Laser scabbling of cementitious materials

by

Ben Peach

A thesis submitted in partial fulfillment for the requirements for the degree of Doctor of Philosophy

University of Sheffield
Faculty of Engineering
Department of Structural and Civil Engineering

July 2015

"Purple rain, purple rain."

Prince

UNIVERSITY OF SHEFFIELD

Abstract

Faculty of Engineering
Department of Structural and Civil Engineering

Laser scabbling of cementitious materials

by Ben Peach

Laser scabbling of concrete is the process by which the surface layer of concrete may be removed through the use of a high power (low power density) laser beam. The aim of this study was to investigate the mechanism(s) responsible for laser scabbling.

This was achieved in three stages. The first stage was a test series used to establish an experimental procedure for assessing the effects of various parameters that may be critical for the effectiveness of the process, such as material composition and initial moisture content. The second stage was a test series investigating the effect of concrete composition on laser scabbling. The first two test series identified that the driving force of laser scabbling in concretes originates from the mortar, therefore, the third test series concentrated on the factors that influence laser scabbling of mortars.

Throughout the study, infra red recordings have been used to quantify laser scabbling behaviour, along with the volume removal due to laser scabbling and characterisation techniques such as XRF, DTA and TGA.

The results suggest that scabbling is mainly driven by pore pressures, but strongly affected by other factors. The removal of free water from mortars prohibits scabbling, but resaturation allows mortar to scabble. A reduced permeability, either due to a reduction in the water/binder ratio or the use of 25% PFA replacement, enhances laser scabbling. Results show that the biggest effect of ageing is due to specimens drying.

Mortars and cement pastes were seen to scabble at a constant rate, whereas concretes experienced a peak rate, after which volume removal reduced dramatically. Basalt aggregate concrete was less susceptible to laser scabbling than limestone aggregate concrete due to vitrification. A higher fine aggregate content increases volume removal and fragment sizes during laser scabbling.

Acknowledgements

First and foremost I would like to thank my supervisors, Mihail, Dirk and Jon, and the technicians, Kieran Nash and Matt Spinks, who made this possible. In addition to these, I would like to thank everyone who has helped me in the Structural and Civil Engineering Department at the University of Sheffield, and those at TWI Ltd, Cambridge, in particular Ali Khan.

Further to this, I would like to thank everyone on the Nuclear First DTC for making that week in Buxton something to look forward to, and the EPSRC for funding the project.

Finally, I would like to thank my friends and family for putting up with all my science chat. In particular I would like to thank my dad for suggesting that I apply to do a PhD and my mum for not asking too many questions. Most importantly, I would like to thank Alison for being a dream boat.

Contents

List of Figures

List of Tables

Chapter 1

Introduction

This section provides an introduction to laser scabbling, highlighting the need for the process within the nuclear industry and the benefits of laser scabbling over alternative concrete decontamination techniques.

1.1 Radioactive waste

Nuclear power is currently going through a renaissance. Many states have reaffirmed their pro nuclear power stance and are building, or planning to build, new reactors. All existing and planned nuclear power stations will need to be decommissioned. Nuclear decommissioning is the process of decontaminating and dismantling a nuclear facility, once its operational lifetime has come to an end. Due to the inherent dangers involved, nuclear decommissioning is a time consuming and technically challenging process, and any methods that could increase safety, productivity, efficiency or reduce the cost of the process should be explored.

Arguably, the biggest challenge within the nuclear industry is the waste. Radioactive waste is hazardous to life and therefore must be restricted. Active elements are unstable and in the process of reaching stability, particles of ionising radiation are emitted. This radiation is harmful to life.

Radioactive waste is classified in the UK in the following manner [13]:

Very low level waste (VLLW): 0.1m^3 of material containing < 400 kBq of beta/gamma activity, or single item containing < 40 kBq. VLLW is disposed of at landfill sites.

Low level waste (LLW): Material that exceeds VLLW contamination boundaries but is less than 4 GBq/te of alpha or 12 GBq/te of beta/gamma activity. LLW is disposed of in shallow burial sites such as that at Drigg, Cumbria where waste is subject to high force compaction, placed in metal containers, grouted with cement and disposed of in a concrete-lined vault.

Intermediate level waste (ILW): Materials that exceed LLW contamination boundaries but do not produce enough heat to require special storage conditions (as in HLW). ILW is currently stored in 500 litre drums where the waste is encapsulated with cement. The current UK government stance on ILW disposal is interim storage followed by disposal at a geological disposal facility (GDF).

High level waste (HLW): Waste that is heat producing due to radioactive decay. The current stance of the UK government for this waste is to store it in interim storage until a GDF is operational, heat produced being accounted for in both conditions. It is unlikely wastes of this sort will be dealt with via laser scabbling as HLW mainly consists of spent nuclear fuel.

The cost of disposal of radioactive waste increases as the the waste classification increases (HLW being the most costly). It is of great economic benefit to reduce the volume of the higher classification wastes as much as reasonably possible. As a matter of social responsibility the amount of hazardous waste inherited by future generations should be minimised.

1.2 Scabbling of concrete

Concrete is commonly used in nuclear facilities. Along with the usual construction benefits (low cost, reliability, vast knowledge base, flexibility of use) concrete is well suited for use as a biological shield due to its high neutron capture cross section and shielding properties can be easily adapted with the addition of materials such as lead or boron.

From nuclear operations it is inevitable that some concrete will become contaminated. Studies have found that contamination is limited to the surface layer of the concrete, generally to a depth of around one centimetre, but it can extend to a depth of tens of centimetres depending on factors such as contamination type, concrete condition and exposure time [14]. The topic of concrete contamination is dealt with in more detail in Appendix A. If the contaminated concrete surface can be removed and contained, the volume of ILW will be greatly reduced. Only the contaminated material that has been removed will be classed as ILW and require disposal in the GDF. The majority of the

concrete will be classed as a lower waste classification, depending on the success of the process this could be LLW, VLLW or standard construction waste.

Scabbling is the process of removing the surface of concrete, it is usually carried out by mechanical means or by high pressure water jetting. Mechanical scabbling requires extensive deployment systems to deal with the large reaction forces, making remote handling difficult. Mechanical scabbling also creates a large amount of dust, which is difficult to contain. High pressure water jetting, on the other hand, creates large volumes of contaminated water, which needs to be subsequently dealt with. A more detailed discussion on alternative concrete decontamination techniques can be found in Appendix B.

1.2.1 Laser scabbling

Application of a high power (low power density) laser on a concrete surface causes concrete fragments to explosively spall from the surface. Lasers of wavelengths around 1 μm can be transmitted down optical delivery fibres several hundred metres in length, allowing expensive laser generation equipment to be stationed away from contaminated areas. As no reaction forces are developed during laser scabbling, relatively lightweight deployment systems can be used, making remote handling a real possibility. Laser scabbling, and surface glazing with subsequent surface removal, was used successfully in the decommissioning of the Japan Atomic Energy Research Reprocessing Test Facility [15].

Previous laser scabbling research is limited and often focused on the processing parameters rather than the fundamental science behind the phenomenon. The studies that did test different concrete compositions highlighted drastic differences in the effect of laser application. The main aim of this study is to identify the mechanism(s) that cause laser scabbling to occur and to determine the effect of concrete composition on the process, all the while giving an insight into process optimisation.

1.3 Scope

Previous research has concentrated on the processing parameters and application of laser scabbling of concrete, rather than on the fundamental science (mechanisms) behind it. This study concentrates on the fundamental science behind laser scabbling. The effects of laser application on concrete ranges from, no effect, to scabbling (surface spalling/explosive ejection of fragments), to vitrification, to ablation. The effects depend

on the concrete composition and laser parameters, but stochastic behaviour has also been reported.

The majority of previous research on laser scabbling was conducted at TWI Ltd, which focused on optimising the processing parameters of laser scabbling for industrial use. TWI Ltd [16] developed a process head, to be mounted on an articulated robot arm, equipped with a vision system, which uses low power lasers and cameras to automatically adjust the robotic arm to accommodate for changes in the concrete topography. A 16 kW vacuum system was also tested which contained 95% of the debris. This means laser scabbling is in the peculiar position of having the technology available for industrial application, while lacking an understanding of the fundamental science which governs it.

1.4 Aim

The aim of this study was to determine the mechanism(s) that cause laser scabbling and the key factors affecting the process.

A study of the mechanism(s) responsible for laser scabbling offers three potential benefits: (1) assess the applicability of laser scabbling on existing facilities, (2) identify any methods that could increase the susceptibility of existing materials to laser scabbling (e.g. wetting the surface), and (3) offer guidance for the design of new materials that will require scabbling at the end of their operational lifetime.

1.5 Objectives

To achieve the aim, the following objectives were set out:

1. Establish an experimental procedure for assessing the laser scabbling behaviour and identify the contribution of each concrete constituent to successive scabbling (hardened cement paste, mortar, concrete and rock specimens) at different degrees of saturation.
2. Quantify the effects of the key factors on successful scabbling (e.g. water/binder ratio, PFA replacement, coarse aggregate type and size, fine aggregate content and free water content).
3. Determine the effect of specimen age on laser scabbling.

4. Clarify the mechanisms responsible for successful scabbling of concrete by focussing on a previously identified key constituents and key compositional factors.

1.6 Outline of the thesis

Chapter 2 *"Literature review"* – A review of the literature related to laser scabbling, including research conducted into laser scabbling and other laser based concrete decontamination techniques, as well as concrete spalling.

Chapter 3 *"Methodology"* – A detailed explanation of the methodology used throughout this study.

Chapter 4 *"Preliminary study"* – A report of the preliminary study carried out in the first test series, identifying major factors of the laser scabbling process which were investigated in detail in the second test series.

Chapter 5 *"The effect of concrete composition on laser scabbling"* – A report of the results from the second test series, an investigation into the key effects of concrete composition on laser scabbling.

Chapter 6 *"Laser scabbling of mortars"* – A report of the third test series, investigating the effect of free water content, water/binder ratio and fine aggregate content on laser scabbling of mortars.

Chapter 7 *"The effect of age on laser scabbling"* – The results of tests conducted on specimens of different ages, including investigations into the effect of ageing on saturated specimens and the effect of prolonged drying.

Chapter 8 *"Summary of results and discussion on laser scabbling"* – A discussion of all the results presented in this study in relation to the mechanism(s) responsible for laser scabbling and the practical application of laser scabbling in nuclear decommissioning.

Chapter 9 *"Conclusions and further work"* – A summary of the conclusions from this study and suggestions for further work to be carried out on laser scabbling.

Chapter 2

Literature Review

This section presents the review of the literature relevant to laser scabbling. Laser scabbling was discovered during laser-concrete interaction trials aimed at developing a method of dealing with radioactively contaminated concrete. To give the background behind laser scabbling, the literature review includes an assessment of alternative phenomena caused by laser interaction with concrete, such as surface glazing, ablation, delamination and melt pool ejection along with laser scabbling itself. The similarities between laser scabbling and concrete spalling are also explored.

2.1 Laser-concrete interaction

When different laser parameters are applied to concrete the material behaves in different ways. Many studies have used different laser parameters to try and deal with contaminated concrete from the nuclear industry in different ways. This section describes some of the different laser applications that have been explored in an attempt to deal with contaminated concrete from the nuclear industry. Table 2.1 summarises the different studies that have been conducted and a comparison of the studies shows an overlap in concrete behaviour between the different techniques, depending on the laser parameters used, including scabbling taking place during glazing trials, and vice versa.

2.1.1 Glazing

Blair studied the feasibility of creating a glazed surface on contaminated concrete to restrict the movement of radionuclides [17]. The process was found to be unsuccessful on limestone concrete due to scabbling of areas where the coarse aggregate was close to the surface. In an attempt to overcome this, a layer of mortar was added to the concrete

TABLE 2.1: Summary of concrete-laser interactions from literature.

Paper	Laser	PFA	Concrete	Power density W/cm^2	Scan speed mm/min	Vitrification Y/N	Explosive scabble Y/N	Depth mm	Volume removal cm^3/min	Conclusions
Hilton	Yb fibre	–	Limestone	177	100	N	Y	22	130	
2010					200	N	Y	20	217	
[16]					300	N	Y	10	185	
Hilton	Nd:YAG	N	Limestone	120	100	N	Y	11	55	Stochastic behaviour
2008				280 - 290	100	Y	N	–	–	Glaze easily removed
[3]			Siliceous	120 - 280	100	N	Y	–	–	Low removal rate
				960	100 - 1400	Y	N	–	–	$<$ 200 mm/min v.hard
			Basalt	280	200 - 300	N	Y	–	–	Low levels of removal
				280	50 - 100	Y	N	–	–	Wet surface insignificant
Nguyen	Yb Fibre	–	Granite	156 - 212	800	N	Y	1.5	–	Composition unknown*
2007			Basalt	52 - 65	400 - 800	N	N	–	–	Cored sample, cut face*
[2]				103 - 212	400 - 800	Y	N	–	–	Wet 103 W/cm^3, no effect
Hirabayashi	Nd:YAG	–		452	80	N	Y	1.7		
2000				423	600	Y	N	4-5		
[15]										
Johnston	Nd:YAG	Y	Limestone	198	30 - 270	N	Y	–	16 - 94	98 W/cm^3 at 94 mm/min
1998				142	30 - 270	N	Y	–	16 - 94	
[1]				106	30 - 270	N	Y	–	16 - 78	
Blair	Nd:YAG	Y	Limestone	298	120	N	Y			Vitrification $<$ 298 W/cm^2
1996										
[17]										

surface which was subsequently glazed by laser application. While the surface of the added mortar glazed successfully, the bond to the concrete was poor. This is possibly a result of the 44% volume increase associated with the rehydration of calcium oxide, left from decarbonation of calcium carbonate present in the limestone aggregates.

Hirabayashi et al. [15] investigated various uses of lasers in the decommissioning of a reprocessing plant. Glazing was defined as the formation of a glassy surface through melting of concrete, removal of which was easily attained. A single pass of a laser with a power of 600 W, scan speed of 80 mm/min and beam diameter of 13 mm yielded a glazed depth of 4-5 mm, with a triple pass yielding a glazed depth of 14 mm.

2.1.2 Heat affected zone (HAZ) delamination

Li [18] reported a technique that used a high power laser to weaken the surface of the contaminated concrete which was subsequently removed by mechanical means. For this method power densities between 700-1200 W/cm^2 and scan speeds of 0.5-5 mm/s were used. The Calcium Silicate Hydrates (CSH) dehydrate fully and hydraulic bonds between cement phases are destroyed once a temperature of 800-900 °C is reached. Dehydration of calcium hydroxide takes place at around 400 °C resulting in a layer of calcium oxide behind the thermally damaged HAZ. Rehydration of the calcium oxide, and the associated expansion, weakens the HAZ. Typically 2-5 mm can be removed in this fashion.

2.1.3 Ablation

Li et al. [18] found that laser vaporisation of concrete and other materials of low thermal conductivity was possible when power densities above 2500 W/cm^2 were used. The depth of material removal can be controlled accurately and a glazed layer is left after vaporisation which has the benefit of restricting the movement of any remaining contamination. The glazed layer did not occur for limestone concrete. MacCallum and Norris [19] found the rate of volume removal by ablation to be too low to be scaled up for use in industry.

Savina et al. [20] investigated pulsed laser ablation using a power density of 226 kW/cm^2. It was found that the hardened cement paste would readily melt, dehydrate and finally vaporise. Mortars with 300 μm or 0.5-1 mm quartz aggregate, on the other hand, showed a tendency to fracture and dislodge from the matrix before melting could take place. This effect was increased for a larger grain sizes. Savina et al. went on to conduct similar experiments [21] using power densities of 226-673 kW/cm^2. It was found that mortars

and concretes tended to fracture due to thermal shock, as long as the temperature gradient was sufficient, rather than vaporise like the hardened cement pastes. It was highlighted that if the heat rate was too low or the material was already hot from an earlier pass, vitrification may take hold which had a twofold effect: (1) energy was wasted in the phase change and (2) the vitrified material could not accommodate induced strain.

2.1.4 Melt pool ejection

Li et al. [18] found melt pool ejection to be suitable only for metals. Laser power densities greater than 6 MW/cm^2 applied to metal surfaces cause molten metal sparks to be violently ejected. These were subsequently collected by a compressed air/water mist system.

More recently Anthofer [22] reported results of experiments involving a technique whereby up to 5 mm of the concrete surface is melted with a 10 kW diode laser and dislodged by pulsed compressed air jets. Molten material solidifies in air and hard glassy spheres are collected by a suction device. The removed material is in a form suitable for disposal and dust creation is eliminated. For a mixed quartzite-calcite concrete, a power density of 2222 W/cm^2 and scan speed of 400 mm/min yielded removal rates of 2.16 m^2/h with an average depth of removal of around 5 mm.

2.1.5 Conclusions of alternative laser-concrete interaction studies

1. Alternative laser-concrete interactions tend to be more power intensive, have lower removal rates and smaller depths of removal than laser scabbling.

2. The effect of laser application on concrete depends on the laser parameters used (power density and scan speed). A higher intensity of laser energy results in more extreme concrete behaviour which may affect the success of laser scabbling, for example, vitrification reduces the thermal shock effect [21].

3. For fixed laser parameters, the effect of laser application depends on the concrete composition with cement pastes, mortars and concretes acting in different manners [17, 20, 21].

2.2 Laser scabbling

Application of a high power laser, perpendicular to the concrete surface, causes concrete fragments to be violently ejected, this process is known as laser scabbling. Compared

to glazing, ablation, HAZ delamination and melt pool ejection, the power densities used for laser scabbling are relatively low.

Previous studies on laser scabbling are sparse. It was discovered during concrete glazing trials [18] and is often mentioned in studies investigating glazing [15, 17]. The bulk of the work done on laser scabbling is unpublished. TWI Ltd. conducted several trials from 1998-2010 [1–3, 16, 23] to determine the feasibility of laser scabbling in nuclear decommissioning activities.

2.2.1 Laser scabbling mechanisms

It must be noted that the following proposed mechanisms for laser scabbling stem from research that is not based on systematic experimental investigations (with the exception of [17]) and, as a result, most of the suggested mechanisms are merely assumptions, not supported by clear experimental evidence.

Li et al. [18] identified laser scabbling as laser thermal shock fractures. Layers of concrete or mortar exploded from the surface after laser application, which was attributed to the rapid expansion of free water and interlayer and chemically bound water released due to dehydration of the cement paste. Aggregate type, porosity distribution and moisture content were identified as key factors in the process. Removal depths of between 1-4 mm were obtained after laser application with power density in the range 400-800 W/cm^2 and scan speeds between 30-300 mm/min.

Hirabayashi et al. [15] also identified laser scabbling as spalling due to rapid expansion of water. Spalling occurred with laser power of 1200 W, 600 mm/min scan speed and 13 mm beam diameter; yielding an average depth of 0.7 mm but continuous spalling was not achieved.

Blair [17] observed explosive scabbling during glazing trials on limestone concrete and considered it an inconvenient phenomena. It was concluded that increased pore pressures, caused by the release of carbon dioxide during the decarbonation of calcium carbonate ($CaCO_3$) present in limestone, was the cause. Bubbles found in the glazed surface were also attributed to decarbonation of $CaCO_3$ present in the cement matrix; the low concentrations present being insufficient to create the pressures necessary for explosive scabbling to occur. Blair [17] found explosive scabbling occurred only when aggregates were near the concrete surface. The relatively low laser powers used in the study ($<$ 1 kW) meant heat energy could not penetrate far beyond the surface. It was suggested that glazing would occur only in areas where the cement paste was deep enough to thermally insulate the aggregate.

A comparison between tests on cut faces and 'as cast' faces was reported [17]. Cut faces exhibited a greater volume of ejected material, however, as power was increased the 'as cast' acted more like cut face samples, suggesting greater heat penetration would heat aggregate embedded deeper in samples as power increased.

Blair [17] also suggested an alternative mechanism responsible for the explosive scabbling. Rapid thermal expansion of the concrete exposed to the laser beam results in a ring of tensile stress beneath the heat affected zone. Once tensile stresses exceed the ultimate tensile strength of the concrete fracture will occur.

MacCallum and Norris[19] suggested that the mechanism responsible for laser scabbling was the build up of strain in the interfacial transition zone between the aggregate and hardened cement paste. Multiple passes were ineffective suggesting a critical strain may have been reached during the initial pass. The authors concluded that scabbling was caused by expansion of aggregates, and hence the beam diameter had to be sufficiently large to heat whole aggregate pieces.

Studies undertaken at TWI Ltd tended to concentrate on maximising the efficiency of laser scabbling through operating parameters. Comments on the mechanism(s) responsible for laser scabbling were brief. Nguyen [2] explained the low scabbling rates of whinstone aggregate by suggesting that laser scabbling may be dependent on the aggregate type used and that whinstone aggregate concrete may not be suitable for scabbling. Hillton [3, 16] stated that the expansion of residual water vapour in the aggregates and the cement matrix, or differential thermal expansions between constituents were the most probable causes of laser scabbling.

2.2.2 Laser parameters

Laser parameters play a large role in the outcome of laser scabbling. If the energy input is too high it will result in glazing of the concrete [17–19, 23], too low and temperatures required for laser scabbling will not be obtained. The results of laser scabbling trials using different laser parameters is detailed in Table 2.1. The energy input is dependant upon the scan speed (mm/s) and the power density (W/mm^2), which is a combination of the laser power (W) and the beam diameter at the concrete surface (mm). Blair [17] found that trials with high power density and high scan speed resulted in the same concrete behaviour as low power density and low scan speed trials; suggesting that energy input is the factor determining the concrete behaviour.

Blair [17] found that the power density of the laser would govern the effect of laser application on (limestone) concrete. For low power densities just a 'charred' path was

left on the concrete surface. This was accredited to burning of the organic plasticiser. As the power was increased, a white band which flaked off easily was identified within a 'charred' ring. The white material was a result of thermal decomposition of calcium hydroxide. As power increased further, a 'glittery' brown vitrified material was left in the centre of the path. As power increased further still, the width and depth of vitrification increased.

Several authors [17–19, 23] have identified that the diameter of the laser beam needs to be larger than the aggregates used in the concrete. Blair [17] found that for a fixed power (150 W) and scan speed (2 mm/s), a beam diameter greater than 8 mm was required for scabbling to take place. It was suggested that an increase in beam diameter increased the limestone aggregate-cement paste ratio in the heat affected zone. This resulted in more carbon dioxide being released from calcium carbonate decarbonation, yielding higher pore pressures capable of ejecting entire pieces of aggregate. Smaller diameters only heat a portion of an aggregate piece which releases insufficient amounts of carbon dioxide to raise the pore pressure high enough to fracture the concrete. MacCallum and Norris [19] also suggested that laser scabbling was highly dependant upon the ratio of beam diameter to aggregate size but as a result of thermal expansion of the aggregates rather than decarbonation. Thomas et al. [23] found that for fixed scanning speeds, the depth of material removal increased as the beam diameter was increased (up to 55 mm after which the removal rate per unit area was constant, however a reduction in depth occurs). The effect was more prominent for higher laser powers.

Thomas et al. [23] found that the removal rate and depth were proportional to the scanning speed, reporting that the maximum removal rate for all power densities tested existed for a scan speed of 1.5 mm/s. As the scan speed was increased the variation in results between different power densities reduced.

2.2.3 Wavelength of laser light

Johnston and Spencer [1] conducted a comparative study between the effectiveness of a 4 kW Nd:YAG laser and the relatively established technology (at the time) of the CO_2 laser. The two lasers have wavelengths of 1.06 μm and 10.6 μm respectively, therefore comments on the effect of the wavelength of the laser on laser scabbling could be made. Limestone aggregate concrete was used throughout the study. Each of the laser types yielded similar removal rates and depths for fixed beam parameters. Slight variations were identified between the profile of the scabbled troughs: the CO_2 laser made a trough similar to the Gaussian power distribution of the laser, whereas the 'top hat' power distribution of the Nd:YAG laser resulted in flatter bottom of the trough

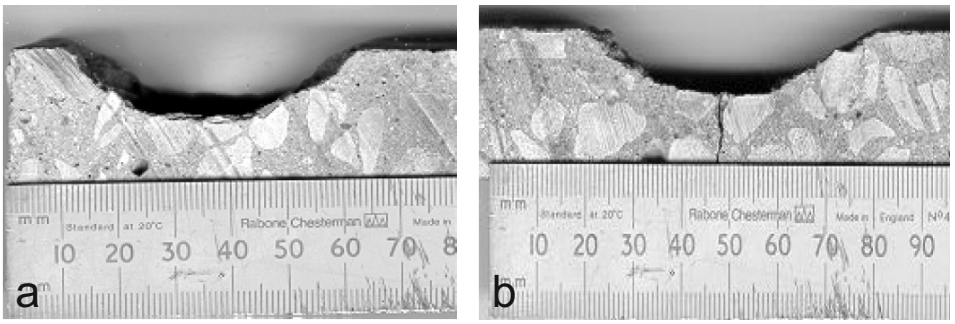

FIGURE 2.1: Images of limestone concrete specimen trough profiles (taken from [1]) that were exposed to identical laser parameters but different laser types. (a) A CO_2 laser caused a gaussian trough profile similar to it's power distribution and (b) a Nd:YAG laser caused a flatter trough bottom due to the 'top hat' power distribution.

(Figure 2.1). It was concluded that the wavelength of the laser beam had little effect on the scabbling process).

2.2.4 The effect of moisture content

Despite some authors suggesting the rapid expansion of water is the cause of laser scabbling, very little work has been done on the effect of moisture content. In Blair's [17] experiments (on limestone aggregate concrete), an increased moisture content only affected specimens that experienced scabbling, not those that glazed. Specimens that were submerged in water over night were seen to eject more material than dry specimens, with the volume of material removed increasing as laser power was increased. Hilton et al. [3] found that wetting the surface of limestone concrete led to an increase in the width of the scabbled track of up to 60%, increasing the rate of volume removal, but the depth was unaffected. Hilton also reported that wetting the surface increased volume removal for siliceous aggregate concrete slightly, but had no effect on basalt aggregate concrete.

Hilton et al. [3] went on to report scabbling trials carried out with specimens submerged in water. No material removal was identified for specimens submerged under depths exceeding 2 mm. Two possible explanations were identified: (1) transmission of the laser light (1 μm wavelength) through water was too low, and (2) the large mass of water on the surface of the specimen acted as a heat sink removing heat from the specimen and reducing thermal gradients.

2.2.5 The effect of concrete composition

Several authors [2, 3, 20] report that the effect of laser interaction with concrete depends on the concrete composition.

Nguyen [2] reported trials on two concrete types provided by British Nuclear Group (BNG), a purposely cast block of granite concrete and whinstone concrete samples bored from a concrete structure used on a nuclear facility. Whinstone is the name given to rocks of a basalt nature found in the north of England. It should be noted that the whinstone concrete was considerably older than the granite concrete and had been exposed to repeated heat-cool cycles. The whinstone concrete samples had a 'cut face' rather than an 'as cast' face like the granite concrete samples. An 'as cast' face will contain a smaller proportion of coarse aggregate at its surface which may have an effect upon the laser scabbling process. The granite concrete consistently scabbled to a depth of 1.5 mm (Figure 2.2-a) for the following laser parameters: power of 6 kW, beam diameter of 60-70 mm and scan speed of 800 mm/min. For identical laser parameters the whinstone concrete scabbled to depths of 0.5 mm and 2.2 mm on the first two runs, but any subsequent trials (of any laser parameters) on this concrete type failed to scabble. Reruns on the samples that were initially successful also failed. Localised melting and carbonation occurred to varying degrees depending upon the laser parameters used (Figure 2.2-b).

Hilton [3] reported experiments carried out on concretes representative of those commonly used in the nuclear industry. Precast concrete slabs of similar mix design using three different aggregate types (siliceous, basalt and limestone), were sourced from a local supplier. Scabbling of siliceous concrete was largely unsuccessful. A range of speeds (100-1400 mm/min) and power densities (120-960 W/cm^2) were used, resulting in different extents of vitrification. Any scabbling that took place was of small quantities. Trials conducted on basalt concrete used only one power density of 280 W/cm^2. For scan speeds of 50 and 100 mm/min vitrification took place, whereas scan speeds greater than 100 mm/min had minimal effect.

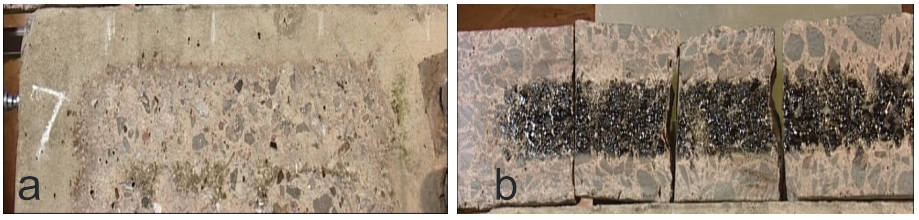

FIGURE 2.2: Photos of specimens after laser application, taken from [2]. (a) Successful scabbling of granite concrete and (b) vitrification and carbonation of whinstone concrete after exposure to high powered laser.

Hilton [3, 16] reported no vitrification during trials on limestone concrete which exhibited varied degrees of scabbling success which depended on the power density and scan speed used. The most successful trials used a power density of 120 W/cm^2 and travel speed of 100 mm/min yielding a removal rate of 55 cm^3/min for a single pass, 65 cm^3/min for a double pass over the top of the original, and 63 cm^3/min for a side by side double pass with approximately 50% overlap. Figure 2.3 illustrates the difference between basalt and limestone concretes after laser application of identical laser parameters.

Hilton [3] highlighted the effect of concrete composition on laser scabbling further with trials on cementitious flagstones of unknown compositions. All flagstones were tested with a power density of 640 W/cm^2 and the scan speed was changed. The first flagstone of uniform grey appearance vitrified at scan speeds of 500 mm/min but scabbled to a depth of 2 mm at 2500 mm/min. This is in stark contrast with the third flagstone, red/brown in appearance, where vitrification did not occur until the scan speed was reduced to 200 mm/min and a maximum depth of 10 mm was observed for 300 mm/min. Flagstone 2, also of red/brown appearance but with the addition of large aggregates, did not successfully scabble for any laser parameters. These trials highlight the effect of composition on the success of laser scabbling, and the need for a screening process to determine the suitability of laser scabbling and give indications of which laser parameters will be successful.

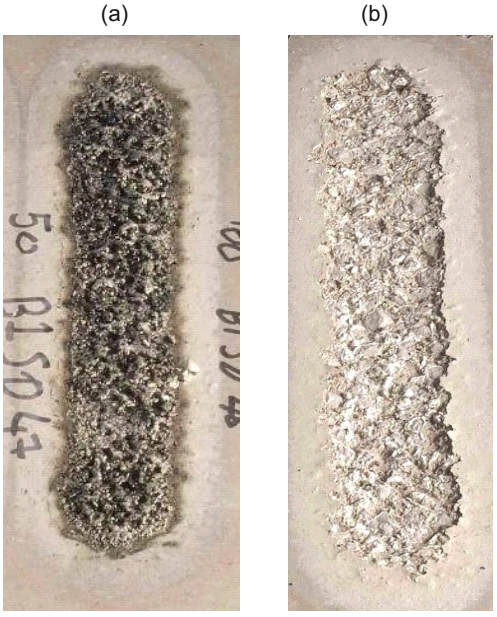

FIGURE 2.3: Images of (a) basalt and (b) limestone concrete specimens after laser application. Both samples underwent identical laser parameters; scan speed=100 mm/min, power=4 kW, diameter=43 mm, power density=275 W/cm^3. Images taken from [3].

2.2.6 Stochastic behaviour

A number of studies have reported stochastic behaviour during laser scabbling trials. Nguyen [2] first highlighted the effect when four specimens of cored whinstone concrete were tested with a 6 kW Yb fibre laser, using a power density of 670-490 W/cm^2 and a scan speed of 800 mm/min. Two of the samples scabbled successfully to depths of 0.5 mm and 2.2 mm, and the remaining two underwent vitrification with no material removed. The two that were initially successful, did not scabble on subsequent tests.

Hilton [3] found identical laser parameters (power density of 120 W/cm^2 and scan speed 100mm/min) to scabble successfully on one slab of precast limestone concrete, showing a removal rate of 55 cm^3/min for a single pass, but another slab, sourced from the same factory with supposedly the same mix design, was unaffected. Higher power densities (smaller beam diameter) on the same slab resulted in a weakly bonded black and white residue which could be easily removed by a wire brush which equated to a removal rate of 60 cm^3/min.

2.2.7 Laser scabbling conclusions

The following laser scabbling related conclusions can be drawn from the previous laser-concrete interaction studies;

(I). A large beam diameter (relatively low power density compared to alternative laser interaction methods) is necessary for scabbling, a small diameter beam is more likely to cause vitrification [17, 20], due to the increased power density.

(II). An increased moisture content generally increases laser scabbling. [3, 17, 18]

(III). Stochastic behaviour has been reported during laser scabbling trials. [2, 3]

(IV). Concrete-laser interaction is highly sensitive to concrete composition. [2, 3, 20]

(V). Energy input governs laser-concrete interaction; power density and scan speed can be adjusted accordingly. [17]

2.3 Concrete spalling

Spalling of concrete is defined as the violent or non violent breaking off of fragments from a concrete surface when exposed to high and rapidly rising temperatures [5]. Spalling damages reinforced concrete structural members, reducing the strength and exposing

reinforcement to the high temperatures of fire, which has the potential of reducing the strength and fire rating dramatically. The potential threat to the safety of structures in fire conditions has led to many studies on concrete spalling. The main factors of the process have been identified as: moisture content, permeability, concrete strength, heat rate and final temperature. The similarities between spalling and laser scabbling (discussed in Section 2.4) means the wealth of knowledge available on spalling should not be ignored.

2.3.1 Types of spalling

It is generally agreed that there are four types of spalling (Figure 2.4);

Aggregate spalling concerns thermal damage concentrated specifically in the aggregate. Splitting and bursting of the aggregate leaves small craters, 5-10 mm [8] in depth, on the heated concrete surface. Damage is generally deemed insignificant as craters are too shallow to reveal reinforcement or affect fire resistance. Researchers are divided on the mechanism behind the phenomenon, and both mineralogical characteristics [24] and a form of thermal shock [25] have been suggested.

Corner spalling is a result of thermal degradation causing the break down of bonds in the concrete [8]. Effects are often seen at corners and on structural elements such as beams and columns, where there are often two faces heated and less physical restraint. Corner spalling has been known to reveal reinforcement and cause failure of structural elements.

Surface spalling is a violent form of spalling often treated as a less serious form of explosive spalling [8]. Fragments of 25-50 mm depth are ejected in a violent manner due to pore pressures or thermal stresses beneath. Large areas can be affected making the effect potentially serious.

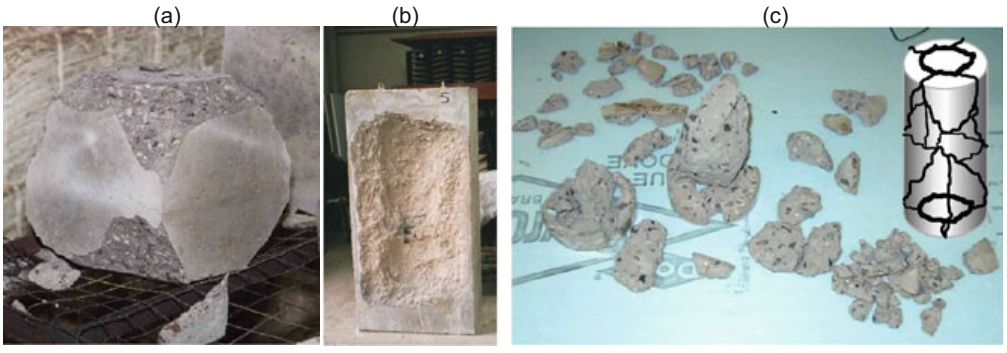

FIGURE 2.4: Examples of different spalling types, taken from [4]. (a) Corner spalling, (b) surface spalling, (c) explosive spalling.

Explosive spalling concerns violent ejection of large fragments, 100–300 mm length, 15–20 mm depth [5]; often differentiated from surface spalling purely by the extent of damage. The potential for catastrophic failure posed by explosive spalling means that this is the most researched area and as a result the area that is concentrated on here.

2.3.2 Spalling of rocks

In the interest of fire safety of tunnels cut into natural rock, Zhang et al. [26] investigated spalling of three common Swedish rocks. Granite was found to spall in large flakes (maximum size 40 mm wide, 3 mm thick), gabbro rock spalled in small fragments and schist underwent delamination. The cause of rock spalling was put down to thermal stresses caused by differences in thermal properties of the specific minerals within the rocks. The granite contained a number of different minerals with different thermal expansions (including quartz), the gabbro was largely made up of one mineral (plagioclase feldspar) which therefore resulted in minimal differential expansions, and the schist was composed of two minerals (muscovite and quartz) in layers which underwent delamination on heating. It was reported that a higher moisture content increased the extent of spalling but pore pressure spalling was discounted as the mechanism responsible due to extensive thermal cracking experienced by all rock types.

2.3.3 Flame cleaning

Flame cleaning [27], like laser scabbling, involves utilising spalling to the benefit of the user, this differs from typical spalling studies where the aim is to limit the process. An acetylene flame (temperature approximately 3100 °C) is used to remove the surface layer of concrete to a depth of up to 4 mm. The depth of removal is affected by changing the scan speed: too slow and the surface melts and becomes fragile (it can be subsequently removed with a wire brush). Johansson reported that moisture content had the greatest effect on the process with soaked specimens yielding a more uniform removal. High strength concrete was slightly more effective than low strength concrete and aggregate type had no effect on the process. Only the upper 2 mm of the remaining concrete was exposed to the damaging temperatures of over 200°C, limiting damage to the remaining material.

2.3.4 Explosive spalling mechanisms

There is no consensus between researchers on the mechanism responsible for explosive spalling. Due to the large amount of factors influencing explosive spalling it is likely that

the phenomenon is a result of a combination of mechanisms, depending on the specific parameters of each individual case.

2.3.4.1 Pore pressure spalling

Water is present in concrete as free water in the capillary pores and aggregates, interlayer water within the gel pores, and chemically combined water within the cement hydration products [28]. When concrete is heated the water present will vaporise and turn to steam undergoing an increase in volume during the phase change increasing pore pressures within the concrete. The different types of water will vaporise at different temperatures: free water around 100 °C, and interlayer water at slightly higher temperatures around 120-140 °C. Chemically combined water will be released at different temperatures depending upon the hydration product in question, for example dehydroxylation of calcium hydroxide takes place around 450-550 °C. In addition to the water vaporisation, decomposition of other phases, such as the decomposition of calcium carbonate present in carbonated cement paste and/or limestone aggregates, will result in the release of carbon dioxide contributing to the increase in pore pressures.

The moisture clog mechanism first proposed by Shorter and Harmathy [29] is the most widely accepted pore pressure spalling mechanism. Mass migration within concrete at ambient temperatures is governed by diffusion, whereas at elevated temperatures the behaviour is governed by pressure, moisture and temperature gradients [5]. As the surface is heated, some of the developed gases will escape through the surface and some will be forced to retreat within the concrete. This creates a dry zone close to the surface, a drying zone deeper in the concrete, and if the permeability is low enough, a saturated zone (or moisture clog) will form where the steam condenses (Figure 2.5-a). This saturated zone will act as an impermeable membrane resulting in the build up of pore pressures, which will cause an explosive fracture once the pore pressures exceed the tensile strength of the concrete.

Pore pressure spalling depends on a number of interconnected factors. A low heat rate and/or a high permeability will allow pore pressures to dissipate, while the moisture content of the concrete, which is largely dependant upon the concrete age, will dictate the amount of free water present. The low permeability of high strength concrete is often used to explain the higher susceptibility to explosive spalling of high strength concretes compared to low strength concretes [5].

Fu [4] suggested spalling is governed by the development of cracks and pore pressures. If cracks develop before the development of sufficient pore pressures, spalling will be avoided (and vice versa). At elevated temperatures, exaggerated by high heat rates,

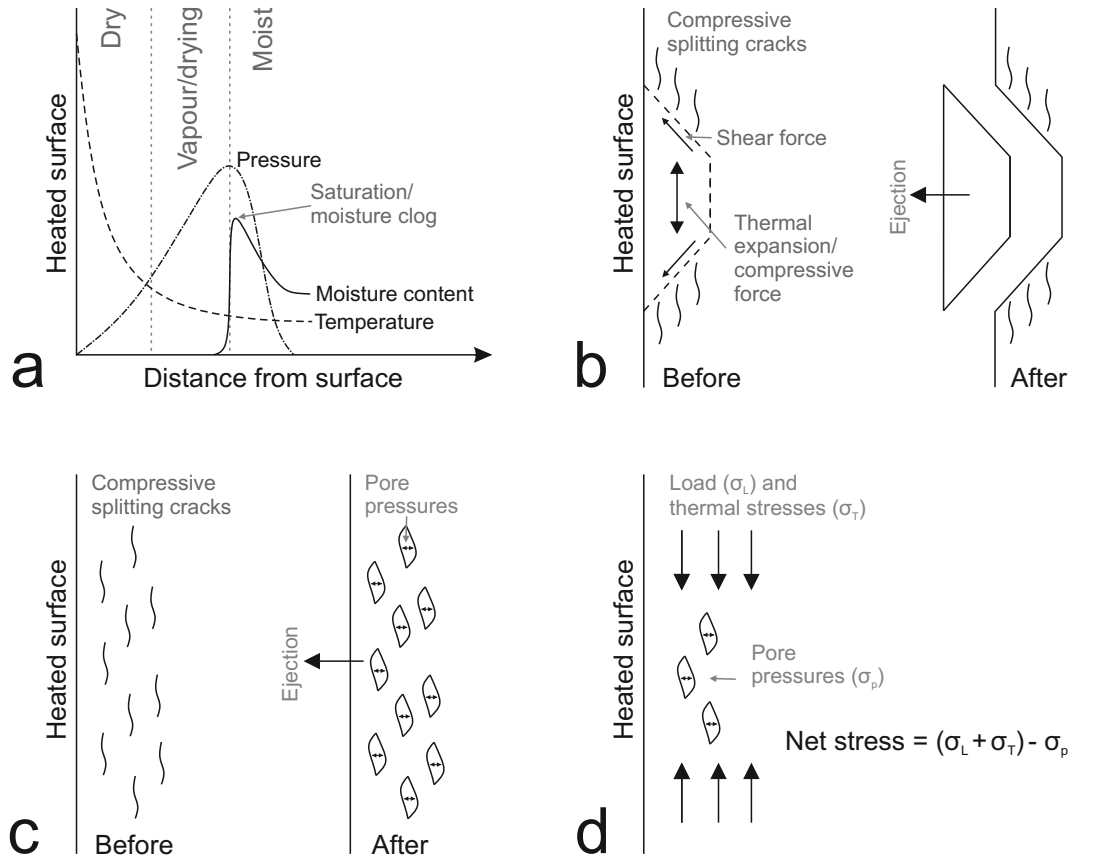

FIGURE 2.5: Spalling mechanisms; (a) Pore pressure spalling (moisture clog) adapted from [5], (b) thermal stress spalling adapted from [6], (c) and (d) combined mechanisms adapted from [7] and [8] respectively.

many factors can cause cracking in concrete: dehydration and thermal decomposition of cement phases, differential thermal expansion, release of evaporable and non evaporable water, temperature gradients etc. Furthermore, the distribution of these cracks are affected by many factors: the spatial difference of constituents, the pore network, defects and pre existing cracks.

2.3.4.2 Thermal stress spalling

A combination of the low thermal conductivity of concrete (which reduces further as concrete is dried [30]) and the high heat rates developed during a fire, result in severe thermal gradients. The higher temperatures at the surface of the concrete will cause compressive stresses to build parallel to the heated surface, due to restrained thermal expansion, causing splitting cracks parallel to the surface and conical shear cracks [6] (Figure 2.5-b). Once the shear cracks develop a concrete fragment is removed from the bulk. Bazant [6] suggests pore pressures could contribute to the triggering of spalling,

providing the slight imperfection (crack) for shear cracks to form. Loading or prestress increases the effect of thermal stress spalling as they are super imposed, increasing the compressive stresses, postponing the crack initiation and allowing buildup of tensile stresses. Proponents of this mechanism often fail to explain the effect of moisture content reported by many authors [4, 31–34].

2.3.4.3 Arguments against pore pressure spalling and in favour of thermal stress spalling

Jansson and Boström [35] found that pore pressures developed in concrete during fire conditions were lower than the tensile strength of concrete, concluding that pore pressures could not be the sole driving force for explosive spalling. Spalling occurred only in specimens not containing polypropelene (PP) fibres, despite recorded pore pressures in specimens containing PP fibres being higher than pressures in specimens without the fibres [35]. This led Jansson and Boström to explore alternative explanations for the effect of moisture content and PP fibres on spalling, other than the traditional reduction in pore pressures. Jansson and Boström accepted that the permeability of the concrete will increase when PP fibres melt around 200°C, but suggested two explanations for this reducing spalling, other than the release of pore pressures. Firstly due to the incompressible nature of water, if pores are saturated and put under stress they cannot deform, as long as the water movement is restricted (i.e. low permeability). This would cause the Young's modulus of the cement matrix to increase, or in other words become stiffer, as it is stressed. Once temperatures rise and aggregates undergo thermal expansion the stiff matrix will crack parallel to the face being heated. Melting of PP fibres will reduce the moisture content in the area affected by heating, reducing the Young's modulus and the stiffness of the cement matrix, reducing cracking. Jansson and Boström pointed out that there is some contradiction in the literature about the effect of moisture content on the Young's modulus of concrete especially under sealed conditions. The second potential mechanism of PP fibres is related to the phenomenon of drying creep that relaxes stresses in the cement matrix. As drying creep is governed by the transport of moisture, specimens with polypropylene fibres will undergo more drying creep, relaxing the thermal stresses and reducing thermal stress spalling.

Similar results were reported by Mindeguia et al. [36]. Mindeguia et al. measured the pressures within concrete specimens exposed to heat following fire curves according to ISO 834-1:1999 and found no correlation between spalling depth and internal pressure, in some occasions higher pressures were reported in specimens that did not spall than in those that did spall. In all cases, pore pressures developed during heating were lower than the tensile strength of concrete.

Bazant [6] suggests pore pressure spalling is an unfeasible mechanism for explosive spalling as once a crack appears the pore pressure will reduce to zero, and repressurisation from the surrounding concrete would be too slow. Therefore pore pressures can only be responsible for cracking, potentially triggering the spalling, but not actually driving the explosive spalling.

2.3.4.4 Combined mechanisms

Sertmehemetoglu [7] also found that pore pressures developed during spalling tests were insufficient to be the primary driver of explosive spalling. Building on a finding of Dougill [37] that cracks form parallel to the heated concrete surface, Sertmehemetoglu suggested that it is the pore pressure buildup in these cracks that subsequently gives the explosive force necessary to remove the surface (Figure 2.5-c).

Khoury [5] and Connolly [8] both suggest that thermal stress spalling and pore pressure spalling work against one another, and the net effective stress will dictate which mechanism takes hold. The sum of the applied load and thermal stresses, minus pore pressures gives a net stress which, if sufficient, induces spalling (Figure 2.5-d). The effective stress is said to depend upon a complicated combination of thermal expansion, pore pressures, permeability, moisture content and compressive strength.

2.3.4.5 Thermal incompatibility

Differential thermal expansion between the different concrete constituents will take place but it is unlikely to be a primary driver for explosive spalling. The cracking induced by thermal incompatibility will cause weakening of the material and an increase in permeability resulting in reduced pore pressures. Piasta found hardened cement paste to undergo shrinkage up to 200 °C [38], whereas aggregates expand at a constant rate until thermal reactions specific to different minerals take place, such as the alpha to beta quartz transition at 573 °C or the decarbonation of calcium carbonate around 600-900 °C [30].

2.3.5 Factors of explosive spalling

There are a number of mechanisms that contribute to spalling each with their own factors. As a result there is no single threshold of factors which will induce spalling.

2.3.5.1 Moisture content

Many authors have highlighted the relationship between moisture content and spalling. A higher moisture content yields a greater degree of spalling [4, 31–34]. It has also been reported that the higher the concrete strength the lower the moisture content required for spalling to take place [32]. It must be noted that this is most likely due to concrete properties related to concrete strength (porosity, permeability) rather than a direct effect of concrete strength. Hertz [31] found that dry specimens experienced spalling too, suggesting that thermal stresses may be responsible or that chemically bound water contributes towards pore pressure spalling.

Copier [34] found that concrete with a moisture content below 5% (by volume, approximately 2.5% by mass) will not spall. In reality, however, concrete will always have a moisture content of 7–10% (by volume, approximately 3–5% by mass). Eurocode 2 [39] details that explosive spalling is unlikely to occur when moisture content of concrete is below 3% (by mass).

Mindeguia [36] found that specimens oven dried at 80 °C had lower pore pressures than air dried or saturated specimens, with the effect reduced for concretes with a lower water/binder (w/b) ratio. It was concluded that evaporable water at 80 °C was responsible for pore pressure development, however no comment was made on the effect of thermal damage due to oven drying, potentially leading to an increase in permeability. It was also found that pore pressures were lower in saturated specimens than in air dried specimens. This was accredited to gases escaping due to audible cracks, not experienced in oven dried or air dried specimens.

Sertmehemetoglu [7] suggested that moisture content affects spalling indirectly, in that a higher moisture content ensures more complete hydration reducing the permeability rather than it being the source of vapour.

2.3.5.2 Permeability, water/cement ratio (w/c) and strength

It has been extensively reported that high strength concrete (w/c ratio below around 0.4) has a tendency to spall more than normal strength concrete (w/c ratio above around 0.5) [5, 8, 40–43]. This is usually explained in relation to pore pressure spalling and the relationship between permeability and w/c ratio. Normal strength concrete will have a higher permeability than high strength concrete, allowing pore pressures within the pore network to dissipate more readily. Permeability, w/c ratio and strength grade are linked, so that a lower w/c ratio will result in a cement matrix with a lower porosity

and a higher strength [28]. Permeability is defined as the interconnectivity of pores and as a result, is usually, but not necessarily, related to porosity.

Bazant [6] explained the effect of concrete strength on explosive spalling in terms of thermal stress spalling. He suggested that high strength concrete is more susceptible to thermal stress spalling as it is able to develop more strain energy and is known to be more brittle than normal strength concrete. Connolly [8], on the other hand, suggested that compressive strength would oppose thermal stress spalling, as greater thermal stresses would be required for fracture to occur.

Eurocode 2 states that high strength concrete, of grades above 80/95 MPa, or concrete containing more than 6% by weight of silica fume (a pozzolanic cement replacement material, known to reduce permeability), must undergo spalling preventative measures, such as the addition of propylene fibres or a reinforcement mesh.

2.3.5.3 Aggregate Type

A number of sources have commented on the effect of aggregate type on explosive spalling. Connolly [8] conducted spalling experiments on 75 mm diameter, 20 mm depth cylinders made of limestone, basalt and Lytag (a lightweight aggregate) aggregates. It was found that gravel aggregates were most susceptible to spalling, and limestone aggregate and the lightweight aggregate were less susceptible to spalling. When the lightweight aggregate did spall however, it was more violent than the gravel or limestone aggregates with fracture taking place within the aggregate itself. For specimens using gravel or limestone aggregates fracture took place exclusively in the cement paste. It was suggested that the greater porosity of lightweight aggregates allows pore pressures to build within the aggregates causing them to explode. Connolly [8] also suggested that the use of lightweight aggregate as a preventative measure against spalling only holds true if the concrete is of a low moisture content. It is possible that saturation of the specimen may cause the moisture content of the aggregate to exceed that of the cement paste, in which case the use of lightweight aggregates may encourage spalling rather than mitigate against it.

BS 8110-2:1985 [44] states that aggregates with a higher silica content are more likely to undergo spalling than limestone aggregate, with lightweight aggregates being identified as having the lowest probability of spalling due to their high permeability. Contrary to this, Mindeguia [36] suggested that thermal damage due to differential thermal expansions experienced in specimens containing siliceous calcareous aggregates increased permeability and limited spalling, similar to the melting of polypropylene fibres.

2.3.5.4 Aggregate size

Connolly's [8] results suggested 5 mm aggregates increased spalling, however he accredited this to poor experimental technique as the aggregate:cement paste ratio was larger for specimens using smaller aggregates. Connolly suggested that larger aggregate size increased the susceptibility to spalling.

More recently, Pan [45] carried out a study on the effect of aggregate size on spalling of concretes with different binders; geopolymer (water/binder = 0.33) and OPC (w/b = 0.42 and 0.61). Crushed basalt aggregate of three different sizes were used as the coarse aggregate; 2.36–4.75 mm (small), 4.75–10 mm (medium) and 10 mm–14 mm (large). Specimens were heated at a rate of 5 °C/min up to a maximum temperature of 800 °C. It was found that specimens of small and medium aggregate sizes spalled at 380 +/− 50 °C but specimens with large aggregate size failed to spall. The same outcome was true for each binder composition leading to the conclusion that spalling was dependant on aggregate size, with larger sizes being less susceptible to spalling under the conditions used in the study.

2.3.5.5 Heat rate

Many authors have commented on the effect of heat rate on spalling, often reporting different results. Fu [4] stated that heat rates above 3 °C/min are required for spalling to occur, whereas other authors such as Hertz [31] found that heat rates as low as 1 °C/min can cause spalling in specific conditions. Hertz [31] found that the heat rate required for spalling to take place decreased from 10 °C/min to 1 °C/min with addition of 7% silica fume (in a concrete using expanded clay aggregate known to have a high moisture content).

Phan [42] suggested that steep thermal gradients caused by a high heat rate may result in microcrack formation giving pore pressures a method of release. Phan found that specimens heated at 25 °C/min developed smaller pore pressures than specimens heated at rates of 5 $°C/min$. Similar results were reported by Mindeguia et al. [36].

2.3.5.6 Loading conditions

Several researchers have commented on the effect of loading of the specimen during spalling trials. While it is agreed that loading increases the chance of spalling, the explanations given for this vary. Some report that loading and prestress are superimposed onto surface compressive stresses, caused by thermal gradients, increasing the chances of

thermal stress spalling [5, 6, 34]. Copier [34] found that the magnitude of the compressive stress applied to concrete during explosive spalling tests to be of little importance; the presence of a compressive force of any magnitude increased the effect of explosive spalling. Connolly [8] suggested that low level applied loads may mean higher pore pressures are required for pore pressure spalling to occur, whereas Sertmehemetoglu [7] suggested a higher load would densify the matrix, decreasing permeability, enhancing the effect of pore pressures.

2.3.6 Conclusions on spalling

Concrete is a variable material which has many interconnected properties. The literature suggests explosive spalling is a result of a complex combination of interconnected factors. As a result of the similarities between laser scabbling and explosive spalling, this is most likely to be true for laser scabbling too. The following conclusions can be drawn.

(I). There is no consensus on the mechanism responsible for explosive spalling. It is suggested that pore pressures, thermal stresses or a combination of both are responsible for spalling.

(II). Pore pressure spalling is a function of moisture content, permeability (including cracking) and heat rate.

(III). Pore pressures of a sufficient magnitude to induce explosive spalling have not been measured in previous tests.

(IV). Thermal stress spalling is affected by the thermal conductivity, the exposed heat rate and loading conditions.

(V). Explosive spalling is dependant on concrete strength. This may be a result of the strength itself or the permeability which is inversely proportional to the strength.

(VI). Concrete using polypropylene fibres, which melt at around 200 °C increasing the permeability of concrete, are less susceptible to explosive spalling.

(VII). A higher heat rate does not necessarily result in higher pore pressures.

2.4 Discussion of the comparisons between explosive spalling and laser scabbling

Both explosive spalling and laser scabbling concern the ejection of material from concrete as a result of the application of an external heat source. In the context of fire

safety, concrete spalling is an unfavourable process and research is aimed at limiting it. On the contrary, the aim of laser scabbling is to remove the required depth of concrete over the shortest time scale. While differences exist between laser scabbling and explosive spalling, the similarities between the two phenomena, and the wealth of research associated with concrete spalling, must not be ignored.

Explosive spalling and surface spalling strike similarities with the desired laser scabbling process (summarised in Table 2.2), but some scabbling trials have yielded results similar to the other types of spalling. The non explosive scabbling behaviour reported by Hilton [3] and the HAZ delamination reported by Li [18] are similar to that of corner spalling.

TABLE 2.2: Summary of similarities and differences between laser scabbling and explosive spalling. (* = Taken from results presented in this study)

	Explosive spalling	Laser scabbling
Heat rate	1-700°C/min [31, 36]	200°C/s [*]
Timescale	30-40 mins [5]	0.5+ secs [*]
Debris depth	15-20 mm [5]	0-10 mm [3]
Debris width	100-300 mm [5]	10-30 mm [3]
Stochastic behaviour	Yes [5]	Yes [3]
Moisture content	Increases [5]	Increases [3]
Reduced permeability	Increases [5]	?

2.4.1 Heat source

The differences between the two processes originate from the heat source. High powered lasers used for laser scabbling have the potential to exert much more energy to the concrete surface than that of fires that result in explosive spalling. A higher energy input will induce a higher heat rate, more severe thermal gradients and higher surface temperatures. The heat rates imparted on the concrete during laser scabbling (200°C/s) are far higher than those developed in concrete during fire conditions, which result in explosive spalling (1-700°C/min [31, 36]). It should also be noted that the method of heat transfer differs between the heat sources: a laser transfers energy by radiation only whereas a fire will transfer energy by radiation, convection and potentially conduction from the source. Therefore changes to the absorption or reflective properties of a material will have a greater effect on laser scabbling than explosive spalling.

The area heated also differs: laser scabbling heats a relatively small localised area (20–100 mm diameter, 60 mm in this study), whereas in fire conditions large areas of concrete can be exposed, potentially from more than one direction. This suggests heat loss will

be more prevalent in laser scabbling reducing the depth of heat penetration compared to that of concrete exposed to fire conditions (explosive spalling).

The different heat sources and heat rates result in different concrete behaviour. Ejected debris is smaller and it takes less time for ejection to occur. Thermal reactions such as vaporisation of water (free, interlayer and chemically combined, in the form of C-S-H, calcium hydroxide and some other phases), decarbonation of calcium carbonate and structural or phase changes occur at different temperatures. These thermal reactions are potential factors in both explosive spalling and laser scabbling. The higher maximum temperature induced during laser scabbling will trigger thermal reactions not seen in explosive spalling trials i.e. vitrification, and the higher heat rate will cause thermal reactions to take place over a shorter time scale.

2.4.2 Effect of composition

Previous laser scabbling experiments have reported that concretes of different compositions exhibit different behaviour under laser application. Limestone concrete is seen to scabble successfully, whereas basalt or granite concretes are less successful and susceptible to vitrification [3], which hinders the laser scabbling process. On the other hand, it is reported that siliceous aggregates are more susceptible to explosive spalling and limestone concretes are seen as thermally stable aggregates [8, 44]. The contradictory results may be a result of the different heating regimes causing different thermal reactions to occur at different rates. Calcium carbonate, the main constituent of limestone concrete, decarbonates between 600–900 °C, weakening the material and producing carbon dioxide, which may increase pore pressures to induce pore pressure spalling. Basalt and granite have a relatively low melting point of around 1200 °C, and quartz is known to undergo crystal transformations causing volume changes, such as the alpha-beta quartz inversion at 573°C [30].

2.4.3 Potential mechanisms

The effect of the higher heat rate of laser scabbling compared to explosive spalling can be seen by the difference in material behaviour (smaller debris size, smaller timescale and vitrification). This difference in material behaviour suggests the mechanisms responsible for the processes will also differ. In terms of pore pressure spalling, the increased heat rate will cause moisture to vaporise at a higher rate, creating a greater volume of vapour in a shorter timescale. It is likely this will affect the movement of vapour and potentially cause the moisture clog to form at a much lower depth. In relation to thermal stress spalling, the higher heat rate will cause more severe thermal gradients to be formed in

the concrete over a shorter time-scale, increasing localised thermal stresses within the concrete.

2.4.4 Stochastic behaviour

Stochastic behaviour has been reported in both explosive spalling [5] and laser scabbling [2, 3] trials. Identical experimental parameters by the same researchers in the same trials yield very different results. Stochastic behaviour is unexplained but may be a result of the variability of concrete: differences in conditioning, storage, mix variations, and/or moisture content affect concrete properties. The source of stochastic behaviour must be understood if the process is to be used in nuclear decommissioning.

2.4.5 Summary of comparisons between explosive spalling and laser scabbling

Previous studies show that there are some similarities between explosive spalling and laser scabbling. Both processes result in explosive fragment ejection, are influenced by moisture content and may exhibit stochastic behaviour. On the other hand, the (limited) previous research on laser scabbling showed some very significant differences between the two processes. The heating rates and maximum temperatures reached during scabbling are higher and aggregate type affects the two processes in opposite ways: siliceous aggregates tend to enhance explosive spalling but hinder laser scabbling. When a high power laser beam is applied to concrete surfaces the material either scabbles (explosive ejection of fragments) or vitrifies, although stochastic tendencies have also been reported. A threshold input energy per unit area ($W/(s \cdot mm^2)$) exists, below which the material scabbles, and above which it vitrifies (and further scabbling is hindered). The process of laser scabbling is also highly sensitive to aggregate type and a higher moisture content enhances the process.

2.5 Relevance of the previous literature to the current research

2.5.1 Experimental procedure

The fundamental differences between explosive spalling and laser scabbling, namely the difference in heat sources, mean the majority of the aspects of the experimental procedures used in the explosive spalling studies are extraneous to laser scabbling experiments.

The previous laser scabbling studies [1–3, 15–18, 23] have highlighted the interconnectivity of the laser parameters and the complications that arise from varying too many of the parameters at once. For instance changing either the scan speed, beam diameter or laser power will affect the amount of energy imparted to a unit area of the concrete surface, and as a result, interpreting the results can be difficult when more than one of these parameters is changed. To avoid this, the experimental procedure for this study was simplified making comparisons of results simpler.

As laser scabbling is an industrial process it was assumed that the highest productivity would be desired, i.e. a higher power and higher scan speed would be preferred over a lower power and lower scan speed, as a result, the laser power used in this study was kept constant at the highest available power (5 kW).

To simplify experiments, a static beam was used in this study, rather than a scanning beam. In order to offer comparisons between different amounts of energy imparted per unit area, the laser interaction time was varied, which can in turn be converted to a scan speed if necessary.

The beam diameter was also kept constant in this study. Previous research [1–3, 16, 23] investigated this factor in some detail, as a result, the beam diameter that yielded the highest volume removal (60 mm [16]) has been used in this study.

2.5.2 Factors affecting laser scabbling and explosive spalling

The literature review has highlighted that many of the factors of explosive spalling and laser scabbling are similar and those factors have been used to design the experimental programme for this study. The main aim of this study was to determine the mechanism(s) responsible for laser scabbling. Observations of the effects of changing the main factors of laser scabbling have been the main tool used to identify the mechanisms involved.

The concrete composition has been highlighted as a key factor of laser scabbling [2, 3] and explosive spalling [5, 8, 36, 40–43, 45], as a result, this has been the main factor concentrated on throughout this study. In particular factors affecting the permeability of materials, such as the water/binder ratio and PFA content, and factors of the aggregate, such as aggregate type, content and size, have been investigated in detail. Furthermore, a key variable to the industrial application of laser scabbling is likely to be the effect of concrete composition, as this is known to vary geographically between different nuclear power plants.

Moisture content has been highlighted as a key factor in explosive spalling studies, whereas relatively little work [3, 17] has been carried out in regard to this factor in laser scabbling studies, despite it being a key factor of the most commonly mentioned mechanism (pore pressure spalling). In an attempt to fill this gap in the research, the effect of the moisture content of materials tested in this study has been investigated.

2.5.3 Stochastic behaviour

Stochastic behaviour has been identified explosive spalling [5] and laser scabbling studies [2, 3]. It is of the opinion of the author that the stochastic behaviour is not truly stochastic, but the result of poor experimental procedure or the intrinsic variability of concrete. As a result, this study has tried to eliminate the stochastic behaviour by ensuring the experimental procedure and the specimen preparation was carried out in a meticulous manner.

Chapter 3

Methodology

This Section outlines the methodology used for all experimental programmes. Differences between the experimental procedures of the separate experimental programmes, in particular the compositions and preconditioning methods, are detailed at the start of the relevant sections.

3.1 The experimental approach

The project was split into three successive test series, with each subsequent programme designed around the outcome of the previous programme. The preliminary test series (Chapter 4) was designed to establish an experimental methodology and assess a wide range of factors in order to identify what should be investigated in more depth in the following programmes (objective I). The second test series (Chapter 5) looked into the effect of concrete composition in detail, by investigating cement pastes, mortars and concretes (objective II). The first and second test series highlighted the dominance of the mortar in the laser scabbling process, as a result, the third experimental programme (Chapter 6) concentrated on the factors influencing laser scabbling of mortars (objective II). The fourth experimental programme (Chapter 7) tested specimens cast at the same time as those tested in the first (Chapter 4) and second (Chapter 5) experimental programmes at a later date to assess the effect of specimen age on laser scabbling (objective III). The results from each experimental programme were assessed in relation to the potential mechanisms responsible for laser scabbling (objective IV).

3.2 Materials and Specimen Preparation

The material compositions selected for this study (Table 3.1) were based on the concrete composition of the pre-stressed concrete pressure vessel of the advanced gas cooled reactor (AGR) in the Heysham-2 nuclear power station in Lancashire, UK. The 20 mm aggregate proportion was directly replaced by 10 mm aggregate to make a more uniform concrete (unless otherwise stated). The specific compositions used in the experimental programmes are reported in the relevant sections.

TABLE 3.1: AGR mix composition, which was used as the base composition. Other mix compositions were modifications of this mix design.

	Mass ratio
Water	0.42
OPC	0.75
PFA	0.25
Fine agg.	1.84
Plasticiser	0.0045
10mm agg.	1.05
20mm agg.	2.16

The materials used for preparing the test specimens were: Hanson CEM I OPC (BS EN 197-1:2000 strength class 52.5N) in the first two test series (Chapters 4 and 5), and Lafarge CEM 1 OPC was used in the third test series (Chapter 6); CEMEX pulverised fuel ash (PFA; LOI-B and fineness-s); fully graded marine dredged quartzitic sand from Hoyle Bank (particle size distribution detailed in Table 3.2), Morecombe Bay, UK; crushed basalt rock sourced from High Force Quarry, Durham, UK; and crushed limestone rock from Longcliffe Quarry, Derbyshire, UK. All coarse aggregate used passed through a 10 mm sieve and was stopped by a 6 mm sieve, unless otherwise stated.

TABLE 3.2: Particle size distribution of the sand used in this study.

Seive size (mm)	Mass retained (g)	Cumulative mass retained (g)	Cumulative mass passed (g)
8	0	0	100
5	2.3	0.6	99.4
2.36	17.2	5.0	95.0
1.18	34.3	13.8	86.2
0.6	56.9	28.4	71.6
0.3	130.6	61.9	38.1
0.15	133.5	96.2	3.8
0.075	0.8	96.4	3.6
0	14.1	100	0

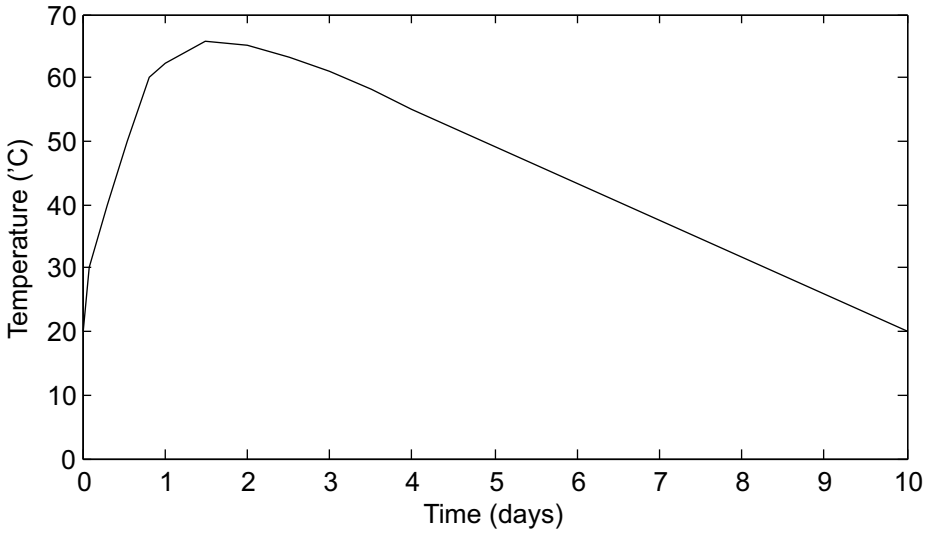

FIGURE 3.1: Temperature-time history for the temperature matched curing.

All mixes underwent 30-60 seconds dry mixing followed by 3-5 minutes wet mixing. The slurry was transferred to 100 mm cube moulds which were 3/4 filled and vibrated for approximately 10s before being filled and vibrated again for approximately 10s, and the cast face trowelled smooth. All specimens underwent a ten day temperature matched curing regime reaching a peak temperature of 65°C after 36 hours, gradually returning to 20°C after 240 hours (Figure 3.1). After curing, the 100 mm cubes were cut in half using a diamond saw, creating 100 mm x 100 mm x 49 mm (+/- 1 mm) cuboid specimens, which were stored in a mist room at ≈100% relative humidity and approximately 20°C for 50 days. Laser scabbling is a surface procedure and therefore all experiments were carried out on a 'cast' surface rather than cut and polished surface.

3.3 Laser Beam Parameters

All scabbling tests were carried out using an IPG Photonics YLS-5000 (5 kW) YB-fibre laser. The specimens were subjected to a static, continuous, diverging laser beam with a stand off distance of 340 mm from the focal point.This setup is different from normal laser scabbling applications, where the beam moves along the surface at a predetermined speed. The static beam was chosen to allow better control of the experiments.

In the preliminary studies (Chapter 4) specimens were tested with the vertical laser beam applied to the horizontal face of the specimens. This allowed debris to land back on the heat affected zone and as a result all further testing (Chapters 5, 7 and 7) was done using a horizontal beam (Figure 3.2).

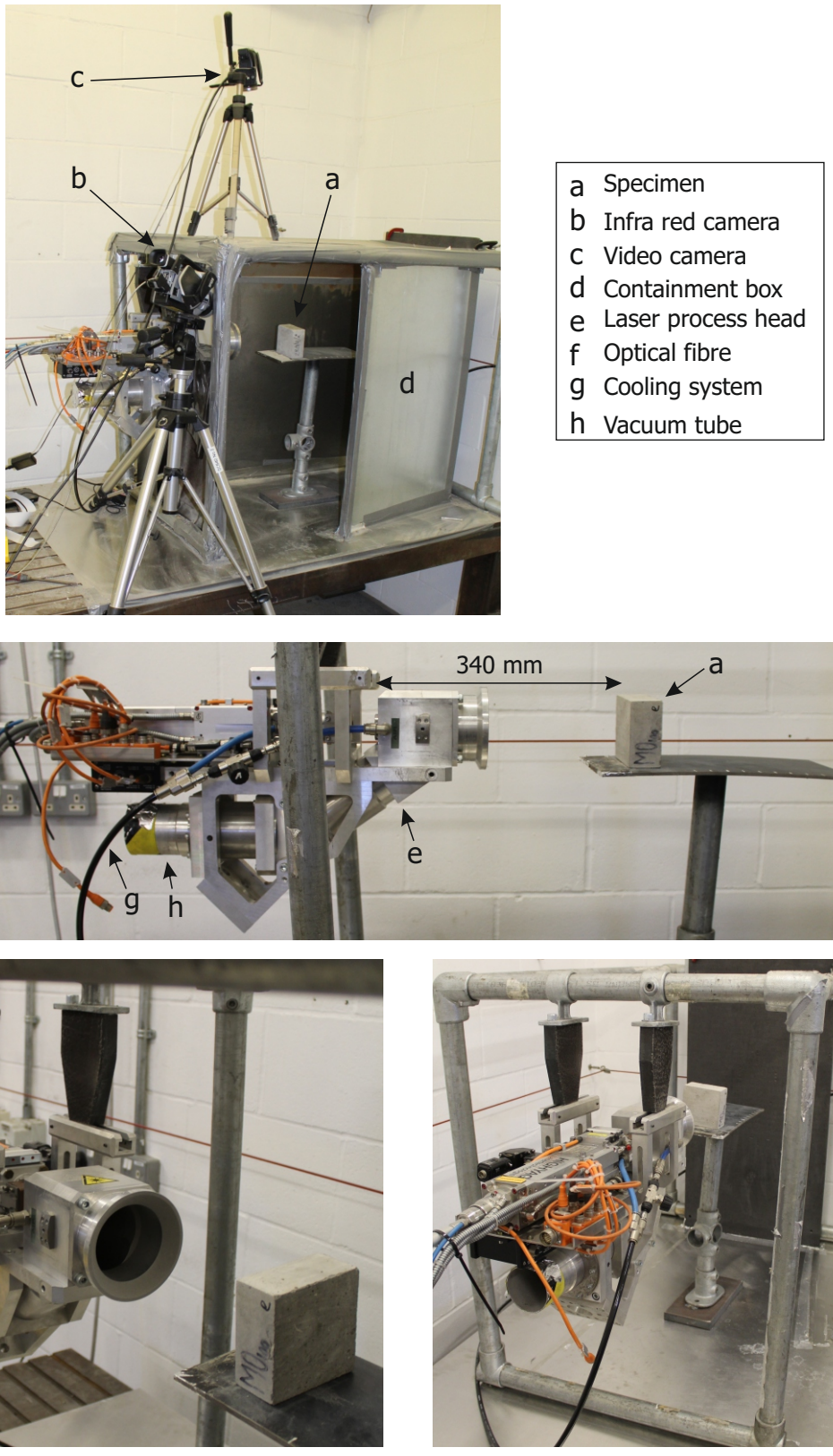

FIGURE 3.2: Experimental setup.

Laser parameters used in this study (4.76 kW power at the workpiece, 60 mm nominal diameter) were similar to those that gained the deepest trough profile in the most recent NDA funded trial at TWI Ltd [16]. A scabbling depth of 22mm was reported after application of laser beam using laser parameters of 5 kW requested power, 60 mm nominal diameter and 100 mm/min scan speed, on limestone concrete. The maximum interaction time for any area of concrete (the centre of the beam) equates to 36 s, which is why 40 s laser interaction was used in the first test series.

3.4 Data Acquisition and Analysis

3.4.1 Specimen properties

The density of the different compositions was determined using BS EN12390-7:2009 [46]. Porosity, moisture content and degree of saturation were subsequently determined using values found in the density tests:

$$\text{Porosity} = 100 * ((m_{sat} - m_{od})/(m_{sat} - m_{sub})),$$

$$\text{Moisture content} = 100 * ((m_t - m_{od})/m_t),$$

$$\text{Degree of saturation} = 100 * ((m_t - m_{od})/(m_{sat} - m_{od}));$$

where m_{sat}, m_{od}, m_{sub} and m_t are saturated, oven-dried, submerged and as received masses respectively.

3.4.2 Volume change

The change in mass due to laser application was determined as the difference in mass of the specimen measured before and after testing. The mass change was converted to volume by dividing the mass by the density determined in accordance with BS EN12390-7:2009 [46]. The volume removal data presented are mean values of the repeats for each interaction time tested with standard deviation error bars, with connecting lines being present as a guide for the eye. The average surface temperature histories, however, are real time temperatures for one or two (depending on the temperature ranges required) tests.

To test the accuracy of this method, the calculated values were compared against values measured using a 3d scanner (reported in Appendix C). A 3D scanner (Geomagic Faro ScanArm 3D scanner) was used to detect the surface profile of scabbled specimens. A plane representing the original specimen surface was made in the Geomagic Studio

software using three points on the surface that were unaffected by scabbling. The volume between the scanned profile and the original specimen surface was calculated using the 'volume to a plane' function in the software; this value has been used as the volume removal due to scabbling. Small discrepancies between the two methods meant the quicker method of mass measurement was opted for in the test series after the preliminary studies (Chapters 5 and 6).

3.4.3 Thermal imaging

The scabbling process in the tests was monitored by recording thermal images of the surface using a FLIR SC 640 infrared camera. The transmission of the infra red window used to protect the camera from debris and the emissivities of specimens was determined experimentally and used in the analysis of infra red data, carried out by using a software package ThermaCam Researcher Professional 2.8 SR-3 (FLIR Systems, Inc). The methods used for determining the IR window transmission and the emissivities of the compositions are described in Appendix D.

The emissivity of the different compositions was calculated using the reference emissivity material method suggested by ISO 18434-1 [47] (Appendix D). Specimens were partially coated in scotch electrical tape (of known emissivity 0.97) and then heated to around 80°C. The temperatures of the taped and untaped areas were compared and the emissivity of the specimens calculated.

In order to record the entire temperature range, at least two experiments were conducted on separate (nominally identical) specimens of each material, using two different camera ranges: 0-550°C and 200-2000°C. All thermal images from the tests were processed to produce average surface temperature histories. Two types of temperature histories were used in the analysis of test data: average and maximum surface temperatures of the heat affected zone (HAZ). The HAZ was defined as the surface area that exceeded 100°C after 1.0 s of interaction time. The time histories of maximum temperature were obtained by identifying the maximum temperature in each frame, regardless of its location in the HAZ. The thermal images were acquired at a time step $\Delta t=(1/30)$ s. Average surface temperature histories were used primarily for analysis in this study, as described in Appendix E. The repeatability of the average surface temperatures has been assessed in Appendix F.

The time histories of maximum surface temperature were only used to assess the reliability of the average surface temperature data. The time histories of average surface temperature, showing the temperature fluctuations due to ejection of fragments (their amplitudes corresponding to size of fragments), were used as key data in characterisation

of the scabbling behaviour of each material. Temperatures and times at the onset of scabbling (T_{os} and t_{os}), pre-scabbling heating rates, as well as heating rates and temperature fluctuations during scabbling were identified from trends in the time histories of average surface temperatures for each test (Figure 3.3a). The frequency and amplitudes of surface temperature fluctuations were used to quantify the frequency of ejections and size of the fragments (Figure 3.3b).

In the first test series, the temperature at the onset of scabbling (T_{os}) for each material was compared with DTA/TGA results of the corresponding composition. Thermal reactions that took place prior to the temperature at the onset of scabbling were identified (Figure 3.3c). Data on water loss from cement phases taken from TGA results found in literature [9] (heat rate of 10°C/min, 50mg sample size, in nitrogen with flow rate 15 ml/min) was used in conjunction with the temperature at the onset of scabbling to indicate the extent of cement phase decomposition at the onset temperatures (Figure 3.3d).

The frequency and amplitudes of surface temperature fluctuations were used to quantify the frequency of ejections and size of the fragments.

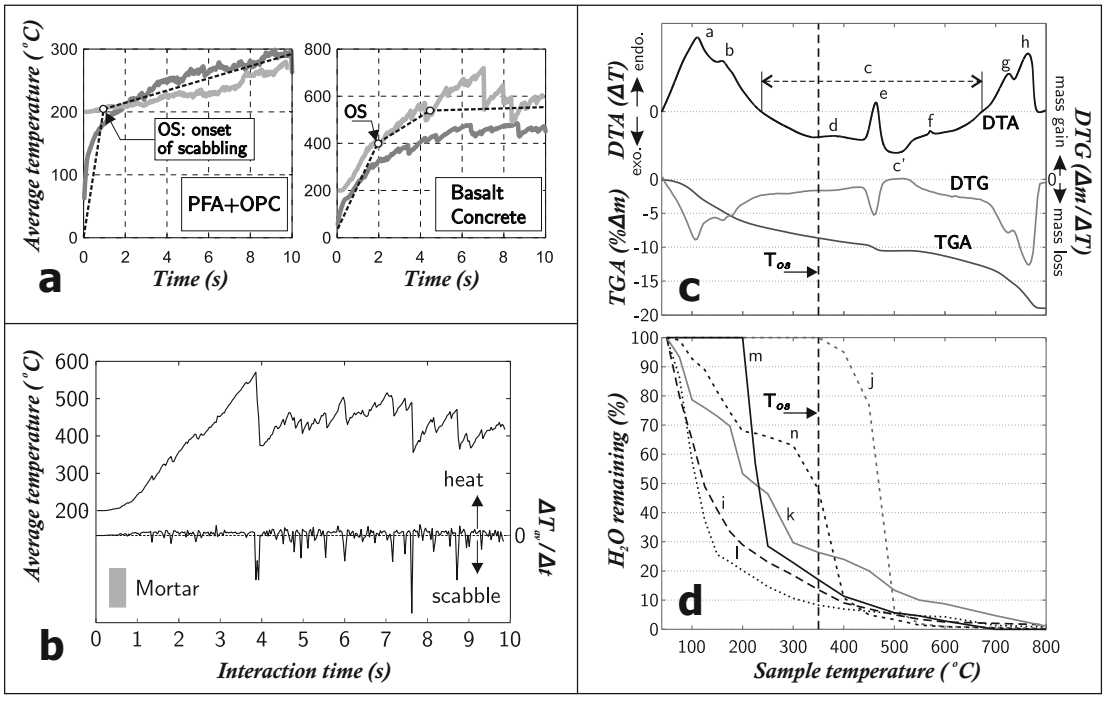

FIGURE 3.3: (a) Examples of how the onset of scabbling was detected, (b) time histories of average temperature and average temperature rate ($\Delta T_{av}/\Delta t$), (c) Graphical representation of differential thermal analysis (DTA), thermo-gravimetric analysis (TGA) and the first differential of the thermo-gravimetric analysis (DTG), and (d) moisture (H_2O) loss from cement phases (taken from TGA data in literature [9]).

3.4.4 High speed camera

In parallel with the infra red camera, a high-speed camera (Phantom V5.1) was used to record the ejection of fragments. The high-speed camera data was used only to provide qualitative information about the scabbling frequency and size of ejected fragments. This was compared with the data obtained in the analysis of the fluctuations in temperature histories. All debris was collected after each test, but it could not be used for analysis of fragment sizes as ejected fragments were further fractured upon impact with the walls of the chamber.

3.4.5 Chemical composition

The chemical composition of tested materials was determined by using X-ray fluorescence (XRF), a Panalytical Minipal 4 EDXRF benchtop was used. To characterise thermal processes taking place in specimens at elevated temperatures differential thermal and thermogravimetric analyses (DTA/TGA) were carried out using a Perkin Elmer Star 8000 simultaneous thermal analyser up to 1500°C in air, with aluminium oxide pan, aluminium oxide reference material and heat rate of 10°C/minute. The samples used in XRF and DTA/TGA were produced by breaking the control specimens, crushing the fragments and grinding the material (using pestle and mortar) until all material passed a 53 μm sieve. Due to heterogeneity of the two concrete mixes, the small samples were not representative for the material as a whole and therefore the DTA/TGA, and XRF results of these compositions should be taken with reserve.

Chapter 4

Preliminary study

The first test series, described in this section, was designed as a preliminary study of a wide range of parameters, in order to establish an experimental methodology, identify the factors that have a major effect on laser scabbling, and potentially obtain data that can be used to explain the mechanisms responsible for laser scabbling of concrete. The factors identified in this programme have been used as the basis for planning the experiments in the following stages of this project. The preliminary studies are published in the Journal of Construction and Building Materials [48].

4.1 Scope and aim of the preliminary study

The aim of this study was to establish an experimental methodology for detecting the mechanisms responsible for laser scabbling of concrete. To achieve this the investigation focussed on the following objectives:

(1) Detect key characteristics of scabbling behaviour. As laser scabbling is an effect of the introduction of heat energy due to laser application, the effects of laser application on surface temperatures will be monitored (the surface temperature at the onset of scabbling, temperature changes during scabbling and relationship between surface temperature variations will be recorded). To assess the extent of laser scabbling, the volume removal due to laser scabbling will be monitored (volume removal rate, size of fragments and frequency of ejections).

(2) Establish relationships between surface temperature, scabbling behaviour and chemical changes in the material.

(3) Determine the differences in scabbling behaviour between different materials (different compositions and initial moisture contents) in order to isolate key factors and/or mechanisms responsible for laser scabbling.

4.2 Specimens and experimental programme

The mix compositions for the specimens tested in this test series are detailed in Table 4.1. The experimental programme and specimen range tested in this series are presented in Table 4.2. Two degrees of saturation were investigated in the test programme: saturated and air dried. Saturated specimens remained at 100% relative humidity until tested, whereas air dried specimens were stored at approximately 40% relative humidity and 20°C from 50 days of age to the time of testing (between 49-65 days of conditioning). Limestone and basalt rock, sourced from the same quarries as the crushed aggregates, was machined to 100 mm x 100 mm x 49 mm (+/- 1 mm) specimens.

TABLE 4.1: Mix compositions (All measurements in mass:binder ratio unless otherwise stated. * AGR mix is included for comparison only; not tested in the experimental programme. ** Basalt and Limestone Concrete refer to concrete mixes using basalt and limestone as coarse aggregates.).

	*AGR	OPC Paste (O)	PFA+OPC Paste (P)	Mortar (M)	**Basalt Concrete (BC)	**Limestone Concrete (LC)
Water	0.42	0.42	0.42	0.42	0.42	0.42
OPC	0.75	1	0.75	0.75	0.75	0.75
PFA	0.25		0.25	0.25	0.25	0.25
Fine agg.	1.84			1.84	1.84	1.84
Plasticiser	0.0045				0.0045	0.0045
10mm agg.	1.05				3.21	3.21
20mm agg.	2.16					
w/c	0.56	0.42	0.56	0.56	0.56	0.56
$\%_{(m)}$ solids	78	0	0	56	78	78
$\%_{(m)}$ cem. paste	22	100	100	44	22	22

TABLE 4.2: Experimental programme and test specimens. Each test using a 40 s interaction time was not repeated, wheras the 10s tests were repeated. (Las. Int.=laser interaction time)

Test/ Spec.	Material Composition	Precon-ditioning	Las. Int. (s)	Age (days)
OS_{40}	OPC	Saturated	40	100
OS_{10a}	Paste	Saturated	10	101
OS_{10b}		Saturated	10	101
OA_{40}		Air dried	40	99
PS_{40}	PFA+OPC	Saturated	40	100
PS_{10a}	Paste	Saturated	10	101
PS_{10b}		Saturated	10	101
PA_{40}		Air dried	40	99
MS_{40}	Mortar	Saturated	40	100
MS_{10a}		Saturated	10	101
MS_{10b}		Saturated	10	101
MA_{40}		Air dried	40	99
BCS_{40}	Basalt	Saturated	40	114
BCS_{10a}	Concrete	Saturated	10	115
BCS_{10b}		Saturated	10	115
BCA_{40}		Air dried	40	113
LCS_{40}	Limestone	Saturated	40	114
LCS_{10a}	Concrete	Saturated	10	115
LCS_{10b}		Saturated	10	115
LCA_{40}		Air dried	40	113
BRA_{40}	Basalt	Air dried	40	-
LRA_{40}	Limestone	Air dried	40	-

4.3 Test results

4.3.1 Vitrification

Figure 4.1 shows the specimens after 40s laser interaction time [10]. It can clearly be seen that all cement and concrete specimens underwent varying degrees of surface removal. Vitrification was identified in basalt rock specimens (BRA) and concrete specimens with basalt coarse aggregate (BCA and BCS). Vitrification was more prominent in saturated than air dried specimens. Slight vitrification can be seen in the mortar of the limestone concrete specimens (LCA and LCS). The saturated OPC paste (OS) showed a large

extent of vitrification (approximately 75% of scabbled area), whereas the saturated PFA+OPC (PS) paste showed only small amounts of vitrification on the periphery of the scabbled area (<10%). The air dried cement pastes (PA and OA) and both mortar specimens (MA and MS) did not show any evidence of vitrification. The experimental set up, whereby ejected debris was able to fall back onto the specimen to receive further laser interaction, increases vitrification. This would be avoided in normal applications where the vacuum would remove any debris.

4.3.2 Volume removal

The trough profiles of the OPC cement paste (OA, OS) were much shallower than those of the PFA+OPC (PS, PA) specimens (Figure 4.1). The air dried PFA+OPC paste (OS) showed a two tiered profile, where the deeper centre had a diameter approximately equal to that of the beam diameter. The trough profiles of the air dried mortar specimen (MA) has a similar depth to the corresponding PFA+OPC (PA) profile, but is wider. The comparison of saturated mortar (MS) and PFA+OPC paste (PS), shows a deeper and narrower profile for the PS (Figure 4.1). The comparison of the concretes show similar profiles for the air dried basalt concrete (BCA) and the two limestone concretes (LCA, LCS), but a shallower profile for saturated basalt concrete (BCS).

Results presented in Figure 4.2 show the volume removal of each of the compositions when exposed to 10s and 40s of 4.76 kW stationary laser beam of 60mm nominal diameter. Two repeats for 10 s laser interaction are included to demonstrate the repeatability which is reasonable. It can clearly be seen that mortar specimens (MA, MS) have the largest volume removal followed by PFA+OPC paste (PA, PS), limestone concrete (LCA, LCS), basalt concrete (BCS, BCA), OPC paste (OA, OS) and finally basalt rock specimen (BRA), while the limestone rock (LRA) experienced no notable volume loss. The large level of vitrification of the saturated OPC paste compared to the PFA+OPC paste is due to the lower volume removal experienced in the OPC paste.

The effect of the two types of preconditioning on volume removal was variable (Figure 4.2). Small variations in volume removal between the saturated and air dried specimens can be seen for the limestone concrete (LCA, LCS), PFA+OPC (PA, PS) and OPC compositions (OA, OS). Saturated specimens of basalt concrete (BCS) and mortar (MS) experienced lower volume removal compared to the corresponding air dried specimens (BCA, MA). In the case of saturated basalt concrete, part of the reduction in total volume removal (in BCS) compared with the air dried basalt concrete (BCA) could be a result of the larger extent of vitrification (Figure 4.1). However, the increased vitrification of the saturated pastes (OS, PS) compared to the air dried pastes (OA, PA),

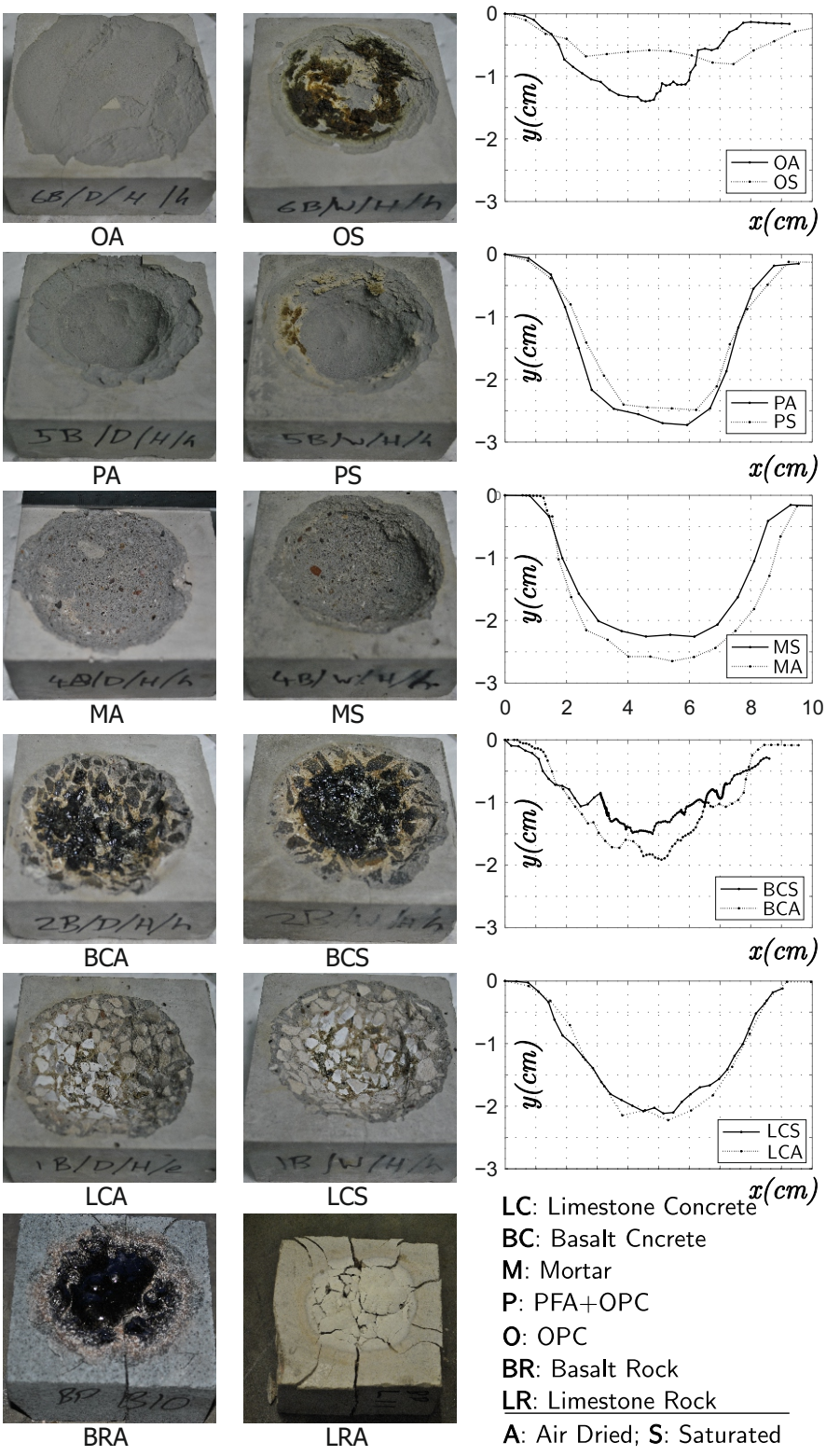

FIGURE 4.1: Photos of specimens of all compositions after 40s of laser interaction and corresponding trough profiles. Centre line trough profiles of specimens of all compositions after 40s of laser interaction [10].

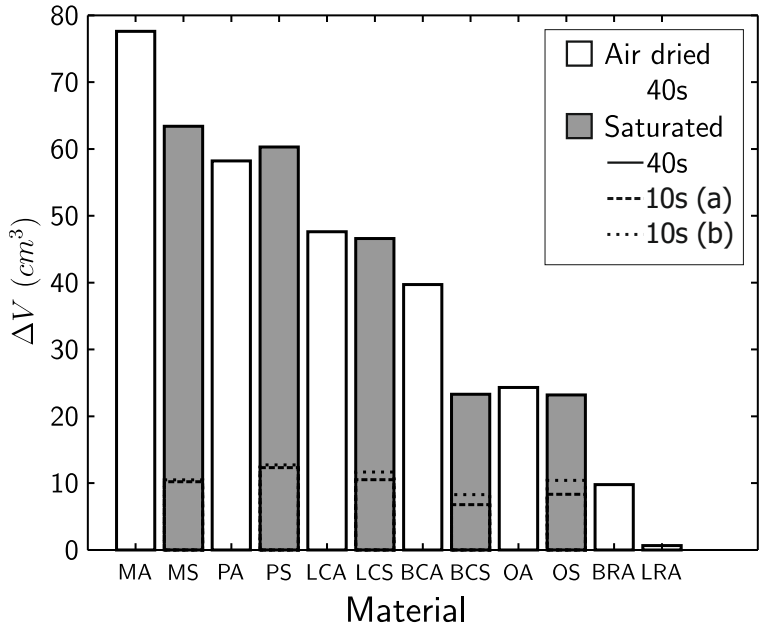

FIGURE 4.2: Volume removal after 10s (2 repeats) and 40s of laser interaction.

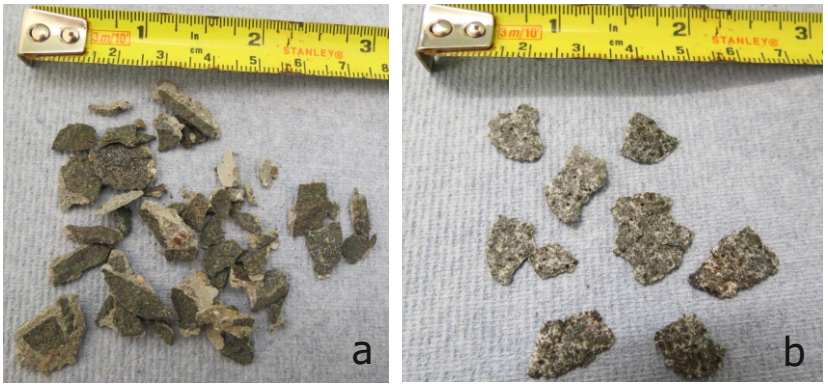

FIGURE 4.3: Debris of (a) air dried basalt concrete, BCA, and (b) basalt rock, BRA, specimens [10].

did not coincide with differences in volume removal between the saturated pastes. The degree of saturation also affected the size of debris, which was smaller for saturated specimens, regardless of composition.

Solid rock specimens showed very different behaviour from that of the corresponding concrete specimens. The limestone rock specimen exhibited very little volume removal, with small fragments ejected in the first few seconds. The end result of laser application on limestoe rock was the remnants of a white powder on the surface, also identified in the limestone concrete specimens (LCA, LCS). The powder is most likely calcium oxide, the product of calcium carbonate decarbonation [3]. The basalt rock specimen showed some scabbling of thin flakes (Figure 4.3b), but by the end of 40s interaction time the specimen had undergone large scale vitrification. Both limestone and basalt rock specimens exposed to 40s laser interaction times underwent extensive fracture after

cooling (Figure 4.1). This was not experienced in the concrete, mortar or cement paste specimens.

4.3.3 Specimen properties

Porosity, moisture content, degree of saturation and density of the different materials (Table 4.3) were determined to identify potential causes for the differences in scabbling behaviour. A greater cement paste content (cement pastes > mortar > concretes as seen in Table 4.1) resulted in higher moisture content, higher porosity and lower density. The higher porosity of PFA+OPC, compared to the OPC paste, is a result of the increase in water/cement ratio, due to the constant water/binder ratio in the two mixes (Table 4.1). Rock specimens had the highest density, lowest porosity and lowest moisture content. Limestone concrete has a slightly lower porosity than the basalt concrete, despite the porosity of limestone rock being an order of magnitude greater than that of the basalt rock. This could be caused by two factors: (i) the limestone rock absorbing more water from the concrete mix and reducing the effective water/cement ratio in the paste, and (ii) the volume of cement paste was larger for the basalt concrete, as the two concrete mixes have the same mass of coarse aggregates, but the density of basalt is higher than that of limestone.

The air dried concrete specimens experienced approximately 30% reduction in moisture content compared to the saturated specimens, the mortar and PFA+OPC specimens

TABLE 4.3: Specimen properties (MC=moisture content, SR=degree of saturation, Em.=emissivity).

Spec.	Porosity %	MC %	SR %	Density kg/cm^3	Em.
OS	38.44	19.76	100	1996	0.941
OA	39.52	14.86	70	1868	
PS	43.49	21.90	96	1902	0.978
PA	42.08	18.16	80	1828	
MS	22.19	9.73	98	2223	0.990
MA	22.44	7.98	77	2186	
BCS	11.60	4.53	98	2518	0.978
BCA	11.27	3.20	71	2500	
LCS	11.07	4.57	99	2385	0.966
LCA	10.76	3.02	67	2395	
BRA	0.20	0.1	-	3006	0.941
LRA	7.37	0.1	-	2465	0.938

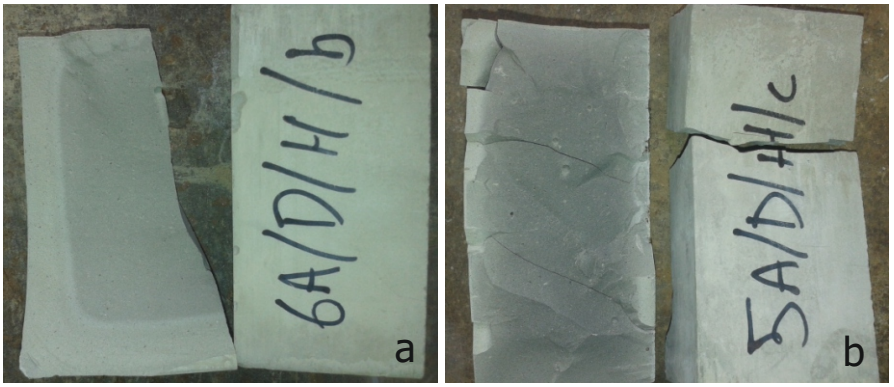

FIGURE 4.4: Cross sections of air dried cement paste specimens; (a) OPC and (b) PFA+OPC.

had approximately a 20% reduction and the OPC cement paste a 25% reduction. This difference in moisture content reduction is illustrated in Figure 4.4 which shows the extent of drying which took place in the air dried cement paste specimens after 50 days of preconditioning, exposed to identical conditions. It can be seen that air dried specimens did not have a uniform moisture content distribution, but a dry surface and a saturated core. The depth of drying was greater in the OPC specimen (8-12mm) compared to the PFA+OPC specimen (1-5mm), indicating lower permeability of the PFA+OPC paste.

4.3.4 Surface temperature histories

Time histories of average surface temperature (Figure 4.5a) show reasonable repeatability in the two (nominally identical) tests in which the thermal images were recorded with two different camera settings. The largest difference recorded for basalt concrete specimens is because this material was heated to temperatures higher than 550°C (Figure 4.5b), which could not be recorded in the first test. Combining the results of the two tests shows that all specimens exhibit bi-linear or tri-linear behaviour (Figure 4.5a), which allows detection of the onset of scabbling (illustrated in Figure 4.5c).

All materials have similar initial heating rates of about about 200°C/s. The onset of scabbling for the two cement pastes can be identified at about 200°C (t_{os}=1s), after which they exhibit an almost constant, reduced heating rate of 10-12°C/s for the rest of the test. The initial heating rate for limestone concrete and mortar is reduced between 200°C and 350°C, a range in which small temperature fluctuations indicate scabbling of small fragments. At about 350°C temperature fluctuations become larger, heating rate drops to 0°C/s, and this temperature can be identified as the onset of scabbling for these two materials. Basalt concrete shows somewhat different, tri-linear behaviour, with an extended range of the initial heating rate to about 400°C, followed by a reduced rate

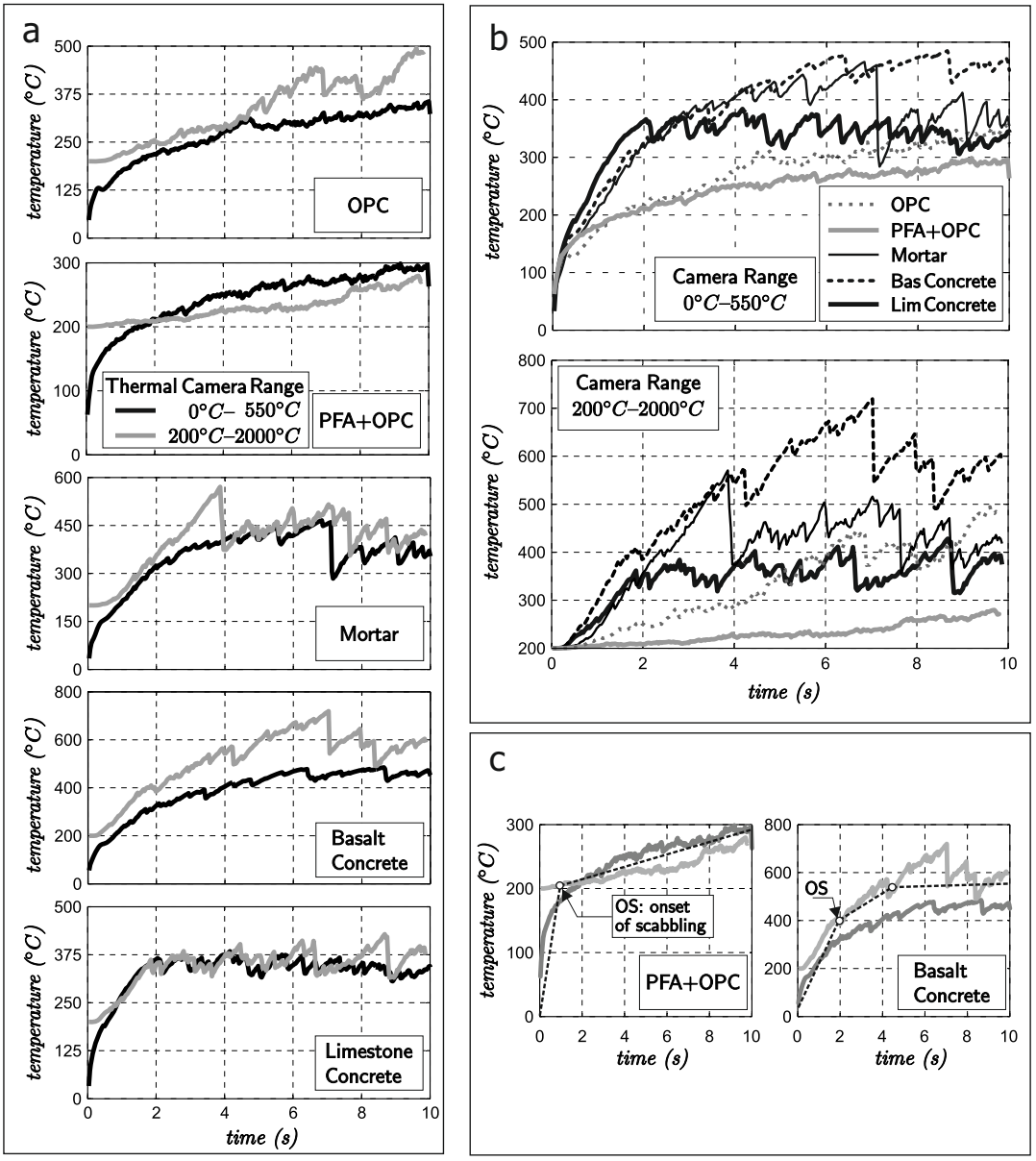

FIGURE 4.5: Time histories of average surface temperatures: (a) histories for each material (saturated) recorded in two tests using two different thermal camera settings, (b) comparison of scabbling behaviour of all materials recorded in the two tests, and (c) detection of phases in scabbling behaviour: onset of scabbling and onset of steady state phase

(about 100°C/s) to 550°C, a range during which there are some significant temperature fluctuations, and then a plateau (0°C/s) characterised with large fluctuations. Hence the onset of scabbling for basalt concrete can be identified at 400°C, and the post scabbling behaviour described as a two-stage process. The values of temperature (T_{os}) and time (t_{os}) at the onset of scabbling for all materials are summarised in Table 4.4a.

4.3.5 Scabbling frequency and fragment sizes

When a fragment is ejected during the scabbling process, the temperature of the exposed surface is lower than that recorded in the preceding frame (Figure 4.6a). Hence scabbling of a larger fragment would result in a larger temperature drop (negative $\Delta T/\Delta t$ rate), followed by a period of temperature increase until the next fragment ejection (positive $\Delta T/\Delta t$ rate).

The frequency and size of negative temperature rate values in the time history of average surface temperatures ($\Delta T/\Delta t$, where Δt=0.033s) was used to identify the frequency and scale of scabbling (Figure 4.6). Here frequency is defined as number of negative

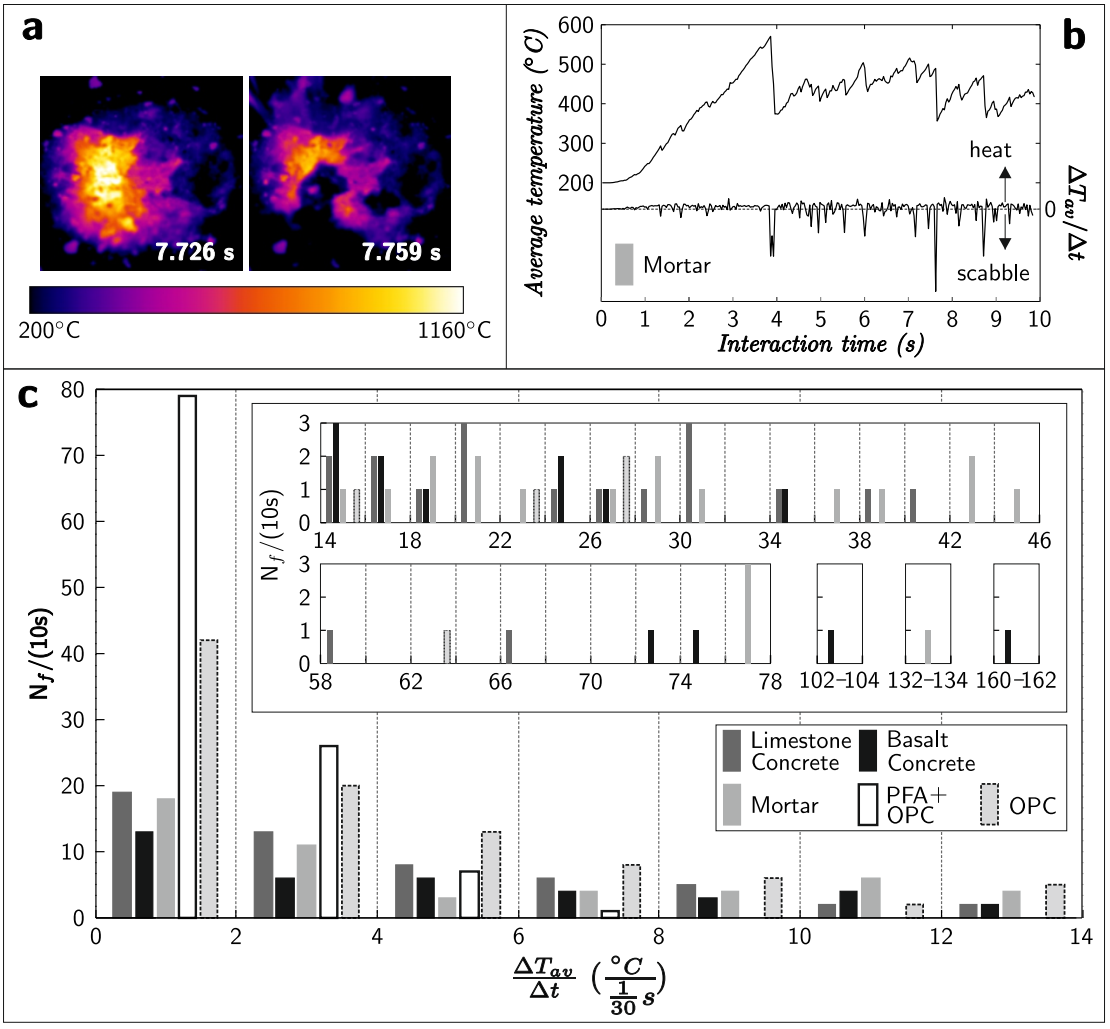

FIGURE 4.6: Frequency distribution of average surface temperature drops (over a 0.033s interval) for each composition. (a) infrared images before and after a large temperature fluctuation for the mortar specimen, (b) time histories of average temperature and average temperature rate ($\Delta T_{av}/\Delta t$) for the mortar specimen, (c) distribution of temperature drops recorded during 10s interaction time for all materials

fluctuations (N_f) of a different magnitude (ΔT, in steps of 2°C), recorded during the laser interaction period (10s, with step Δt=0.033s). The higher frequency of smaller $\Delta T/\Delta t$ fluctuations (0-4°C/Δt) for the cement paste specimens indicates smaller fragment sizes of these compositions when compared to mortar or concrete specimens, which experience a higher frequency of larger temperature fluctuations (above 10°C/Δt). The largest temperature fluctuations (over 100°C/Δt) were recorded for basalt and mortar specimens, suggesting the largest fragment size. The results also show that, compared to the OPC paste, the PFA+OPC scabbling was characterised by a larger number of very small fluctuations ($<$2°C/Δt), as well as a complete absence of larger fluctuations ($>$ 8°C/Δt), suggesting smaller fragment sizes. These results were confirmed by the analysis of thermal and high-speed camera images.

4.3.6 Thermal reactions

The temperatures at the onset of scabbling were combined with DTA/TGA results for all paste, mortar and concrete compositions, to determine which thermal reactions took place before and after the onset of laser scabbling. It should be noted that the heat rate affects the extent to which thermal reactions take place. For example, when higher rates were used the complete thermal decomposition of cement phases occurred at higher temperatures [49, 50]. This means that the results from combining the temperature at the onset of scabbling (heat rates of 175-200°C/s) with DTA/TGA results (heat rate 10°C/min) should be used only qualitatively. This method is suitable for detecting reactions that may take place (although to a lesser extent than that shown by the DTA/TGA) and eliminating thermal reactions that occur at higher temperatures.

DTA/TGA results, presented graphically in Figure 4.7.a-e and presented numerically in Table 4.4, identify the thermal reactions that would take place in concrete/cement specimens prior to reaching the onset of scabbling (values in bold). A large endothermic peak and mass loss (point 'a' in Figure 4.7 and Table 4.4) between 90-120°C, for all compositions, is due to evaporation of free and interlayer water [30, 51–54]. A smaller endothermic peak and mass loss ('b') was identified between 130-190° in all samples as a result of decomposition of cement phases. Less pronounced peaks at 'b' are seen for samples with a lower cement paste content. A doublet in this region ('b') was present only in the PFA+OPC paste. Lilkov [55] and Odler [56], who investigated OPC-PFA mixes, suggested similar peaks to be due to thermal decomposition of calcium monosulfoaluminate, with decomposition of calcium-hydrocarboaluminate as a less likely option [55].

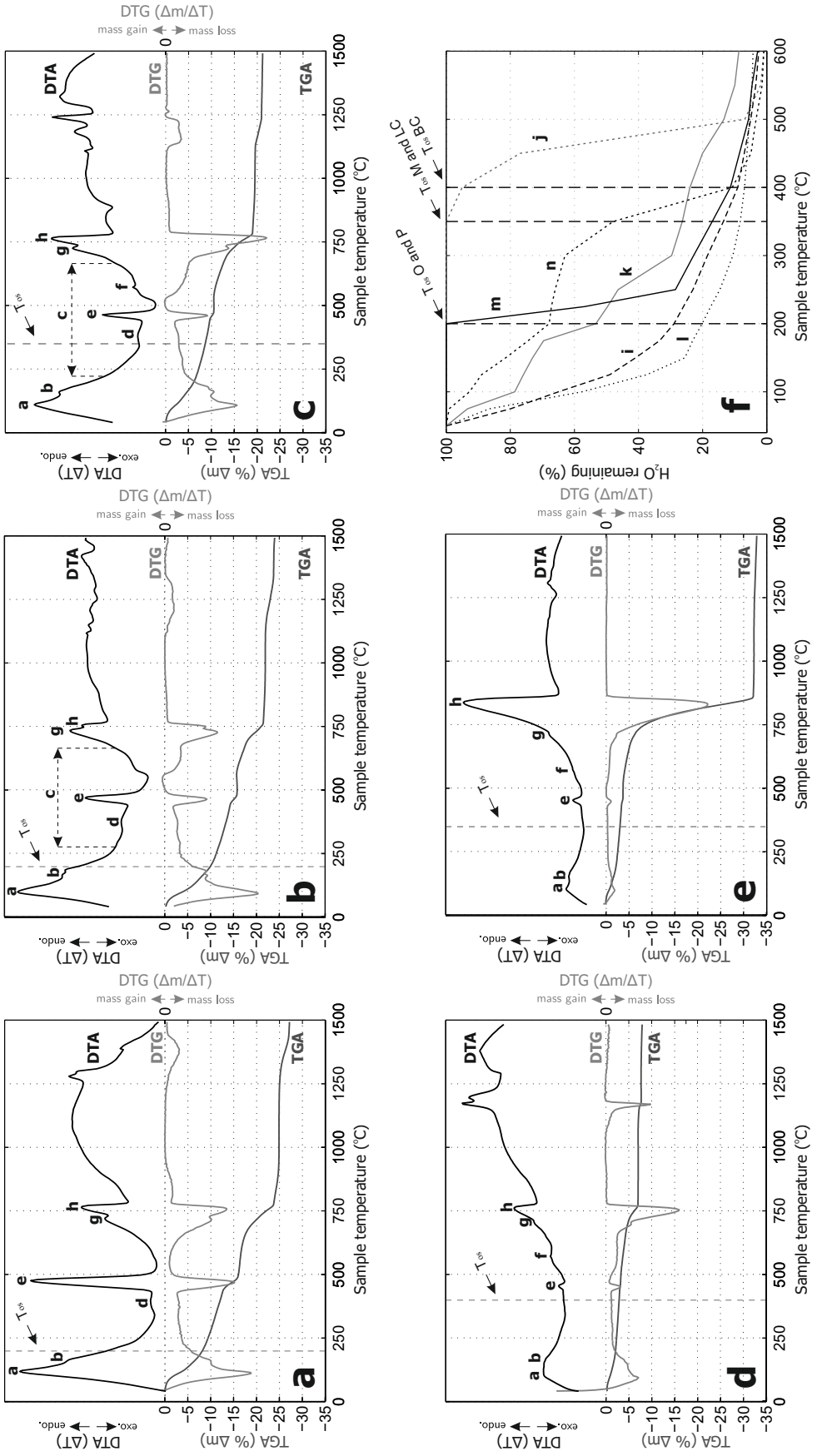

FIGURE 4.7: Graphical representation of relationship between temperature at the onset of scabbling and thermal reactions: differential thermal analysis (DTA), thermo-gravimetric analysis (TGA) and the first derivitive of the thermo-gravimetric analysis (DTG) for (a)OPC paste (b) PFA+OPC paste (c) mortar (d) basalt concrete (e) limestone concrete; thermal reactions 'a-h' are decribed in Table 4.4; and (f) moisture (H_2O) loss from cement phases 'i-n' presented in Table 4.4 (taken from literature [9]).

TABLE 4.4: (A) Temperature, time and heat rate at onset of scabbling, (B) DTA/TGA results: temperature and mass change of thermal reactions in each composition (* due to heterogeneity of concrete mixes, small samples are not representative; results to be taken with reserve.), (C) H_2O loss from cement phases at onset temperatures (TGA results taken from Taylor [9]).

		Material				
		O	P	M	BC	LC
A Onset of scabbling	T_{os} (°C)	200	200	350	400	350
	t_{os} (s)	1	1	2	2	2
	T_{os}/t_{os} (°C/s)	200	200	175	200	175
B Peak	Temperature and mass change of thermal reactions in each composition; values in bold show processes occurring prior to onset of scabbling.					
a Loss of evaporable water	T_{range} (°C)	**40-150**	**40-155**	**40-150**	**40-140**	**40-130**
	T_{peak} (°C)	**117**	**97**	**110**	**107**	**103**
	Δm (%)	**-5.8**	**-7.7**	**-3.9**	***-1.2**	***-1.3**
b Cement phase decomposition	T_{range} (°C)	**150-190**	**155-195**	**150-185**	**140-160**	**130-165**
	T_{peak} (°C)	**160**	**162/185**	**100**	**150**	**150**
	Δm (%)	**-2.0**	**-2.0**	**-1.1**	***-0.3**	***-0.6**
c Exothermic behaviour	T_{range} (°C)		**255**-677	**238**-677		
c' Oxidation of metalic phases	T_{range} (°C)		510-561	496-511		
	Δm (%)		+0.1	+0.01		
d Cement phase decomposition	T_{range} (°C)	340-430	340-440	**340**-435		
	Δm (%)	-1.5	-1.4	-0.5		
e Portlandite dehydroxy -lation	T_{range} (°C)	435-510	440-500	440-490	440-475	435-470
	T_{peak} (°C)	475	472	464	455	453
	Δm (%)	-3.5	-1.6	-0.7	*-0.2	*-0.3
f Quartz transformation	T_{peak} (°C)		550-585	572	572	572
g Vaterite decarbonation	T_{range} (°C)	700-733	675-745	685-738	660-712	645-720
	T_{peak} (°C)	719	733	716	706	713
	Δm (%)	-1.9	-3.2	-2.3	*-0.7	*-7.7
h Calcite decarbonation	T_{range} (°C)	733-785	745-767	738-787	712-777	720-870
	T_{peak} (°C)	765	754	764	760	838
	Δm (%)	-2.8	-0.7	-2.5	*-2.0	*-25.6
C Curve	H_2O loss from cement phases at onset of scabbling temperatures ($T = T_{os}$); taken from Taylor [9] (see Figure 3.3d)					
i C-S-H	Δm (%)	71	71	86	91	86
j Portlandite	Δm (%)	0	0	0	6	0
k Afm phases	Δm (%)	46	46	73	76	73
l Aft phases	Δm (%)	80	80	92	93	92
m Hydrogarnet	Δm (%)	0	0	83	88	83
n Hydrotalcite	Δm (%)	33	33	51	90	51

Mortar and PFA+OPC paste samples show exothermic behaviour ('c') between 238-677°C, with slight mass increases ('c') around 500°C, most likely due to oxidation of metallic impurities present in PFA. The lower range of this reaction is below 350°C, the onset temperature of mortar, but above the onset of the PFA+OPC paste (200°C). The absence of PFA in OPC pastes or its reduced proportion in the mass of concrete samples explains why this process is not observed in the DTA/TGA results for these compositions.

A wide endothermic hump and slight mass loss ('d') due to dehydration of hydration products such as calcium hydrosilicates, calcium hydroaluminates and ettringite [55] was present around 340-440°C in mortar, PFA+OPC and OPC samples. Mortar is the only composition where this reaction occurs below the temperature at the onset of scabbling. An endothermic peak and mass loss ('e') due to portlandite (calcium hydroxide) dehydroxylation [54, 57–60] was observed in all samples between 430-510°C. This reaction occurs below the temperature of the onset of scabbling only for the basalt concrete.

An endothermic peak at 572 °C ('f') occurs with no mass loss due to the α-quartz to β-quartz inversion [17, 30], most prominent in specimens with the largest sand content. The change in crystal structure gives rise to a 0.85% volume expansion [28]. The inversion is present in all specimens except the OPC paste, but only below the temperature of onset for the basalt concrete.

Decarbonation of calcium carbonate phases vaterite ('g') and calcite ('h') at around 650-850°C [17, 30, 52, 54] are identified above the temperature of onset for all samples.

Table 4.4c shows the percentage of water loss in specific cement phases (taken from literature [9]) at the onset of scabbling temperatures for each of the compositions (illustrated in Figure 4.7f). These results have been recorded at a heat rate of 10°C/min. The actual dehydration could be much lower at the onset temperatures (Tos), where the heat rates were of up to 1200°C/min. In the absence of test data recorded at high heat rates, the values shown in the table can only be used as indication that: (i) some dehydration of all cement phases would take place below Tos=400°C (basalt concrete); (ii) in limestone concrete and mortar (Tos=350°C), some dehydration will be expected in all phases with the exception of portlandite ('e' in Figure 4.7a-e or'j' in Figure 4.7f); (iii) dehydration would occur in cement pastes before the onset of scabbling (Tos=200°C) to a lesser extent than that of the mortars and concretes, with hydrogarnet ('m' in Figure 4.7f) and portlandite ('e' in Figure 4.7a-e or'j' in Figure 4.7f) being unaffected. The cement phase decomposition would continue after the onset of scabbling as surface temperatures increase with the increase of interaction time.

4.3.7 Chemical composition

XRF data (Table 4.5) shows that OPC replacement with PFA increases silicon (silica) and aluminium (alumina) content while decreasing calcium (calcium oxide, lime) content following the trend of the constituents. The high silicon content of sand means the mortar has the highest silica content followed by the basalt concrete, limestone concrete and the two cement pastes (PFA+OPC and OPC).

DTA (Table 4.4b) identified the decreased portlandite content of the PFA+OPC compared to the OPC sample. Portlandite is a product of OPC hydration and therefore the OPC paste sample has the greatest content. OPC replacement with PFA reduces portlandite content in two ways, (i) by reducing OPC content and (ii) by using the portlandite as a reactant in the pozzolanic reaction. Calcium carbonate content is higher in the OPC due to carbonation of portlandite during specimen preparation, therefore a lower portlandite content will result in a lower calcium carbonate content [61].

4.4 Discussion of results

4.4.1 Potential mechanisms

The results of explosive spalling studies, summarised by Khoury and Anderberg [5], suggest that explosive spalling is a result of one of two mechanisms. Pore pressure

TABLE 4.5: Results of XRF analysis: chemical composition (% atomic mass) of specimens (LC=limestone concrete, BC=basalt concrete, M=mortar, P=PFA+OPC paste, O=OPC paste) and constituents (Bas.=basalt aggregate, Lime.=Limestone aggregate). XRF equipment used does not identify elements with atomic number lower than 16 (sulfur), therefore values presented do not add up to 100%.

	Constituents					Specimens				
	OPC	PFA	Sand	Bas.	Lime.	O	P	M	BC	LC
Mg	1.32	0.76	0.41	2.72	-	0.26	0.56	0.18	1.76	0.32
Al	2.88	17.31	3.09	10.96	0.16	1.97	4.56	3.34	7.16	3.00
Si	9.82	33.26	51.95	33.24	0.23	7.81	12.17	31.28	32.31	23.07
P	-	-	0.13	0.38	0.04	0.22	0.24	0.22	0.24	0.24
SO	2.55	1.51	0.67	0.64	-	1.43	1.59	1.03	0.91	0.97
K	0.94	4.81	1.56	1.33	-	1.59	1.39	1.20	1.29	1.02
Ca	59.96	2.69	9.17	10.05	72.04	50.02	42.00	19.87	14.29	68.47
Ti	0.23	1.07	0.21	2.03	0.02	0.20	0.42	0.22	1.28	0.28
Fe	2.27	10.71	1.97	13.81	0.04	2.11	4.13	2.26	9.31	2.61

spalling is the process of steam retreating within the concrete where it condenses to form an impermeable saturated zone, which further restricts mass migration causing a build up of pore pressures. Permeability and moisture content are identified as key factors for this mechanism. Thermal stress spalling is caused by high heat rates and the low thermal conductivity of concrete inducing severe thermal gradients and subsequently differential thermal expansions that cause fracture. The two mechanisms work against each other. For example, a higher moisture content is likely to increase pore pressures but reduce thermal stresses due to the cooling effect caused by evaporation and increasing conductivity.

It has been reported that a higher silica content increases the susceptibility of a concrete to explosively spall during fire conditions due to the crystal transformation that takes place in quartz at around 572°C [8, 44] (reaction 'f' in Figure 4.7 and Table 4.4b). This study and early studies on laser scabbling of concrete [2, 3, 16] found that the siliceous aggregates tested (granite and basalt) hindered the scabbling process, but limestone aggregate concrete scabbled successfully. All specimens in this study underwent scabbling at temperatures below that of the quartz inversion, suggesting that this reaction is not necessary for scabbling to take place.

Thermal reactions detected in DTA/TGA results are likely to affect scabbling in a number of ways. Thermal decomposition reactions, such as cement phase dehydration and calcium carbonate decarbonation, will release gases increasing pore pressures and also weaken the structure, reducing the stresses required for scabbling to take place. On the other hand, thermal decompositions and thermal mismatch between constituents will increase permeability, allowing dissipation of pore pressures, reducing scabbling.

The fact that mortar and PFA+OPC paste showed similar volume removals, while concrete specimens (with much reduced cement paste content) experienced lower volume removals and rock specimens almost no scabbling, suggests that the mechanism responsible for laser scabbling takes place within the cement matrix, where addition of fine aggregates introduces a secondary effect which increases debris size and slightly enhances volume removal.

The temperatures at the onset of scabbling vary between compositions. The two cement pastes have similar values (200°C), with the mortar and concrete specimens having higher onset temperatures ($350 - 400$°C). The results show that a higher cement paste content allows scabbling to take place at lower temperatures, further supporting the suggestion that the scabbling process takes place within the cement matrix. This could be due to more free, interlayer and chemically combined water being available to aid pore pressure spalling, and therefore a lower surface temperature is required to produce sufficient pressures.

All cement paste and concrete compositions underwent some degree of volume removal suggesting the stochastic behaviour reported in previous studies [2, 3, 16] was not detected in this study. Concrete age was not reported in previous studies, hence the young age of specimens used in this study (99-114 days) may be a determining factor.

4.4.2 Scabbling of cement pastes: effect of PFA replacement

Results presented in this study show that the use of PFA as a cement replacement material enhances the volume removal of hardened cement paste during laser scabbling, suggesting a mortar or concrete without PFA (not tested here) would experience lower volume removals than a mortar or concrete with PFA replacement.

The PFA+OPC paste had a larger water/cement ratio when compared to OPC paste (Table 4.1). Water not chemically combined during hydration remains as free water which forms capillary pores [28], resulting in higher moisture content and higher porosity [62]. This increase in porosity is the cause of the lower density of the PFA+OPC cement paste and potentially of a reduced strength at the age of testing (99-114 days).

While PFA replacement increases total porosity [62], it has been reported that the larger proportion of foil like C-S-H produced by the pozzolanic reaction reduces pore connectivity and as a result permeability is reduced [9]. The reduced drying experienced by the air dried PFA+OPC specimen when compared to the air dried OPC specimen seen in Figure 4.4 supports this.

Use of PFA changes the chemical composition of the system causing different hydrates and phases to be formed. This in turn affects the thermal and mechanical properties of the material. The DTA/TGA results show a doublet between 155-195°C in the PFA+OPC sample, while the OPC specimen displays a plateau. This difference is most likely due to the different phases and/or different proportions of similar phases. This could also be the reason for the exothermic hump 'c' in DTA results (Table 4.4b), which is more prominent in the PFA+OPC than the OPC sample.

The pozzolanic reaction and reduction in OPC content in the PFA+OPC paste will reduce the portlandite content compared to the OPC paste. This can be seen by the reduced mass loss due to portlandite dehydroxylation ('e') in the TGA (Table 4.4b). It can be seen from Table 4.4.c that C-S-H ('i') decomposition begins prior to the temperature at the onset of scabbling (200°C), whereas portlandite ('e') does not undergo any dehydroxylation until around 400°C. The replacement of portlandite with C-S-H that occurs during the pozzolanic reaction and the higher moisture content will mean more

water is released at the onset temperature in the PFA+OPC paste (7.7% mass loss due to loss of free water for the PFA+OPC paste compared to 5.8% for the OPC paste).

Dehydration of cement phases will cause weakening of the cement matrix and increase pore pressures due to release of water vapour. The low temperatures at the onset of scabbling of cement pastes indicate that scabbling is driven by the evaporation of free and interlayer water and the release of chemically combined water during cement phase decomposition. The higher content of both free water and C-S-H in the PFA+OPC paste, compared to those for OPC, results in greater loss of evaporable water and cement phase decomposition detected in the TGA. Combined with the probable reduced permeability of PFA+OPC paste, this suggests that pore pressure spalling is the mechanism responsible for the larger volume removal of the PFA+OPC paste compared with the OPC paste. Assuming that the two cement pastes have similar thermal gradients, as they are both homogeneous materials, the large difference in volume removal indicates that thermal stress incompatibilities are not the cause of scabbling in cement pastes.

4.4.3 Scabbling of mortar and concrete: effect of aggregate addition

The mortar experienced slightly higher volume removal (Figure 4.2) and larger debris sizes (inferred from the larger temperature fluctuations in Figure 4.6) compared to the PFA+OPC cement paste. The increased size of debris suggests that the sand particles act as reinforcement causing larger fragments to be removed. This can also be inferred from the deeper and narrower shape of the trough profiles of PFA+OPC paste compared to the wider and shallower profile of the mortar (Figure 4.1), which indicates that the reinforcement effect of the sand caused more material removal outside of the hotter central area of the laser beam.

Concrete specimens experienced less volume removal than the mortars. The reinforcement effect would essentially be the same, but the larger size of coarse aggregates makes them more difficult to dislodge than sand particles. In the absence of coarse aggregates (i.e. mortars) a fracture plane can form in the weaker cement paste surrounding the fine aggregate particles (Figure 4.8.a), avoiding the need for the higher strength sand

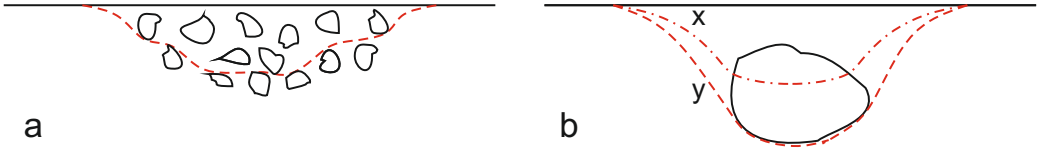

FIGURE 4.8: Comparison between fracture planes formed in (a) mortars and (b) concretes.

particles to be fractured. When coarse aggregates are included in the material (i.e. concretes), material ejection will take place if either the coarse aggregate is fractured (fracture plane x in Figure 4.8.b), as a result of thermal degradation, or a deeper fracture plane is formed beneath the larger coarse aggregates (y in Figure 4.8.b). Both mechanisms require extra energy and longer interaction times.

An alternative cause for variation in volume removal could be the difference in thermal properties of the specimens. The high porosity of cement paste results in lower thermal conductivity [30]. Therefore by replacing part of the cement paste content with aggregate, the overall thermal conductivity will be increased allowing for greater heat transfer and less severe thermal gradients. While mortar will have a high proportion of conductive silica sand, the larger cement paste content (Table 4.1) will mean the mortar will have a lower thermal conductivity than the concretes.

Inclusion of aggregates reduces the content of cement paste greatly, increasing the rock content from 0% for the cement pastes, to 56% for the mortar and 78% for the concretes, which in turn causes vast reductions in porosity, moisture content (Table 4.3) and permeability. As a result there is less free, interlayer and chemically combined water available within the specimens to be released and aid pore pressure spalling. Combining this with the greater resistance to material removal due to the 'reinforcing effect', it leads to greater temperatures being required for the onset of scabbling to occur.

The temperature of the onset of scabbling for the basalt concrete is higher than that for the limestone concrete. The higher porosity of the limestone rock (Table 4.3) may enable pore pressures to build within the aggregate pieces, reducing the reinforcement effect and increasing scabbling. The temperature of the onset for mortar is similar to that of limestone concrete, as the increased proportion of cement paste may have a similar effect as the high porosity of the limestone rock (compared to the basalt). The temperature at the onset of scabbling of cement pastes is even lower. Considering the larger proportion of cement phases (and therefore available water) in the cement pastes and the the lack of reinforcing particles, lower temperatures would increase pore pressures and reduce resistance sufficiently to trigger scabbling.

Hilton [3, 16] found that limestone concrete scabbled effectively but concretes with basalt or granite aggregates vitrified, preventing scabbling. In this study basalt concrete experienced a lower volume removal than limestone concrete, with some vitrification (Figure 4.1), but the volume of material removal from basalt concrete was still far greater than what has been reported in the literature [2, 3]. The mineralogical composition of the basalt was not analysed in this study (nor reported in the earlier studies [2, 3]), but since the melting temperatures of all minerals in basalts (olivine, pyroxene and plagioclase) are above 1000°C [63], and the scabbling of concrete occurred at a lower temperature

range (400-700°C), it can be assumed that the difference in volume removal is due to different cement paste characteristics of the two materials. Increased vitrification noticed in the earlier study indicates a lower rate of scabbling. Small amounts of vitrification in the mortar surrounding the aggregates can be seen in the limestone concrete specimens (LCA, LCS in Figure 4.1) along with the whitening of the exposed limestone aggregate, the cause of which could be decarbonation of the calcium carbonate, similar to that seen in the limestone rock specimen (LRA). Blair [17] suggested the release of carbon dioxide during decarbonation of calcium carbonate in limestone aggregates was responsible for increasing pore pressures and subsequently inducing fracture. Scabbling takes place at temperatures below that of calcium carbonate (vaterite or calcite) decarbonation for all specimens tested in this study, suggesting that calcium carbonate decarbonation is not the primary mechanism responsible for laser scabbling.

4.4.4 Scabbling of rock

The rock specimens had much lower volume removals compared to the concrete specimens with corresponding aggregates. Limestone rock experienced almost no volume removal whereas basalt rock underwent small scale scabbling. Basalt rock is more heterogeneous than limestone rock and as a result more differential expansion between constituents could be the cause for the greater degree of volume removal.

Basalt rock debris was thinner than basalt concrete debris (Figure 4.3) suggesting different mechanisms were responsible for the scabbling of each specimen. Vitrification of basalt rock debris showed that higher temperatures were reached in trials on basalt rock than those on basalt concrete, again indicating that different mechanisms were causing the scabbling.

The lower volume removal of limestone rock compared to the basalt rock suggests the greater porosity of the limestone (Table 4.3) was not a determining factor of scabbling success.

4.4.5 Scabbling of cement pastes, mortar and concretes: effect of saturation

The laser scabbling process took place in both saturated and air dried specimens. The volume removal was similar in some cases, and different in others, with no clear trend. According to EN 1992-1-2:2004 [39] and Copier [34], a moisture content of 3% and above (by mass) is required for explosive spalling to occur. In this study all tested specimens had a moisture content above 3% (Table 4.3).

The two cement pastes (PFA+OPC and OPC) and the limestone concrete showed little difference in volume removal for the two moisture contents. Larger volume removals were recorded for air dried than saturated specimens of basalt concrete (70%) and mortar (20%). The expected increase of scabbling with the increase in degree of saturation was not observed for any of the investigated compositions. This suggests that the increase of pore pressures due to evaporation of free water was not a critical mechanism driving the scabbling.

It has been identified that vitrification was more prominent in saturated specimens compared to air dried specimens. At this stage of the investigation the reason for this was unknown and requires further investigation.

It should be noted that the saturated cement pastes produced smaller debris sizes than the air dried cement pastes. Smaller debris sizes for similar volume removal suggests a higher frequency of smaller fragment ejections in saturated specimens. This indicated that the higher moisture content would increase the effect of pore pressure spalling, whereas the materials with lower moisture content would require longer interaction times, allowing more time for thermal stresses to develop, and resulting in a combined mechanism of pore pressure and stress gradient spalling.

4.5 Conclusions

The aim of this study was to detect key mechanisms that control laser scabbling of concrete. The first step was to establish an experimental procedure for characterizing the scabbling behaviour of concrete. This procedure was then applied to a wide range of specimens with different material characteristics, that may have a significant effect on the process.

4.5.1 Key characteristics of scabbling behaviour

The results of this study show that the scabbling behaviour of each material can be characterized by time histories of average surface temperature of the exposed area of the specimens. These temperature time histories provide data on (i) time and temperature at the onset of scabbling, (ii) rate of temperature changes during scabbling, and (iii) temperature fluctuations during scabbling. The temperature at the onset of scabbling can be related to results of DTA/TGA and used to detect which thermal reactions are critical to the initiation of scabbling. Temperature fluctuations during scabbling (their amplitudes and frequency), combined with mass loss measurements, provide data on

the effectiveness of the process (mass removal), as well as size of debris, which indicates a particular mechanism. The results showed distinct differences between these characteristics of scabbling behaviour for different materials.

4.5.2 Effects of material composition on scabbling

The results show that the laser scabbling process is significantly affected by the material composition, with clear differences between cement pastes with different binder mixes; between cement pastes, mortars and concretes; and between concretes with the two different types of aggregates used in this study.

The use of 25% OPC replacement with PFA has a major effect on scabbling in cement pastes, in this case increasing the volume removal by almost 3 times for 40s interaction time, regardless of the degree of saturation of the material. This could be a result of the increased amount of water (free and bound) and/or reduced permeability of PFA+OPC paste, both contributing to an increase in pore pressures, as well as changes in the chemical composition of the cement phases, which would contribute to both the release of chemically bound water and a reduction in tensile strength of the material.

The temperature at the onset of scabbling is higher for compositions with lower cement paste content. This could be a result of two mechanisms: (i) by introducing aggregates and reducing the content of cement paste (per unit volume), a higher temperature is required to release sufficient water from cement phase decomposition to produce sufficient pore pressures, and (ii) aggregates act as reinforcement, increasing the tensile strength of the material and postponing scabbling.

This study suggests that thermo-mechanical effects of aggregates are more prominent than their thermo-chemical effects. The results show that calcium carbonate decarbonation and the α-quartz to β-quartz inversion are not the primary mechanisms responsible for laser scabbling, as these processes occur at temperatures that are higher than the temperatures at the onset of scabbling for all materials. In basalt concrete the melting of aggregates creates a vitrified layer that prevents further scabbling; whereas the limestone concrete continues to scabble over a longer period, maintaining a nearly constant surface temperature. The largest volume removal in mortar specimens can be explained by the combined action of the two main mechanisms: larger pore pressures compared to concrete (due to larger cement paste content), and higher scabbling temperatures (due to increased tensile strength), resulting in less frequent scabbling, but much larger fragments when compared to the cement pastes.

These results suggest that laser scabbling is generally driven by processes that take place in the cement paste, with aggregates (fine and coarse) influencing the process by increasing tensile strength and thermal conductivity, which postpones the onset and increases the size of fragments during scabbling.

4.5.3 Effect of degree of saturation

While only a narrow range of degrees of saturation were tested in this test series, the results showed that the size of fragments was generally smaller, and vitrification was more prominent, for saturated specimens compared to air dried specimens, but the higher degree of saturation did not lead to increased volume removal. This indicates that the difference in free water content, for the two degrees of saturation tested here, does affect the process, but is not a key factor controlling its effectiveness. The effect of the degree of saturation will be investigated further in Chapters 6 and 7.

Chapter 5

The effect of concrete composition on laser scabbling

This chapter describes the second test series: an investigation into the effect of concrete composition on laser scabbling [64]. The experimental methodology established in the preliminary study (Chapter 4) was applied in tests on hardened cement pastes, mortars and concretes to determine the scabbling behaviour for different compositions.

5.1 Scope and aim of the research

The aim of this test series was to determine the relationship between laser interaction time, volume removal and surface temperatures for different compositions in order to identify the effect of concrete composition on laser scabbling behaviour: rate of volume removal, temperature at the onset of scabbling, surface temperature during scabbling, fragment ejection frequency and fragment sizes (Figure 5.1). These observations were then used to form conclusions on the mechanisms responsible for laser scabbling.

The compositions selected for investigation in this study (Table 5.1) were designed to isolate factors of the laser scabbling process identified in the first test series (Chapter 4).

The reasons for choosing the compositions tested in this series are as follows:

(I). Cement pastes with different w/b ratios were investigated to determine the effects of permeability and strength on laser scabbling;

(II). Concretes, mortars and hardened cement pastes with two different binder compositions (OPC and PFA+OPC) were analysed to determine the effect of PFA replacement in different materials;

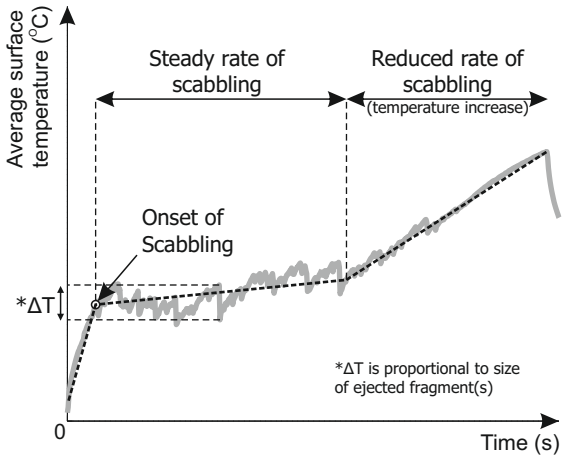

FIGURE 5.1: Example average surface temperature graph, showing trilinear behaviour with different stages of scabbling behaviour highlighted.

(III). Limestone and basalt aggregate concretes using OPC and PFA+OPC binders were tested to characterise the effect of different aggregate/binder combinations;

(IV). Concretes with two coarse aggregate gradings (10 mm and 20 mm) were tested to determine the effect of aggregate size;

(V). A wide range of interaction times were applied to each composition to determine the relationship between laser interaction time and volume removal for each composition (only 10 s and 40 s interaction times were used in the first series).

5.2 Specimens and experimental programme

The material compositions used in this study are given in Table 5.2. The laser interaction times, number of repeats and age of specimens at the time of testing are given in Table 5.3 for the pastes and mortars and Tables 5.4 and 5.5 for the concretes. Hardened cement paste samples were cast 3 months after the mortar and concrete specimens and as a result underwent less ageing/curing. Tests in this series were conducted with the

TABLE 5.1: The scopes of the 1st series (Chapter 4) and the 2nd series (presented here).

	1st series	2nd series
w/b ratio of cement pastes	0.42	0.32 & 0.42
Binder of concretes and mortars ($OPC\%/PFA\%$)	75/25	75/25 & 100/0
Coarse aggregate size	10 mm	10 mm & 20 mm
Laser interaction time intervals	10 s, 40 s	5 s, 10 s, 20 s, 30 s, 40 s, 50 s, 70 s

TABLE 5.2: Mix compositions (all measurements in mass:binder ratio unless otherwise stated. * AGR mix is included for comparison only; not tested in the experimental programme. ** Basalt and Limestone Concrete refer to concrete mixes using basalt and limestone as coarse aggregates.)

	Water	OPC	PFA	Fine agg.	Plast -iciser	10mm agg.	20mm agg.
*AGR	0.42	0.75	0.25	1.84	0.0045	1.05	2.16
OPC Paste							
O_{42}	0.42	1	0				
O_{32}	0.32	1	0				
PFA+OPC Paste							
P_{42}	0.42	0.75	0.25				
P_{32}	0.32	0.75	0.25				
Mortar							
Mp	0.42	0.75	0.25	1.84			
Mo	0.42	1	0	1.84			
****Bas. Concrete**							
Bp	0.42	0.75	0.25	1.84	0.0045	3.21	
Bo	0.42	1	0	1.84	0.0045	3.21	
****Lime. Concrete**							
Lp	0.42	0.75	0.25	1.84	0.0045	3.21	
Lo	0.42	1	0	1.84	0.0045	3.21	

laser beam applied to a vertical concrete surface to avoid debris falling back onto the specimen during testing (in situ the vacuum used to remove the debris would eliminate this problem). This differs from the first series (Chapter 4) where the laser was applied to a horizontal concrete face.

TABLE 5.3: Experimental programme and test specimens: Mortars and cement pastes.

Test/ Spec.	Material Composition	No. of Repeats	Int. time (s)	Age (days)
$O_{42}10$	OPC	2	10	77
$O_{42}20$	Paste	2	20	77
$O_{42}30$	($w/b = 0.42$)	2	30	77
$O_{42}40$		2	40	71-72
$O_{42}70$		2	70	77
$O_{32}10$	OPC	2	10	77
$O_{32}20$	Paste	2	20	77
$O_{32}30$	($w/b = 0.32$)	2	30	77
$O_{32}40$		2	40	71-72
$P_{42}10$	PFA+OPC	2	10	77
$P_{42}20$	Paste	2	20	77
$P_{42}30$	($w/b = 0.42$)	2	30	77
$P_{42}40$		2	40	72
$P_{42}70$		2	70	77
$P_{32}10$	PFA+OPC	2	10	77
$P_{32}20$	Paste	2	20	77
$P_{32}30$	($w/b = 0.32$)	2	30	77
$P_{32}40$		2	40	71-73
Mo5	Mortar	3	5	234
Mo10	(OPC	3	10	232
Mo20	binder)	3	20	234
Mo30		3	30	234
Mo40		3	40	232-234
Mo50		2	50	238
Mo70		1	70	238
Mp5	Mortar	3	5	234
Mp10	(PFA+OPC	3	10	232
Mp20	binder)	3	20	234
Mp30		3	30	234
Mp40		3	40	232-234
Mp50		2	50	238
Mp70		1	70	238

TABLE 5.4: Experimental programme and test specimens: Basalt concrete and rock specimens

Test/ Spec.	Material Composition	No. of Repeats	Int. time (s)	Age (days)
$Bo_{10}5$	Basalt	3	5	220
$Bo_{10}10$	Concrete	3	10	220
$Bo_{10}20$	10 mm agg.	3	20	220
$Bo_{10}30$	(OPC	3	30	220
$Bo_{10}40$	binder)	3	40	219-220
$Bo_{20}5$	Basalt	3	5	221
$Bo_{20}10$	Concrete	3	10	221
$Bo_{20}20$	20 mm agg.	3	20	221
$Bo_{20}30$	(OPC	3	30	221
$Bo_{20}40$	binder)	4	40	219-224
$Bp_{10}5$	Basalt	3	5	220
$Bp_{10}10$	Concrete	3	10	220
$Bp_{10}20$	10 mm agg.	3	20	220
$Bp_{10}30$	(PFA+OPC	3	30	220
$Bp_{10}40$	binder)	3	40	218-220
$Bp_{20}5$	Basalt	2	5	221
$Bp_{20}10$	Concrete	3	10	221
$Bp_{20}20$	20 mm agg.	3	20	221
$Bp_{20}30$	(PFA+OPC	3	30	221
$Bp_{20}40$	binder)	5	40	219-224
BR40	Basalt	2	40	-

TABLE 5.5: Experimental programme and test specimens: Limestone concrete and rock specimens

Test/ Spec.	Material Composition	No. of Repeats	Int. time (s)	Age (days)
$Lo_{10}5$	Limestone	3	5	207
$Lo_{10}10$	Concrete	3	10	207
$Lo_{10}20$	10 mm agg.	3	20	207
$Lo_{10}30$	(OPC	3	30	207
$Lo_{10}40$	binder)	5	40	204-211
$Lo_{20}5$	Limestone	3	5	207
$Lo_{20}10$	Concrete	3	10	207
$Lo_{20}20$	20 mm agg.	3	20	207
$Lo_{20}30$	(OPC	4	30	207
$Lo_{20}40$	binder)	3	40	205-207
$Lp_{10}5$	Limestone	3	5	207
$Lp_{10}10$	Concrete	3	10	207
$Lp_{10}20$	10 mm agg.	3	20	207
$Lp_{10}30$	(PFA+OPC	3	30	207
$Lp_{10}40$	binder)	3	40	204-210
$Lp_{20}5$	Limestone	3	5	207
$Lp_{20}10$	Concrete	3	10	207
$Lp_{20}20$	20 mm agg.	3	20	207
$Lp_{20}30$	(PFA+OPC	3	30	207
$Lp_{20}40$	binder)	3	40	205-210
LR40	Limestone	3	40	-

5.2.1 Specimen properties

The specimen properties detailed in Table 5.6, porosity, moisture content, density and compressive strength, follow the trend expected from evidence in the literature [28]. Hardened cement paste with a higher water/binder ratio and/or use of 25% PFA replacement result in a weaker, more porous, less dense structure with a higher moisture content. Concretes and mortars using 25% PFA replacement show a similar trend but to a lesser extent as the properties of the aggregates become more dominant.

TABLE 5.6: Specimen properties; porosity, moisture content (MC), density and compressive strength (Fc). All values are the mean of three repeats.

Spec.	Porosity (%)	MC (%)	Density (kg/m^3)	F_c (MPa)
Lp	12.4	5.0	2417	70
Lp_{20}				68
Lo	11.0	4.5	2439	72
Lo_{20}				67
Bp	14.2	5.7	2478	79
Bp_{20}				75
Bo	12.2	4.7	2555	82
Bo_{20}				86
Mp	21.1	9.3	2252	61
Mo	20.2	9.0	2250	61
P_{42}	40.4	21.1	1908	54
P_{32}	33.0	16.4	2002	74
O_{42}	38.5	19.3	1993	64
O_{32}	31.9	15.2	2093	86

5.3 Volume removal and average surface temperature-time history results

5.3.1 Hardened cement pastes

Volume removal results for all cement pastes tested in this study are shown in Figure 5.2a. For the same w/b ratio the PFA+OPC paste experienced larger volume removals due to laser scabbling than that of the OPC pastes. The reduction in w/b ratio from 0.42 to 0.32 resulted in a dramatic increase in the OPC paste (25-69%, depending on interaction time), and marginally affected the volume removal of the PFA+OPC paste (4-13%).

The time histories of average surface temperature in Figure 5.2b show an almost identical temperature at the onset of scabbling (≈220 °C), followed by different scabbling behaviour for the four compositions. After the onset of scabbling, the average surface temperature of the two PFA+OPC pastes continue to increase with a heat rate of around 2.5 °C/s with very small fluctuations (up to a maximum of around 20 °C). The OPC_{32} paste shows similar behaviour to the PFA+OPC pastes but with a higher constant heat rate of around 5 °C/s and slightly larger temperature fluctuations (up to a maximum of around 40 °C). The average surface temperature is controlled by scabbling activity: as fragments are removed the average surface temperature is reduced by exposure of cooler areas. The low and steady rate of temperature increase in the two PFA+OPC pastes and OPC_{32} is a result of volume removal (Figure 5.2).

The OPC_{42} paste shows very different behaviour after the onset of scabbling: average surface temperature increases to 700 °C in the first 37 s (at a higher rate of about 13 °C/s), with larger (up to 120 °C), but less frequent, temperature fluctuations, as a result of lower rates of volume removal.

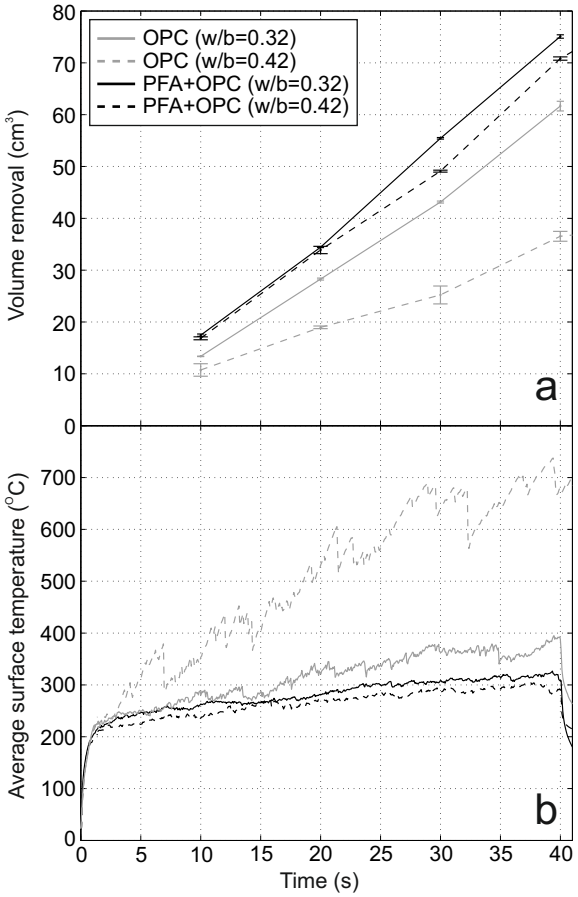

FIGURE 5.2: Cement pastes; (a) volume removal and (b) time histories of average surface temperatures for OPC_{42}, OPC_{32} $(PFA+OPC)_{42}$ and $(PFA+OPC)_{32}$ paste compositions.

The two cement pastes with w/b = 0.42 were also exposed to 70 s interaction time (Figure 5.3). The results for the $(PFA+OPC)_{42}$ show no change in behaviour after 40 s, either in the rate of volume removal or in the rate of increase of average surface temperature. The rate of volume removal for the OPC_{42} drops dramatically between 40 s and 70 s, from 0.9 cm^3/s to 0.3 cm^3/s. The surface temperature reaches about 700 °C at 40 s, and then oscillates around this value. The vitrification of the OPC_{42} starts at about 40 s and develops further, covering almost 50% of the surface after 70 s (Figures 5.4b and d). $(PFA+OPC)_{42}$ pastes show no vitrification for either 40 s or 70 s exposure (Figures 5.4a and c).

5.3.2 Mortars

Figure 5.3 shows volume removals and average surface temperature histories of the mortar and cement pastes with the same w/b of 0.42. The effect of different binder compositions is much less pronounced in the mortars than in the cement pastes. The OPC_{42} mortar did not experience a drop in rate of volume removal observed in the

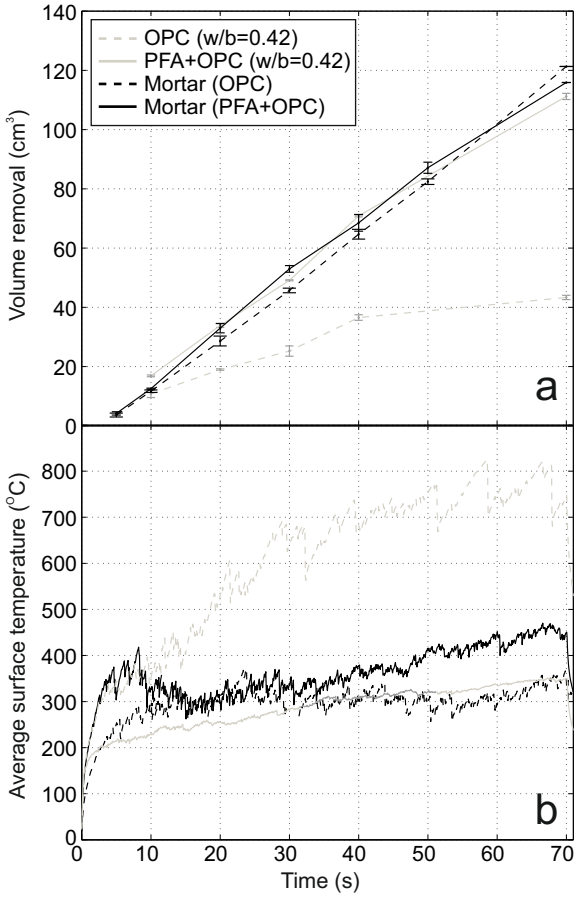

FIGURE 5.3: Mortars and cement pastes (w/b=0.42); (a) volume removal and (b) time histories of average surface temperatures for the OPC_{42} and $(PFA+OPC)_{42}$ paste compositions, and the OPC_{42} and $(PFA+OPC)_{42}$ mortar compositions.

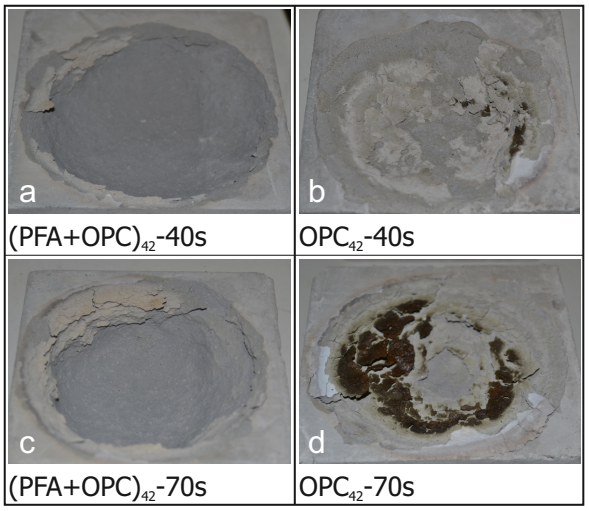

FIGURE 5.4: Photos of cement paste specimens after laser exposure, highlighting the extent of vitrification in OPC_{42} samples: (a) $(PFA+OPC)_{42}$ after 40 s exposure, (b) OPC_{42} after 40 s exposure, (c) $(PFA+OPC)_{42}$ after 70 s exposure, (d) OPC_{42} after 70 s exposure.

OPC_{42} paste (Figure 5.3a). The two mortars show very similar volume removal rates to the $(PFA+OPC)_{42}$ paste.

The two mortars show different surface temperatures in the initial stage. Both the initial heating rate and the temperature at the onset of scabbling are higher for the mortar with PFA+OPC binder (150 °C/s and 300 °C) than those for the mortar with OPC binder (110 °C/s and 240 °C). To illustrate the repeatability of this result, Figure 5.5 shows all average surface temperatures recorded for the mortar specimens: one recording in the 0–550 °C temperature range for each composition (Figure 5.5b), and two recordings in the 200–2000 °C temperature range for each composition (Figure 5.5a). All three OPC_{42} mortar average surface temperature-time histories show a lower initial heat rate compared to the data for the $(PFA+OPC)_{42}$ mortars. The results in Figure 5.3b show that after the onset of scabbling, the two mortars show almost identical average surface temperatures and temperature fluctuations until 35 s (≈300°C) , after which the temperature of PFA+OPC mortar increases at a rate of around 4 °C (to 450 °C after 70 s), whereas the surface temperature of the OPC mortar remains nearly constant at 300 °C.

Figure 5.3 shows that these differences in surface temperatures are reflected in the volume removal: the volume removal in the PFA+OPC mortar is larger at the beginning, and this difference remains almost constant for exposure intervals of up to 30 s, when it starts reducing, and it is finally reversed for longer exposures (between 50 s and 70 s), with a slightly larger volume removed from the OPC mortar after 70 s exposure as seen in Figure 5.3a. (It should be noted however, that there are no repeats of the tests using 70 s interaction time on the mortars).

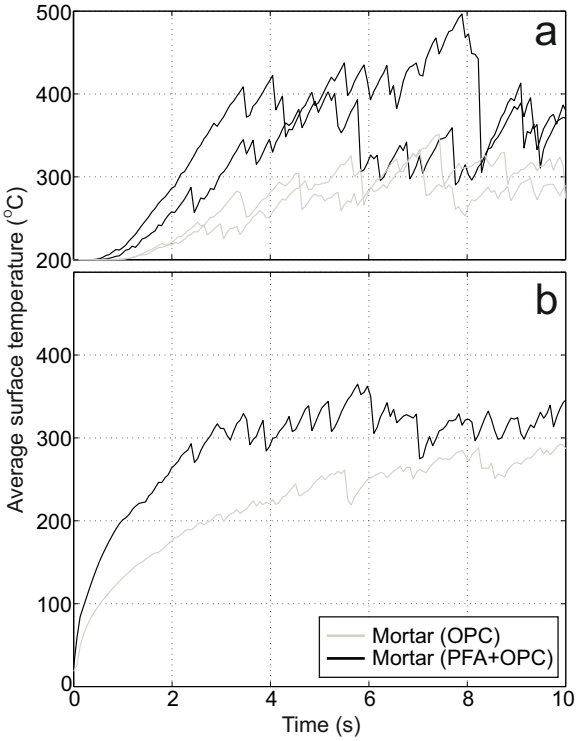

FIGURE 5.5: Mortars; time histories of average surface temperatures for the OPC_{42} and $(PFA+OPC)_{42}$ mortar specimens: camera ranges (a) 200–2000 °C and (b) 0–550 °C. Both temperature ranges are included to highlight the repeatability of the lower initial heat rate of the OPC_{42}-mortar compared to the $(PFA+OPC)_{42}$-mortar.

5.3.3 Concretes

All concretes had lower volume removal than the mortars (Figure 5.6), with basalt concretes consistently showing lower volume removal than limestone concretes, and concretes with $(PFA+OPC)_{42}$ binder showing 5-10% higher volume removal than concretes with OPC_{42} binder. All concretes undergo similar initial heat rates of around 100 °C/s until the onset of scabbling, which differs at around 400-510 °C for the basalt concretes and 300 °C for the limestone concretes. Following this are the scabbling phases, which are very different for the concretes with different aggregates.

The surface temperature plot for the PFA+OPC basalt concrete shows scabbling activity until 15 s exposure with large fluctuations around an average surface temperature of 500 °C and volume removal rate of 1.7 cm^3/s, reaching a total of 20 cm^3 (Figure 5.6). After this point the scabbling stops, the volume removal rate drops to zero, the average surface temperature increases to 1000 °C and the concrete vitrifies (Figure 5.7). It should be noted that the volume removal graphs (Figure 5.6a) were constructed using data recorded at 10 s and 20 s. Hence the 15 s exposure is the point at which the rate of volume removal drops to zero was defined from the surface temperature graph (Figure 5.6b), which shows almost no temperature fluctuations after 15 s (a similar

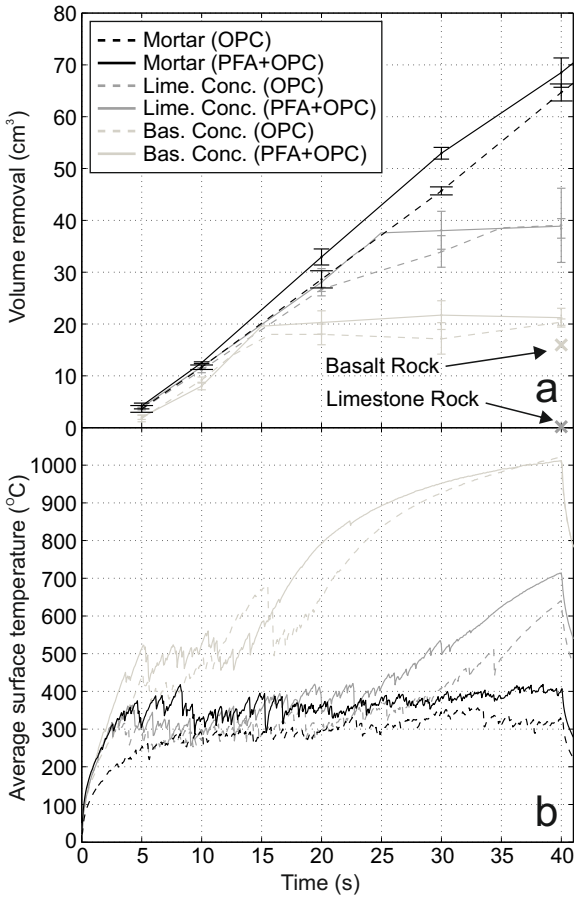

FIGURE 5.6: Concretes (10mm coarse aggregates) and mortars; (a) volume removal and (b) time histories of average surface temperatures for mortar, limestone concrete and basalt concrete compositions using both OPC_{42} and $(PFA+OPC)_{42}$ binder compositions. Concretes made with 10 mm coarse aggregates.

practice has been used for the limestone concrete). The OPC basalt concrete shows similar overall behaviour, but with a lower temperature at the onset of scabbling (400 °C), and about 5-10% lower volume removal.

The scabbling in the two limestone concretes shows two distinct phases. The first is the phase of temperature fluctuations around an almost constant temperature of 300 °C (Figure 5.6b) and constant volume removal rates (Figure 5.6a), which are different for the two limestone concretes: 1.7 cm^3/s, extending to 25 s exposure, for the PFA+OPC concrete; and 1.3 cm^3/s, up to 28 s exposure, for the OPC concrete. This is followed by short intervals (of about 5 s) during which both limestone concretes exhibit reduced volume removal rates and small temperature fluctuations around an increasing average surface temperature (up to 30–35 s of exposure); and finally by 5-10s of zero volume removal rate and monotonic increase of surface temperature to 650-700°C (between 30 and 40s exposure time). The higher temperatures and higher volume removal were recorded for the PFA+OPC limestone concrete specimens (Figure 5.6).

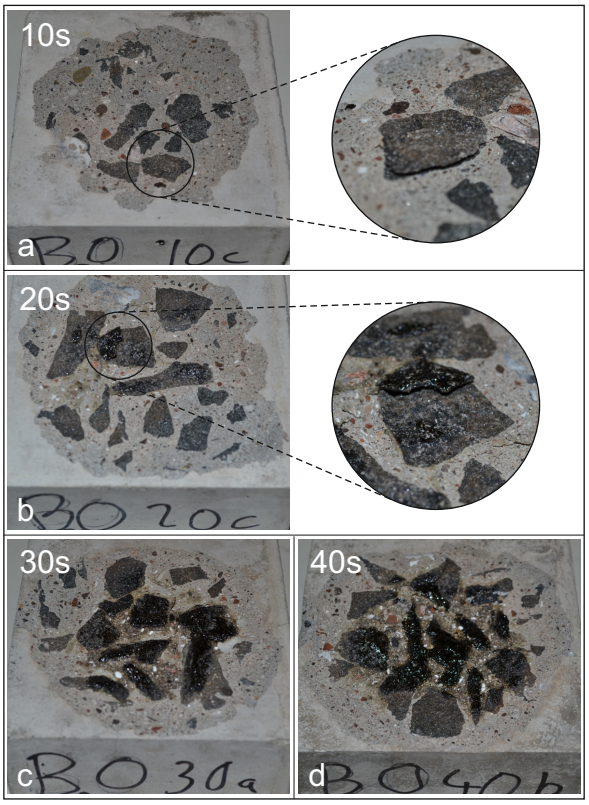

FIGURE 5.7: Photos after laser trials showing vitrification in basalt concrete (Bo_{20}) at different interaction times.

Figures 5.8 and 5.9 show the effect of aggregate size (10 mm vs 20 mm) on scabbling behaviour of concretes (volume removal graphs and surface temperature histories), using both OPC and PFA+OPC, $w/b = 0.42$. The effect of coarse aggregate size on volume removal was minimal with error margins overlapping in most cases. Regardless of type and size of aggregates, the concretes with OPC binder showed lower volume removal than those with PFA+OPC after 30s exposure, but this difference was reduced after 40s. The largest difference of 30% (reduced to 10% at 40 s) was recorded for basalt concretes.

Concretes using larger aggregate sizes (Figure 5.9 for basalt and Figure 5.8 for limestone) generally had slightly higher surface temperatures, but similar temperature fluctuation magnitudes.

5.3.4 Rock specimens

The tests on rock specimens show significant differences between basalt (Figure 5.9) and limestone (Figure 5.8). The limestone rock showed no evidence of scabbling in the average surface temperature-time history, and a much lower heat rate compared to all other compositions. The average surface temperature increases up to 470 °C after 25 s

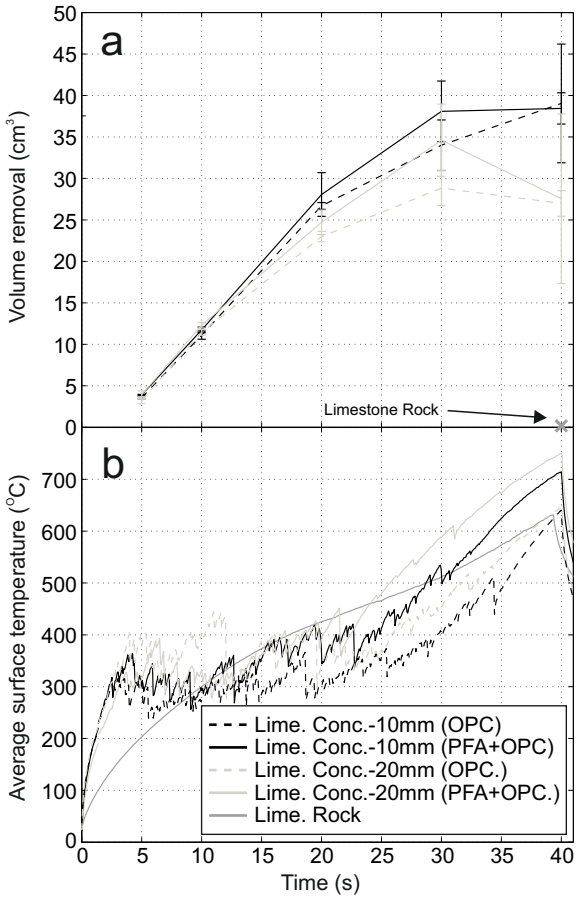

FIGURE 5.8: Limestone concretes and limestone rock; (a) volume removal and (b) time histories of average surface temperatures for the limestone concrete compositions using 10 mm and 20 mm coarse aggregates and OPC_{42} and $(PFA+OPC)_{42}$ binder compositions. 40 s laser interaction on limestone rock specimens also included.

at a decreasing rate. After this, the heating rate starts increasing until the temperature reaches 640 °C at the end of the 40 s exposure interval (Figure 5.8b). Throughout this range there are no temperature fluctuations, which indicates that no scabbling occurred, and is also reflected in the negligible volume removal (Figure 5.8a). The inspection of the specimens at the end of the 40 s exposure showed a thin layer of white powder at the surface.

Basalt rock specimens (Figure 5.9b) underwent an initial heat rate comparable to the concretes of around 110 °C/s, before reaching an onset of scabbling at around 450 °C, after 2 s. The material underwent scabbling (Figure 5.9a) accompanied by a parabolic temperature increase, with fluctuations up to 800 °C (20s), followed by monotonic increase to 1000 °C, when the heating rate approached zero. At this point the surface was fully vitrified. The total volume removal after 40 s was 16 cm^3, or about 80% of the volume removal in basalt concrete.

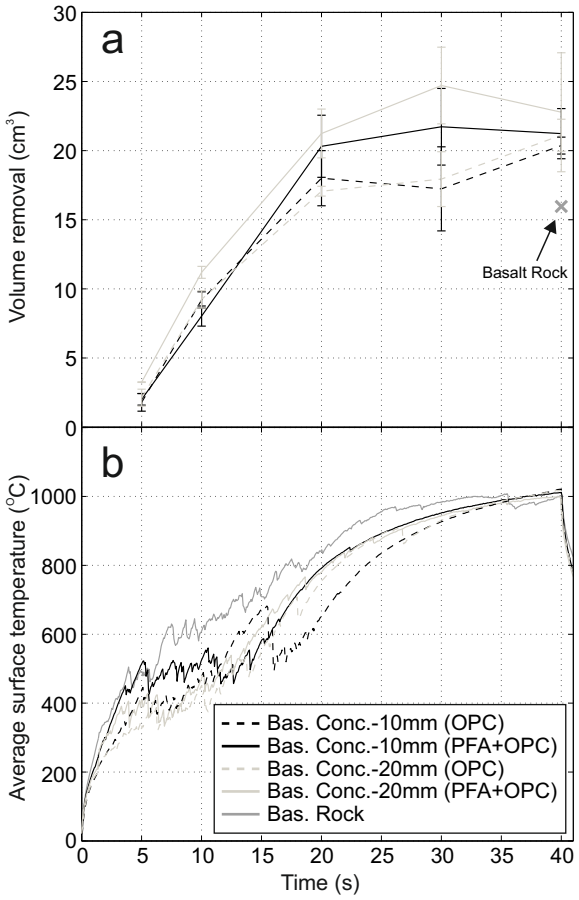

FIGURE 5.9: Basalt concretes and basalt rock; (a) volume removal and (b) time histories of average surface temperatures for the basalt concrete compositions using 10 mm and 20 mm coarse aggregates and the OPC_{42} and $(PFA+OPC)_{42}$ binder compositions. 40 s laser interaction on basalt rock specimens also included.

5.4 DTA/TGA results

DTA, TGA and differential thermogravitimetric analysis (DTG) for the mortar and cement paste specimens are presented in Figure 5.10. The comparison between the DTA/TGA results of the control specimens (solid lines) and scabbled debris (dotted lines) have been used to identify the thermal reactions that have taken place during laser scabbling. The corresponding labels (a–h) are described in Table 5.7.

The main difference in the debris compared to the control samples, identified in all compositions, is the reduction in mass loss due to free and interlayer moisture loss ('a') and a reduction in the definition of the peaks for the DTA for decomposition of cement phases ('b' and 'd').

Unidentified DTA peaks before 100°C (* in Figures 5.10-b, d and f) are present for the PFA+OPC pastes and PFA+OPC mortar compositions. As there is no mass change coinciding with the peaks (not seen in the TGA/DTG), it can be assumed that a structural

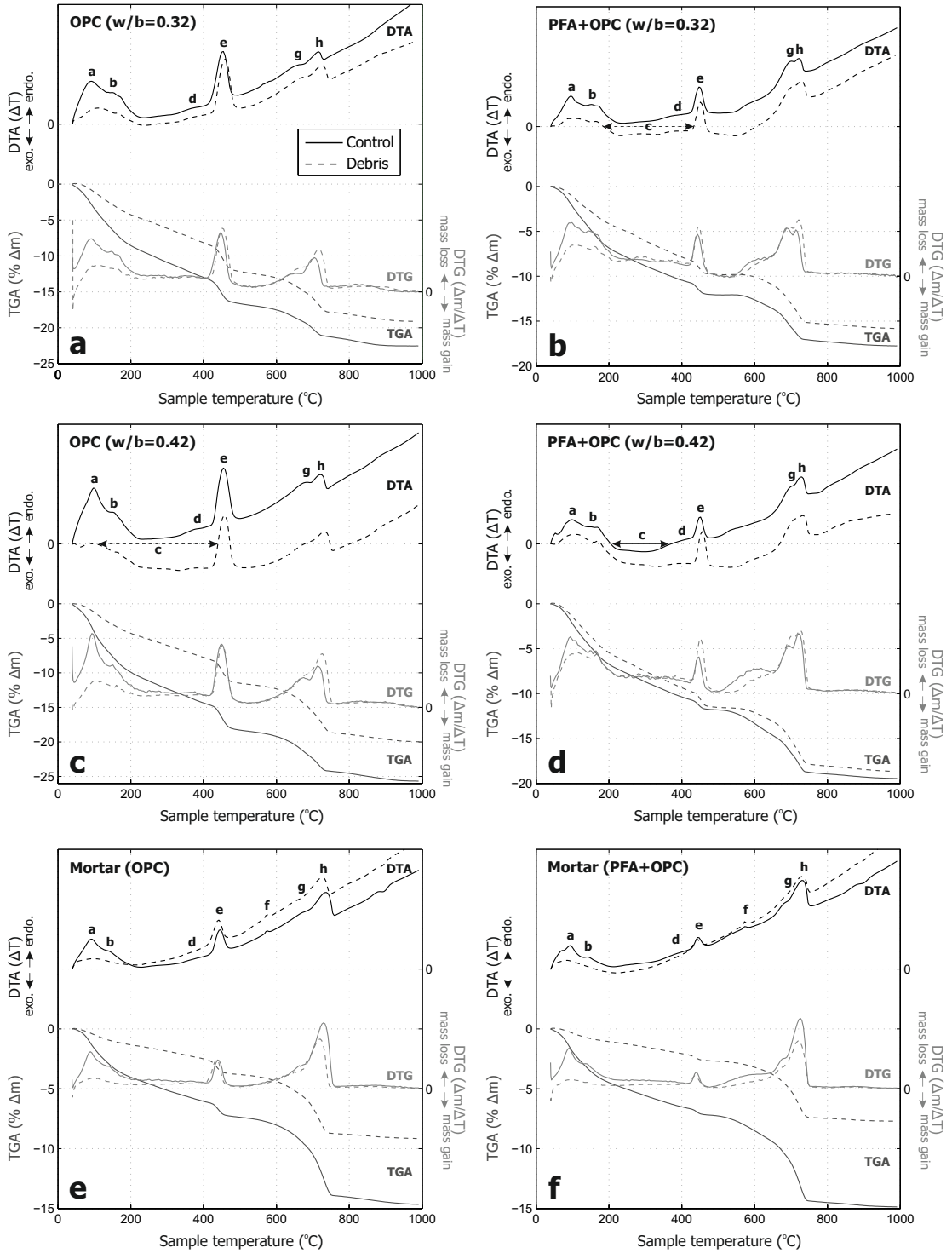

FIGURE 5.10: Graphical representation of DTA, TGA and DTG results of control specimens (solid lines) and debris (dotted lines) samples for (a) OPC $w/b = 0.32$, (b) PFA+OPC $w/b = 0.32$, (c) OPC $w/b = 0.42$, (d) PFA+OPC $w/b = 0.42$, (e) OPC mortar and (e) PFA+OPC mortar.

TABLE 5.7: Thermal reactions highlighted in Figure 5.10, discussed in greater detail in Chapter 4.

	DTA/TGA representation	Thermal reaction responsible
'a'	Endothermic peak, mass loss	Evaporation of free and interlayer water. [30, 52–54]
'b'	Endothermic peak, mass loss	Decomposition of cement phases (calcium monosulfo–aluminate [56] or calcium-hydrocarboaluminate [55]).
'c'	Exothermic behaviour	Potentially, oxidation of metallic impurities in PFA.
'd'	Endothermic hump, slight mass loss	Dehydration of hydration products (calcium hydro-, silicates, calcium hydroaluminates and ettringite) [55].
'e'	Endothermic peak, mass loss	Calcium hydroxide (portlandite) dehydroxylation [54, 57–60].
'f'	Endothermic peak, no mass loss	The reversible α-quartz to β-quartz inversion [17, 30], which involves a volume increase of 0.85% [28].
'g'	Endothermic peak, mass loss	Decarbonation of calcium carbonate (vaterite).
'h'	Endothermic peak, mass loss	Decarbonation of calcium carbonate (calcite) [17, 30, 52, 54].
*****	Endothermic peak, no mass loss	Unidentified structural change.

change, rather than a chemical change (decomposition for example), is responsible.

An endothermic peak is identified in the DTA of the mortars at 573°C ('f' in Figures 5.10-e and f), which is not seen in the cement pastes. The peak refers to the α-quartz to β-quartz inversion which involves a volume increase of 0.85% [28], which will induce thermal stresses in the mortar and could potentially contribute to scabbling; some authors suggest this plays a role in explosive spalling [5]. The quartz inversion is reversible, and as a result would be present in both the debris and the control sample results despite the temperature reached during the scabbling of the debris.

It has been reported that dehydroxylation of calcium hydroxide is a reversible process [57]. The calcium oxide which remains after dehydroxylation can undergo rehydration, but it has been found that the rehydrated calcium hydroxide has a DTA peak at a slightly lower temperature compared to the original crystal [57]. The peaks in DTG graphs for the mortars due to calcium hydroxide ('e' in Figures 5.10-e and f) are of similar intensity for both debris and control samples, but peaks for the debris occurs at slightly lower temperatures, suggesting some dehydroxylation may have taken place. It should be

noted that any calcium carbonate decarbonation is likely to affect the calcium hydroxide detected in the debris, as calcium oxide produced by calcium carbonate decarbonation will readily rehydrate in the presence of water to form calcium hydroxide [17].

The results suggest there is generally more calcium hydroxide ('e') and calcium carbonate ('h' and 'g') in the debris of the cement pastes than the control samples (Figures 5.10-a to d). This could be due to carbonation that took place after the experiments (accelerated in the dried debris compared to the saturated control specimens), rather than being a result of the scabbling itself. In mortars (Figures 5.10-e and f), on the other hand, smaller DTG peaks and smaller mass losses can be seen for the calcium carbonate ('h' and 'g') in the debris compared to the control samples. This suggests some decarbonation of calcium carbonate took place during scabbling of the mortars. The difference between calcium carbonate peaks in the DTG for the debris and control samples is larger for the PFA+OPC mortar than the OPC mortar. This coincides with the higher average surface temperatures and temperatures at the onset of scabbling for the PFA+OPC mortar compared to the OPC mortar. It should be noted that the temperatures reported in Section 5.3 are based on the average surface temperature, which meant that the temperatures within the heat affected zone will vary.

The extent of the difference between the debris and control samples of the pastes generally follows the average surface temperature results: the TGA results of debris of compositions that experienced higher temperatures had lower mass loss than the control samples. A lower w/b ratio and cement pastes including PFA showed smaller differences between debris and control sample DTA/TGA results.

The DTA/TGA/DTG results suggest that cement pastes and mortars experienced free and interlayer moisture loss and decomposition of cement phases during scabbling. Discrepancies between results for the debris and the control samples of the mortars suggests that calcium hydroxide dehydroxylation ('e') and calcium carbonate decarbonation ('g'), and as a result, the α–quartz to β–quartz inversion ('f'), may have taken place to some extent. The decomposition of calcium hydroxide and calcium carbonate will increase pore pressures and decrease the tensile strength of the material. The quartz inversion could cause cracking increasing permeability and/or cause thermal stresses to develop and potentially be super-imposed [5] to the compressive forces which induce the shear forces required for thermal stress spalling to occur.

5.5 Discussion of results

The research literature identifies pore pressure and thermal stress as two key mechanisms responsible for explosive spalling [4–7, 29, 36, 37, 65]. Pore pressure spalling is due to vaporisation of free, interlayer and/or chemically combined water causing a rapid increase in pore pressures which exceeds the tensile strength of the material. Thermal stress spalling is driven by the development of thermal stresses as a result of severe thermal gradients, caused by the high heat rates and low thermal conductivity of concrete. The process is also affected by differential thermal expansions between the constituents causing cracking which reduces both pore pressures and tensile strength. Since laser scabbling can be treated as a form of explosive spalling, albeit at much higher heating rates, the results of the experiments carried out in this study can be interpreted as a consequence of these three mechanisms.

5.5.1 The effect of water/binder ratio

It is generally accepted [28] that a reduction in w/b ratios results in a denser and less porous cement matrix with higher strength and lower permeability. Lower permeability reduces mass migration and causes a build up of pore pressures. Higher strength has two effects: (i) maintains low permeability by delaying formation of cracks, and (ii) increases the tensile strain energy in the matrix; which both contribute to explosive ejection of material. The results of this study show that laser scabbling was less effective on cement pastes with the higher w/b ratio of 0.42, compared to pastes with w/b=0.32 (Figure 5.2a).

5.5.2 The effect of PFA replacement

Two effects of altering the binder composition of cement pastes can be identified from the volume removal and surface temperature time histories of the hardened cement pastes (Figure 5.2). The results show that (i) laser scabbling was more effective on PFA+OPC pastes than OPC pastes, regardless of the w/b ratio, and (ii) the effect of the w/b ratio on the PFA+OPC pastes was much smaller than that on the OPC pastes.

Although not tested in this study, it is well known [28] that use of PFA as a cement replacement material reduces the permeability of hardened cement pastes. The small particle size of the PFA, along with the pozzolanic reaction and/or the 'filler effect' [66] contribute to a reduction in permeability. PFA replacement also reduces the compressive strength of hardened cement pastes (seen in Table 5.6). A reduction in permeability restricts the movement of gas causing pore pressures to build quicker and scabbling

to take place at lower surface temperatures, through more frequent ejection of smaller fragments, as observed in the results on PFA+OPC pastes (Figure 5.2b). The fact that the largest volume removal was observed in the paste that was most likely the least permeable paste, $(PFA+OPC)_{32}$, indicates that the pore pressure mechanism was the primary driver of laser scabbling of the hardened cement pastes. This is further supported by the DTA/TGA results which suggest moisture loss and cement phase decomposition occurred in the debris of the paste during scabbling.

The effect of using PFA as a cement replacement material on volume removal during laser scabbling is less significant in the mortars and concretes compared to the hardened cement pastes. This is mainly due to the reduced paste content, but also due to the fact that the introduction of aggregates to the mix changes the scabbling mechanism. The effects of pore pressure are no longer dominant, and the changes in mechanical properties allow further mechanisms to take effect (such as reinforcing effects of aggregates, thermal stress spalling and vitrification, discussed later).

One unexpected result was the significantly lower initial heating rate in OPC_{42} mortar compared to all the other materials (Figures 5.3b and 5.6b). A more detailed comparison of the two mortars (three specimens of each) is shown in Figure 5.5.

5.5.3 The effect of fine aggregates

The volume removal of the $(PFA+OPC)_{42}$ mortar is very similar to that of the $(PFA+OPC)_{42}$ paste, whereas laser scabbling is far more effective on the OPC_{42} mortar compared to the OPC_{42} paste (Figure 5.3a). The increased volume removal during laser scabbling due to the addition of fine aggregates, as is the case with the OPC_{42} mortar, cannot be explained by the pore pressure mechanism. The replacement of water rich cement paste with anhydrous sand particles (56% by mass), and the creation of highly permeable interfacial transition zones between the aggregates and cement paste [28], will result in a reduction of pore pressure spalling. The reduced effect of the permeability of the paste is supported by the fact that the binder composition had much less effect on volume removal in the two mortars compared to the hardened cement pastes. Although the evidence of moisture loss and cement phase decomposition (including calcium hydroxide and calcium carbonate) during scabbling of mortars, illustrated by the DTA/TGA results, suggest that pore pressure spalling still plays a role to some extent.

An alternative mechanism driving the scabbling could be stresses produced by thermal gradients in the material. The scabbling would occur by accumulation of stresses in a volume of material that expands more than the surrounding cooler material, until they reach the strength (shear and tensile) at the boundaries of that volume, after

which the accumulated strain energy will eject the fragment [5]. Larger and thicker fragments, incorporating a number of sand grains indicate the presence of this mechanism in mortars.

Without the reinforcement provided by the fine aggregates (sand grains), the low tensile strength of the cement paste would result in fracturing without accumulation of strain energy. This would result in damaged material remaining at the surface and getting hotter, until eventually there is enough strain energy (or pore pressure) in the deeper layers to force an occasional ejection of the surface material. This corresponds to the scabbling behaviour observed in OPC_{42} paste. In the case of $(PFA+OPC)_{42}$ paste (and the pastes with w/b=0.32) the lower permeability causes pore pressure spalling to occur before the development of thermal stresses, resulting in frequent ejection of smaller fragments.

5.5.4 The effect of coarse aggregates

At interaction times of up to 20 s, volume removal in concretes is similar to that of the mortars (Figure 5.6a). The distribution of aggregates within concrete means that material removed in the early stages would be mostly mortar in the surface layer and, as a result, concretes will behave like mortars until the coarse aggregates are exposed. The final depth of scabbling in the concretes (a maximum of 15 mm) may be too small for the full effect of the larger 20 mm aggregates to take place, potentially explaining the similarities in scabbling behaviour between the 10 mm and 20 mm aggregate concretes (Figures 5.8 and 5.9).

The reduction in rate of volume removal experienced by the concrete compared to mortar specimens and cement pastes (Figure 5.6a), suggests that the presence of coarse aggregates limits the effectiveness of laser scabbling. This reduction in rate of volume removal must be the result of either a reduction in the driving force responsible for laser scabbling, an increase in the resistance to scabbling or the introduction of a further mechanism which hinders scabbling.

The replacement of mortar with coarse aggregates reduces the amount of free water in the material by 40–50% (Table 5.6) and the amount of chemically combined water (due to a reduction in cement paste content). Consequently, the effects of pore pressure spalling are reduced. The higher compressive strength of the concretes compared to the mortars (Table 5.6), along with the local reinforcing effect of the coarse aggregates, would result in higher tensile strength of the concretes than the mortars, increasing the resistance to scabbling. It could be assumed that after the intial scabbling of the surface layer, when the aggregates are fully exposed, the thermal stresses would not

always be sufficient to cause either fracture of the aggregates or ejection of whole aggregate pieces, and the thermal stress spalling will be greatly reduced. The reduction in both pore pressure spalling and thermal stress spalling will reduce the rate of volume removal, resulting in rapid increase in surface temperatures, which is exactly the scabbling behaviour displayed by the two concretes observed in the tests (Figure 5.6).

Despite the basalt rock scabbling to a greater extent than the limestone rock, limestone concrete scabbles more than the basalt concrete (Figure 5.6a). The average surface temperature histories show the temperature of the basalt rock to be higher (Figure 5.9) than limestone rock (Figure 5.8), despite the larger volume removal in basalt rock. This could be due to higher reflectivity of limestone rock than basalt rock, something that needs to be investigated further.

The small volume removal of solid limestone rock (Figure 5.8a), suggests that the properties of limestone aggregates do not directly enhance laser scabbling. The lower volume removal of the limestone concrete compared to the mortar specimens is a direct result of reducing the content of mortar with rock, reducing the available driving force. This effect does not take place until the surface mortar is removed and the coarse aggregates are fully exposed. At longer interaction times (30–40 s) the rate of volume removal in the limestone concretes is reduced to zero and the average surface temperatures increase rapidly to 650-700 °C (Figure 5.8b), resulting in a limited amount of vitrification in the mortar surrounding the aggregates, and decarbonation of the limestone aggregates (Figure 5.11a).

The tests on basalt rock showed scabbling of thin flakes of material (Figure 5.12a) in a similar fashion to the spalling of granite blocks observed during tests reported by Zhang et al [26]. After 20s of scabbling the basalt rock underwent full vitrification. High speed photography of the process shows that basalt aggregates in the concrete specimens scabbled in a similar manner, as well as in bulk fragments (Figure 5.12b) including aggregate and mortar, similar to the limestone concrete (Figure 5.12c). The volume removal in basalt concrete is lower than that in mortar even in the early stages of the process. This is a result of the early stage vitrification of the basalt aggregates, in addition to the reduction in the mortar content and the increase in resistance (strength and reinforcement).

Figure 5.7a shows evidence of basalt aggregate undergoing partial scabbling in the early stages (10 s exposure), leaving the aggregate fragmented. The fragmented aggregate is unable to develop thermal stresses and as a result would only be removed if the material beneath it was ejected. In this case, the fragmented aggregate blocks the laser radiation, keeping it from reaching the material beneath, leaving the fragmented aggregate prone to vitrification (Figure 5.7b). The phase change that takes place during vitrification uses

up energy from the system that may otherwise increase thermal stresses. Vitrified areas increase the temperature locally, inducing further vitrification of nearby aggregates and mortar, reducing the rate of scabbling further. While large areas of vitrified material were seen to scabble (Figure 5.13) and vitrified material was identified in the debris in the early stages (< 15 s), when the concrete is exposed to longer interaction times a drop in the rate of volume removal coincides with an increase in vitrification (Figure 5.7c and d).

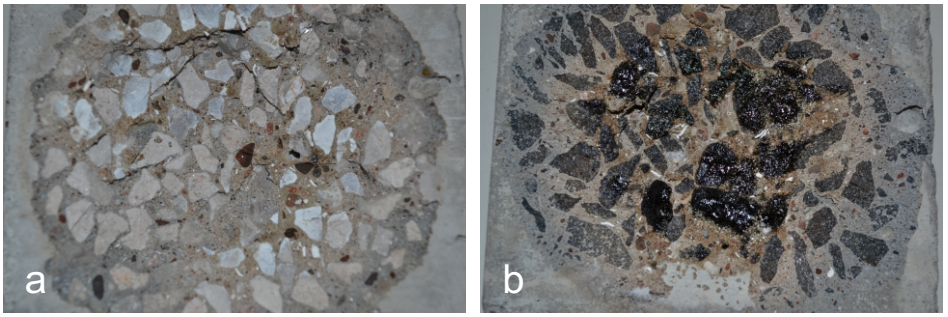

FIGURE 5.11: Photos of specimens after 40s of laser interaction; (a) limestone concrete showing decarbonated limestone aggregates (whiter, brighter aggregates) and vitrification of mortar surrounding aggregates (light brown rather than grey); and (b) basalt concrete showing vitrification of basalt aggregates (darker, glossier aggregates).

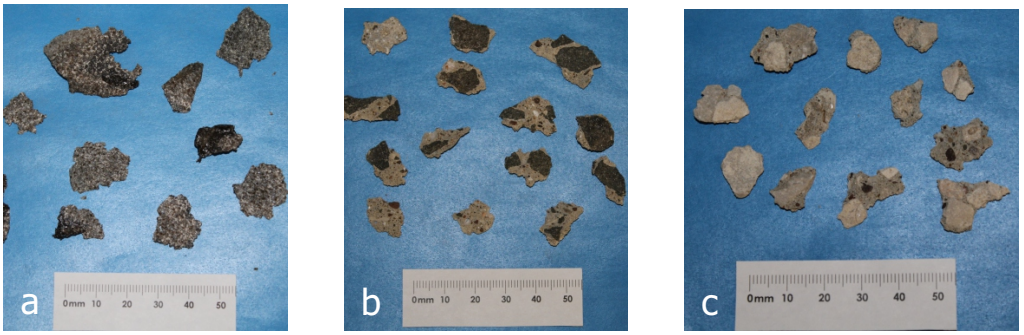

FIGURE 5.12: Photographs of laser scabbling debris (a) basalt rock, (b) OPC basalt concrete and (c) OPC limestone concrete compositions. It should be noted that debris collected is not representative of that initially ejected as it is damaged after ejection (before collection).

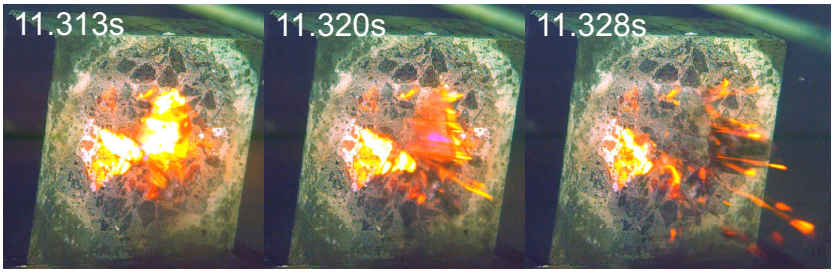

FIGURE 5.13: High speed photography of basalt concrete showing vitrified areas (glowing white) being scabbled.

5.5.5 Repeatability

In previous laser scabbling [2, 3, 16, 19] and explosive spalling [5] experiments researchers reported stochastic behaviour. Identical specimens exposed to identical conditions exhibited different results. In this study no stochastic behaviour has been identified. The largest variations in volume removal, recorded in the most variable specimens (concrete using 20 mm aggregate), were still small enough to enable clear distinction between the tested materials (Figure 5.6). The variations in cement pastes and mortars were even smaller (Figure 5.3).

5.6 Conclusions

The results from this study can be used to make the following conclusions on the mechanism(s) of laser scabbling:

(I). The results suggest that pore pressure spalling, driven by vaporisation of free, interlayer and/or chemically combined water in the cement matrix, is the predominant mechanism in laser scabbling of cement pastes;

(II). Laser scabbling of mortars is driven by a combination of thermal stress spalling and pore pressure spalling (which is reduced due to the reduction of available water in the mortars compared to the cement pastes);

(III). The primary driving force for laser scabbling of concretes is developed from the mortar not the coarse aggregates;

(IV). The low melting point of basalt rock causes vitrification, which hinders laser scabbling of basalt concrete;

(V). The decarbonation of limestone aggregates causes weakening/powdering of the rock, which hinders laser scabbling of limestone concrete.

This study has highlighted the following practical considerations for the laser scabbling proccess:

(I). Laser scabbling of cement pastes is more effective when a lower w/b and/or PFA replacement is used; most likely due to the reduction in permeability;

(II). If a material is not scabbling at a sufficient rate vitrification and/or decarbonation will take place;

(III). Limits on laser interaction times exist for concrete specimens, above which no further laser scabbling will take place. For the laser parameters used in this study (beam diameter = 60 mm , power = 5kW), interaction time on limestone concrete should not exceed 25 s (equivalent to a minimum scan speed = 144 mm/min) and 15 s (minimum scan speed = 240 mm/min) for basalt concrete.

It should also be noted that previously reported stochastic behaviour was not observed in this study.

Chapter 6

Laser scabbling of mortars

The results of the first two test series indicated that the scabbling of concrete is mainly controlled by processes in the mortar matrix, with coarse aggregates generally reducing the amount of volume removal. This chapter describes the third test series: an investigation into the parameters that influence laser scabbling of mortars. Mortars of different compositions have been tested to identify the mechanism(s) that take place during laser scabbling.

6.1 Scope and Aim of the Research

The first two test series suggested that the mortar is responsible for the primary driving force in laser scabbling of concretes. This test series aimed to determine the relationship between laser interaction time, volume removal and surface temperatures for different mortar compositions, in order to identify the parameters affecting the laser scabbling of mortars.

The compositions selected for investigation in this study were designed to isolate the following factors that were highlighted from the previous two test series (Chapters 4 and 5):

(I). Mortars of the same composition with different free moisture contents, to determine the effect of free water content, and its effects on potential operational use of laser scabbling.

(II). Mortars with different w/b ratios, to determine the effects of permeability and strength on laser scabbling of mortars;

(III). Mortars with and without 25% PFA content, to add to previous work on the effect of PFA replacement in the binder on laser scabbling;

(IV). Mortars with different fine aggregate contents, to gain an understanding of the effect of fine aggregate content on laser scabbling;

6.2 Specimens and experimental programme

The mix composition of the mortar used in the free water investigation (Mp) is detailed in Table 6.1. It is the same mix composition as the mortar (M) used in the first test series (Chapter 4) and the PFA+OPC mortar (Mp) used in the second test series (Chapter 5). Specimens tested in the free water investigation were exposed to the preconditioning methods detailed in Table 6.2 until constant mass was achieved (a loss of <2 g/day for oven dried and <0.1 g/day for dessicated and air dried specimens). The moisture content and degree of saturation of specimens exposed to the different preconditioning methods are also given in Table 6.2.

The laser interaction times and age of specimens at the time of testing are given in Tables 6.3, 6.4 and 6.5; each test was repeated three times unless stated otherwise.

TABLE 6.1: Mix compositions of specimens in the three investigations: (i) effects of free water content, (ii) effects of w/b ratio (and binder composition) and (iii) effects of fine aggregate content. All values are mass/binder ratios unless otherwise stated.

	Water	OPC	PFA	Fine agg.
(i) Effects of free water content				
*Mp	0.42	0.75	0.25	1.84
(ii) Effects of w/b ratio				
Mp37	0.37	0.75	0.25	1.84
Mp47	0.47	0.75	0.25	1.84
Mo37	0.37	1	0	1.84
Mo47	0.47	1	0	1.84
(iii) Effects of fine aggregate content				
Mp0%	0.42	0.75	0.25	0
Mp20%	0.42	0.75	0.25	0.36
Mp40%	0.42	0.75	0.25	0.95
Mp60%	0.42	0.75	0.25	2.13

TABLE 6.2: Description of the preconditioning methods used in the free water investigation, including the length of preconditioning, and the resulting average mass change, degree of saturation and moisture content. *The MpDes specimens were air dried for 69 days followed by 99 days stored with silica gel.

Spec.	Type of preconditioning
MpSat	Stored in mist room (>95% relative humidity)
MpAir	Stored at ≈20°C and ≈40% relative humidity
MpDes	Same as MpAir, but stored with silica gel
Mp50	Oven dried at 50°C
Mp105	Oven dried at105°C
MpRS	Mp105 specimens submerged in water

Spec.	Precon. time (days)	Av. mass change (g / %)	Deg. sat. (%)	MC (%)
MpSat	261	0 / 0	100	9.3
MpAir	168	-34.1 / -3.2	66.9	6.2
MpDes	69 + 99*	-43.7 / -4.1	57.5	5.4
Mp50	25	-38.0 / -3.5	63.0	5.9
Mp105	18	-102.8 / -9.5	0	0
MpRS	2	+52.8 / +4.9	51.4	4.8

6.2.1 Specimen properties

The specimen properties for the different compositions are detailed in Table 6.6. Specimen properties of the compositions tested in the w/b ratio investigation (Mp37, Mp47, Mo37 and Mo47) show that the use of a higher w/b ratio and/or the use of PFA as a cement replacement material increases the porosity and moisture content, while reducing the strength and density.

Of the specimens tested in the fine aggregate content investigation the Mp0% (hardened cement paste) has the highest porosity and moisture content, but the lowest density. Increasing the content of fine aggregates (Mp20% and Mp40%) reduces the porosity and moisture content, and increases the density. Hardened cement paste is naturally porous due to the formation of pores during hydration [28], therefore, as the porous cement paste is replaced with dense/low porosity fine aggregates, the porosity and moisture content of the mortar reduces and the density increases. At high fine aggregate contents (Mp60%), however, the reduction in workability causes the porosity and moisture content

TABLE 6.3: Experimental programme and test specimens of the free water content investigation. All specimens have the mix composition of 'Mp' detailed in Table 6.1, but underwent different preconditioning methods as detailed in Table 6.2. *Tests had only 2 repeats rather than three.

Test/ Specimen	Precon- ditioning type	Interaction time (s)	Age (days)
MpSat-10	Saturated	10	261
MpSat-30		30	261
MpSat-50		50	261
MpSat-70		70	261
MpAir-10	Air dried	10	263
MpAir-30		30	263
MpAir-50		50	263
MpAir-70		70	263
MpDes-10	Dessicated	10	263
MpDes-30		30	263
MpDes-50		50	263
MpDes-70		70	263
Mp50 -10	Oven dried	10	263
Mp50-30	at 50	30	263
Mp50-50		50	263
Mp50-70		70	263
Mp105-10	Oven dried	10	263
Mp105-30*	at 105	30	263
Mp105-70*		70	263
MpRS-10*	Resaturated	10	268
MpRS-70*	Resaturated	70	268

to increase and the density to reduce. The compressive strength of the specimens tested in the aggregate content investigations are all similar.

The mass loss due to preconditioning, moisture content and degree of saturation of the specimens tested in the free water content investigation were determined, which are detailed in Table 6.2.

TABLE 6.4: Experimental programme and test specimens of the water/binder investigation. Mix compositions are detailed in Table 6.1. All specimens in the binder composition investigation were tested saturated.

Test/ Specimen	Precon- ditioning type	Interaction time (s)	Age (days)
Mp37-10	$w/b = 0.37$	10	223
Mp37 -30	PFA+OPC	30	223
Mp37 -50		50	223
Mp37 -70		70	223
Mp47 -10	$w/b = 0.47$	10	223
Mp47 -30	PFA+OPC	30	223
Mp47 -50		50	223
Mp47 -70		70	223
Mo37 -10	$w/b = 0.37$	10	223
Mo37 -30	OPC	30	223
Mo37 -50		50	223
Mo37 -70		70	223
Mo47 -10	$w/b = 0.47$	10	223
Mo47 -30	OPC	30	223
Mo47 -50		50	223
Mo47 -70		70	223

6.3 Test results

6.3.1 Results of the free water content investigation

Figure 6.1 shows the volume removal and average surface temperatures recorded in the free water content investigation. The results show that specimens oven dried at 105 °C (Mp105) undergo negligible volume removal and experience a dramatic increase in surface temperature due to laser application, resulting in extensive vitrification (Figure 6.2). In comparison, all non-oven-dried specimens and specimens oven dried at 50 °C act similarly, and experience high rates of laser scabbling.

Oven dried specimens that were resaturated (MpRS) experience scabbling initially. The volume removal after 10s laser interaction, and the average surface temperature behaviour up to around 8 s, was similar to that of the MpAir, MpSat, MpDes and Mp50 specimens. After this the MpRS surface temperatures increase at a similar rate as the Mp105 did initially, but surface temperatures continue to rise to a final temperature

TABLE 6.5: Experimental programme and test specimens of the fine aggregate content investigation. Mix compositions are detailed in Table 6.1. All specimens in the fine aggregate content investigation were tested saturated.

Test/ Specimen	Precon- ditioning type	Interaction time (s)	Age (days)
Mp0%-5	0% agg.	5	246
Mp0%-10		10	246
Mp0%-30		30	246
Mp0%-50		50	246
Mp0%-70		70	246
Mp20%-10	20% agg.	10	247
Mp20%-30		30	247
Mp20%-50		50	247
Mp20%-70		70	247
Mp40%-10	40% agg.	10	246
Mp40%-50		50	252
Mp40%-70		70	252
Mp60%-10	60% agg.	10	247
Mp60%-30		30	247
Mp60%-50		50	247
Mp60%-70		70	247

TABLE 6.6: Specimen properties; MC = moisture content, Fc = compressive strength (the mean of three repeats is reported). All specimen property tests were carried out saturated.

Spec.	Porosity (%)	MC (%)	Density (kg/m^3)	F_c (MPa)
Mp	21.1	9.3	2262	63
Mp37	18.3	8.1	2267	65
Mp47	22.8	10.1	2250	55
Mo37	17.1	7.4	2293	76
Mo47	21.2	9.3	2277	67
Mp0%	42.2	21.8	1937	57
Mp20%	34.8	16.9	2058	60
Mp40%	18.9	8.4	2264	59
Mp60%	26.3	12.0	2188	62

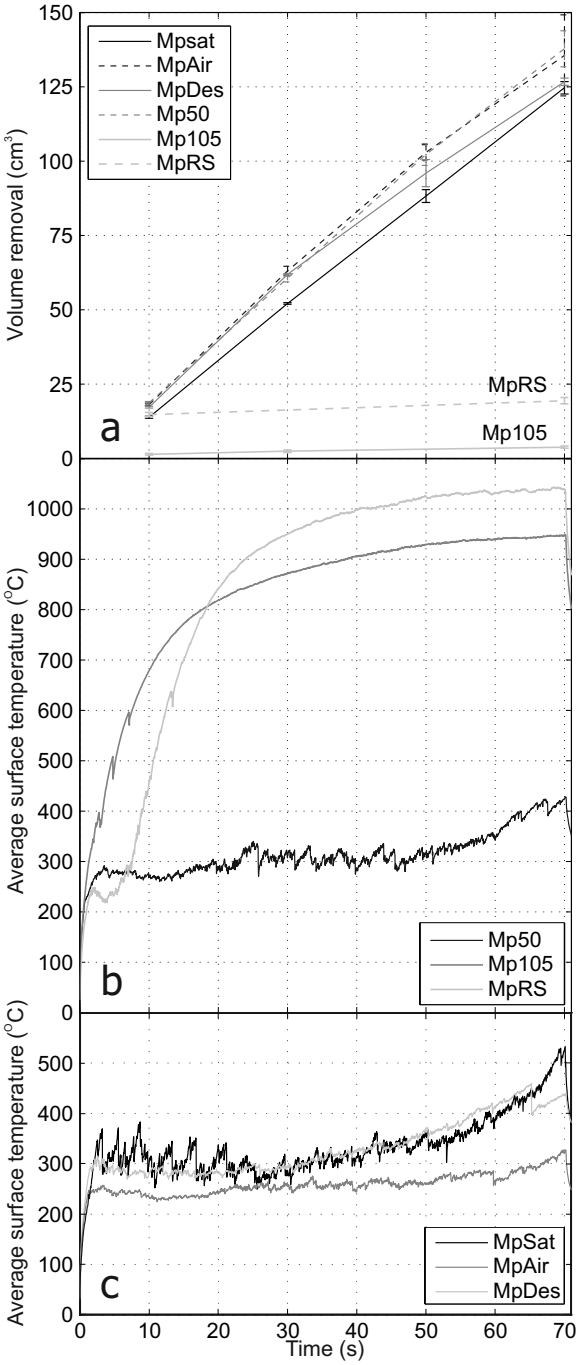

FIGURE 6.1: Results of the free water investigation: (a) volume removal; (b) average surface temperatures of specimens oven dried at 50 °C (Mp50) and 105 °C (Mp105), and those resaturated after being oven dried at 105 °C (MpRS); (c) average surface temperature results of the saturated (MpSat), air dried (MpAir) and dessicated specimens (MpDes).

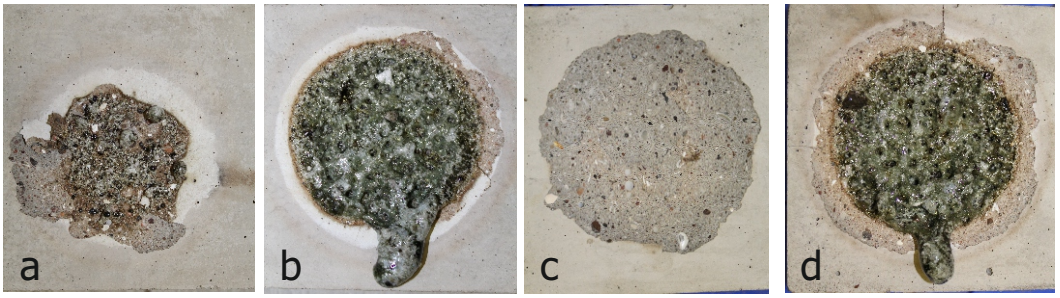

FIGURE 6.2: Photographs of specimens after laser interaction tested in the free water content investigation: (a) Specimen oven dried at 105 °C, exposed to 10 s laser interaction (Mp105-10); (b) specimen oven dried at 105 °C, exposed to 70 s laser interaction (Mp105-70); (c) specimen resaturated after being oven dried at 105 °C, exposed to 10 s laser interaction (MpRS-10); (d) specimen resaturated after being oven dried at 105 °C, exposed to 70 s laser interaction (MpRS-70).

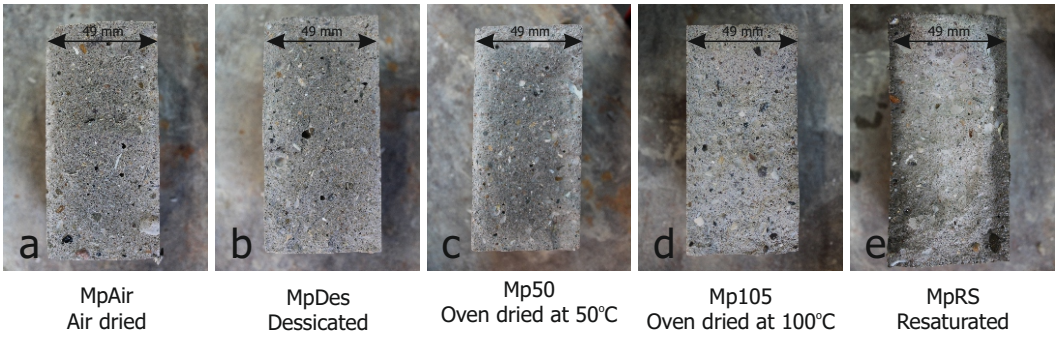

FIGURE 6.3: Photographs of cross sections of specimens tested in the free water investigation. Images show the distribution of moisture within the specimens due to the preconditioning methods.

around 100 °C higher than the Mp105 specimens. Cross sections of specimens after preconditioning, displayed in Figure 6.3, show that the resaturation did not penetrate to a depth beyond ≈1 cm, which explains the short timescale of scabbling behaviour in the resaturated specimens.

The air dried specimens (MpAir), dessicated specimens (MpDes) and specimens oven dried at 50 °C (Mp50) show similar volume removal until between 30 and 50 s laser interaction. After 50 s the rate of volume removal of the dessicated (MpDes) specimens decreases until the total volume removal is equal to that of the saturated specimens after 70 s laser interaction. The saturated specimens (MpSat) consistently experienced lower volume removal compared to the MpAir and Mp50 specimens. Saturated specimens also experienced larger temperature fluctuations than the MpAir, MpDes and Mp50 specimens. The MpAir specimens had lower average surface temperatures than the MpSat, MpDes or Mp50 specimens.

The moisture content and degree of saturation of the specimens tested in the free water content investigation are displayed in Table 6.2. It is clear that the oven drying at 50

°C, desiccating and air drying preconditioning methods did not result in vastly different moisture contents.

6.3.2 Results of the water/binder ratio and binder composition investigation

The volume removal and average surface temperature results for the w/b ratio investigation are shown in Figure 6.4. It can be seen from Figure 6.4b that an increase in w/b ratio from 0.37 to 0.47 causes the volume removal to decrease by 19–24% for OPC mortars and by 8–19% for PFA+OPC mortars. The use of 25% PFA replacement (Mp's vs Mo's) causes the volume removal to increase by 5–18% when a water binder ratio of 0.47 is used, however the effect of PFA in a mortar of w/b ratio of 0.37 is less certain with volume removal increasing for 30 and 50 s (8 and 3%), but decreasing slightly for 10 and 70 s (2 and 3%).

Average surface temperatures for the mortars using different binder compositions are broadly similar. The initial temperatures at the onset of scabbling vary for mortars of different binder compositions; PFA+OPC binder specimens have higher onsets than OPC mortar specimens (Mo47 = 240 °C; Mo37 = 260 °C; Mp37 = 330 °C; Mp47 = 400 °C). Up to around 40 s, the average surface temperature behaviour of the four compositions are fairly similar, but higher w/b ratio mixes have larger temperature fluctuations. After 40 s the average surface temperatures of the compositions using PFA increase at a much higher rate than the OPC mortars, which corresponds to a slight reduction in the rate of volume removal in the PFA mortars.

6.3.3 Results of the fine aggregate content investigation

The volume removal and average surface temperature results for the fine aggregate content investigation are shown in Figure 6.5. The average surface temperature behaviour progressively changes as the fine aggregate content is increased, a simplified diagram illustrating this behaviour can be seen in Figure 6.5c.

The specimen with no fine aggregate (Mp0%) is the same composition, and undergoes similar average surface temperature behaviour, as the $(PFA+OPC)_{42}$ paste tested in the previous study (Chapter 5). The Mp0% composition has a temperature at the onset of scabbling of around 210 °C, after which there is a steady increase in average surface temperature of around 1.9 °C/s with frequent, small temperature fluctuations. The specimens with 20% and 40% fine aggregate content (Mp20% and Mp40%), experience similar volume removals and temperature fluctuations which are both higher than for

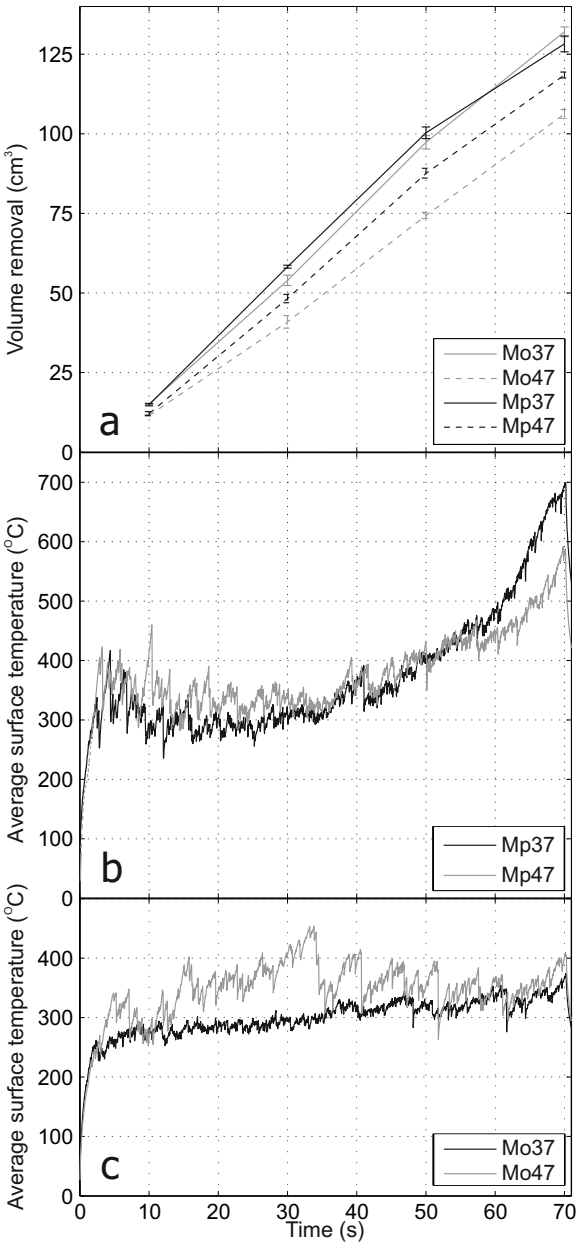

FIGURE 6.4: Results of the water/binder ratio investigation: (a) volume removal; (b) average surface temperatures of PFA+OPC mortars with w/b ratios of 0.37 (Mp37) and 0.47 (Mp47); (c) average surface temperature results OPC mortars with w/b ratios of 0.37 (Mo37) and 0.47 (Mo47).

the Mp0% composition. The Mp40% composition has a higher temperature at the onset of scabbling (335 °C) than the Mp20% composition (240 °C), but both compositions experience similar average surface temperatures after around 30 s laser interaction. The specimens with 60% aggregate content exhibit the highest volume removals, the highest temperature at the onset of scabbling (430 °C) and the largest temperature fluctuations.

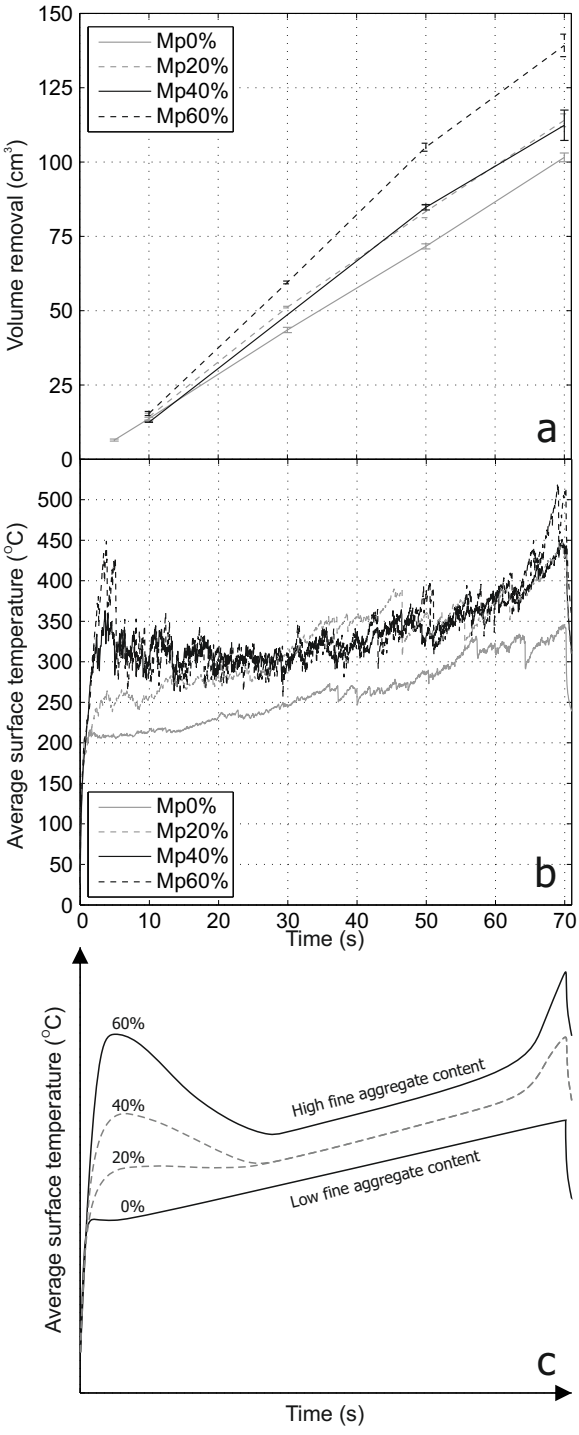

FIGURE 6.5: Results of the fine aggregate content investigation, specimens with fine aggregate content ranging from 0% to 60% (Mp0% ,Mp20%, Mp40% and Mp60%): (a) volume removal; (b) average surface temperatures; (c) simplified graph showing average surface temperature behaviour for mortars of different aggregate content.

6.4 Discussion of results

6.4.1 The effect of free water

The difference in scabbling behaviour between the specimens that were oven dried at 105 °C and those that were resaturated (Figure 6.1) suggests that free water is necessary for scabbling to occur, and that pore pressure spalling is the dominant mechanism. Specimens that were oven dried at 105 °C, effectively, did not undergo scabbling. The specimens that were oven dried at 105 °C and subsequently submerged in water for 48 hours, scabbled for the first 8 s of laser interaction. The only difference between the two specimens was the increased degree of saturation of the surface of the resaturated specimen. The depth of saturation in the resaturated specimens, highlighted by Figure 6.3, indicates that scabbling was only possible in the resaturated surface and once it was removed, scabbling of the oven dried core was not possible due to the absence of free water.

There is evidence in the literature [67, 68] that oven drying at 105 °C damages the microstructure of cementitious materials. The author was concerned this would invalidate the results of scabbling tests on Mp105 specimens. However, the successful scabbling of the resaturated specimens suggests damage due to oven drying is not detrimental to the laser scabbling process.

An unexpected result is that the final average surface temperature of the resaturated specimens (MpRS) was higher than the specimens oven dried at 105 °C (Mp105). A possible explanation for this is the shape of the surface that undergoes vitrification. The Mp105 specimens vitrify almost immediately, meaning vitrification occurs on a flat surface. The MpRS specimens, on the other hand, scabble before vitrification takes place, meaning vitrification takes place on (approximately) a parabolic surface (trough). This shape will insulate the heat affected zone, and potentially increase internal reflection of the laser, raising the surface temperature.

All other preconditioning methods (air dried, dessicated and oven dried at 50 °C, see Table 6.2) left enough free water for scabbling to take place. The threshold degree of saturation for scabbling to take place in the $(\text{PFA+OPC})_{42}$ mortar composition tested here must be between 0–57.5%). Although, the cross sections of the specimens (Figure 6.3) show that the distribution of moisture is not uniform, which may be a factor. The fact that the saturated specimens scabbled less than the MpAir, MpDes and Mp50 specimens suggests an optimum degree of saturation exists between 58% and 100% saturation.

6.4.2 The effect of permeability

The results of previous test series (Chapters 4 and 5), investigating factors known to affect permeability, have suggested that permeability is a key factor in laser scabbling of cement pastes. Results from the w/b ratio investigation (Figure 6.4) show that a lower w/b ratio or the use of PFA will result in a greater rate of volume removal, indicating that a lower permeability mortar will scabble to a greater extent, suggesting that pore pressure spalling is present in laser scabbling of mortars. Furthermore, mortars of a higher w/b ratio (higher permeability) experience higher average surface temperatures and larger fragment ejections (larger temperature fluctuations), suggesting the mechanism of laser scabbling differs slightly as a result of changes in permeability. A lower permeability will allow the pore pressures required for scabbling to build quicker, allowing more frequent, smaller ejections to occur. Although, it must be noted that a lower w/b ratio will also increase the strength of the mortar (Table 6.6), increasing the pore pressure required for scabbling to occur. A higher permeability means vapour will escape at a higher rate. To overcome this, higher surface temperatures are required to liberate vapour from greater depths and build the necessary pore pressures. The increased permeability will also result in more uniform pore pressures, further increasing fragment size.

Alternatively, the higher scabbling temperatures and larger fragment sizes of specimens with higher permeability could be a result of thermal stress spalling. The higher permeability reduces the effect of pore pressure spalling, causing temperatures to rise, and thermal gradients to form, causing thermal stresses to develop.

The average surface temperature results show that PFA+OPC mortars scabble at higher temperatures than the OPC mortars. This result is counter-intuitive, as the suspected lower permeability, due to PFA inclusion, should allow pore pressure spalling to occur at lower temperatures. This result is the opposite of what was seen for laser scabbling of cement pastes (Chapter 5).

6.4.3 The effect of fine aggregates

The average surface temperature behaviour seen in Figure 6.5b and simplified in Figure 6.5c illustrates the effect of fine aggregates on laser scabbling. It can be seen that the hardened cement paste specimen (Mp0%) undergoes consistent, small, frequent fragment ejections, once a relatively low average surface temperature has been obtained (low temperature at the onset of scabbling). Hardened cement paste is water rich (Table 6.6) and free of reinforcing aggregates, therefore, once the free water is heated, and the relatively

low localised pore pressures necessary for scabbling are developed, small fragments are ejected.

The presence of fine aggregates reinforces the paste making it difficult for small fragments to be consistently removed. As the fine aggregate content is increased, so is the amount of reinforcement. For larger fragments to be ejected, higher temperatures are required to develop higher driving forces (either pore pressures or thermal stresses) and/or to induce thermal damage to reduce the resistance to scabbling (weaken the material). Once the material has been heated to a sufficient background temperature, a consistent rate of scabbling can occur. As scabbling of specimens with a higher fine aggregate content results in higher volume removals (Figure 6.5), it shows that less frequent ejection of larger fragments is more efficient than more frequent ejection of smaller fragments.

It is important to note that a lower fine aggregate content will increase the moisture content (Table 6.6) which will contribute to differences in the average surface temperatures. As water is lost from the specimen through evaporation, heat energy is lost resulting in the reduction of average surface temperatures. This effect will increase with moisture content, and therefore, reduce for higher fine aggregate contents.

6.4.4 The effect of thermal conductivity

Results of the saturated mortar shows that the saturated specimens have a reduced volume removal and larger fragment sizes (temperature fluctuations) compared to the MpAir, MpDes and Mp50 specimens (Figure 6.1). A possible explanation for this lies in the effect saturation has on thermal conductivity: as water is more conductive than air, heat will transfer faster through a saturated specimen [30]. This will cause heat (and consequently pore pressures) to spread out deeper within the specimen, and over a larger area, during laser interaction. This means that the temperatures (and pressures) necessary for scabbling must occur over a larger area, causing larger and thicker fragments to be ejected. The lower thermal conductivity of the dried specimens, on the other hand, allows localised areas of high temperature (and pressure) to form allowing smaller, thinner fragments to be ejected at a higher rate.

Furthermore, the increase in scabbling with aggregate content may be a result of an increase in thermal conductivity due to an increase in silica content [30, 69]. Silica is a dense material and as a result, it is naturally a good conductor, whereas the large proportion of pores in hardened cement paste makes it less conductive. Therefore, as the content of cement paste is replaced with fine aggregates, the thermal conductivity of

the specimens is increased. A higher thermal conductivity will allow localised high temperatures to dissipate over the heat affected zone, causing more uniform pore pressures to develop and larger fragments to be ejected.

6.5 Conclusions

The main finding of this study is that specimens oven dried at 105 °C until constant mass did not experience scabbling, but resaturating the surface allowed the surface to be scabbled. This suggests that free water is necessary for laser scabbling to occur. Therefore, it is unlikely that concrete that has been exposed to high temperatures during its lifetime will scabble successfully.

This study also highlighted the following properties of mortars during laser scabbling:

(I). The relationship between degree of saturation (moisture content) and volume removal is not linear: the optimum degree of saturation for maximum volume removal is not 100%, but a value between a threshold (about 58%) and 100%.

(II). Results suggest that a lower permeability aides pore pressure spalling and increases volume removal;

(III). The use of 25% PFA in the binder generally increases both volume removal and average surface temperatures;

(IV). A higher fine aggregate content increases volume removal and the size of fragments ejected, which is mainly due to the reinforcing effect of fine aggregates and changes in thermal conductivity, both resulting in thermal stress redistribution;

(V). The increased thermal conductivity of a saturated mortar causes larger fragments to be ejected.

Chapter 7

The effect of age on laser scabbling

This section describes the fourth test series: an investigation into the effect of age on laser scabbling. In order to identify the effect of concrete age on laser scabbling, specimens cast for previous experimental programmes (Chapters 4 and 5) have been tested at later ages, and compared to the original results. Other than assessing the effect of age on scabbling, the results of this study are important to validate the results and conclusions made in the previous test series.

7.1 Scope and aim of the research

The design life of a nuclear power plant is generally 60 years, which is often extended to improve the economic rewards of the station. Furthermore, the first stage of decommissioning is usually to remove the fuel and leave the structure in a state of passive safety for around 20 years to allow the majority of the short lived radionuclides to decay. As a result, structures undergoing decommissioning will be of the age of around 80-100 years old.

Concrete age is an important factor affecting it's properties, from cement hydration in the early stages to environmental effects in the later stages. For example, initially, the degree of cement hydration is time dependant, and at later ages the effects of external influences such as drying and weathering can affect concrete properties.

This test series aims to determine the relationship between laser interaction time, volume removal and average surface temperatures for different compositions of different ages in order to give an indication into the effect of concrete age on laser scabbling behaviour

(temperature at the onset of scabbling, surface temperature during scabbling, rate of volume removal, fragment ejection frequency and fragment sizes). The compositions reported in this study (presented in Table 7.1) were selected during earlier test series (Chapters 4 and 5) to isolate factors that have a significant effect on the process. The results reported here are grouped into two investigations looking at (i) the effect of age on saturated specimens and (ii) the effect of prolonged drying.

7.2 Materials

Extra specimens were saved from the first two test series to be tested at a later date, in order to determine the effect of age on laser scabbling. These specimens continued to be exposed to the same preconditioning as those that were originally tested (i.e. air dried or saturated).

TABLE 7.1: Mix compositions of specimens tested in the age comparison study. All values in mass/binder ratio. Labels used in the first test series (Chapter 4) and in Section 7.4 are presented in brackets: Lp = LC, Bp = BC, Mp = M, P_{42} = P and O_{42} = O. * AGR mix is included for comparison only; not tested in the experimental programme. ** Basalt and Limestone Concrete refer to concrete mixes using basalt and limestone as coarse aggregates.

	Water	OPC	PFA	Fine agg.	Plast -iciser	10mm agg.	20mm agg.
*AGR	0.42	0.75	0.25	1.84	0.0045	1.05	2.16
OPC Paste							
O_{42} (O)	0.42	1	0				
O_{32}	0.32	1	0				
PFA+OPC Paste							
P_{42} (P)	0.42	0.75	0.25				
P_{32}	0.32	0.75	0.25				
Mortar							
Mp (M)	0.42	0.75	0.25	1.84			
Mo	0.42	1	0	1.84			
Bas. Concrete							
Bp (BC)	0.42	0.75	0.25	1.84	0.0045	3.21	
Bo	0.42	1	0	1.84	0.0045	3.21	
Lime. Concrete							
Lp (LC)	0.42	0.75	0.25	1.84	0.0045	3.21	
Lo	0.42	1	0	1.84	0.0045	3.21	

The compositions of the specimens tested in this study are detailed in Table 7.1.

7.3 The effect of age on saturated specimens

7.3.1 Test programme for saturated specimens

In order to test the effect of age on laser scabbling, extra specimens were made during casting for the investigation into the effect of concrete composition on laser scabbling (Chapter 5). Cement paste specimens were first tested at an age of 3 months and concretes at 8 months. Remaining specimens were then stored in a saturated state in a mist room (≈20 °C, ≈95% relative humidity) until they were tested 14 months later.

The experimental programme (laser interaction times, specimens ages and number of repeats) and specimen range of the investigation into the effect of age on saturated specimens is detailed in Tables 7.2 and 7.3.

TABLE 7.2: Cement pastes: experimental programme and test specimens of the investigation into the effect of age on saturated specimens.

Test/ Spec.	Material Composition	Interaction time (s)	Age (days)	No. of Repeats	Age (days)	No. of Repeats
Cement pastes			3 months		17 months	
$O_{42}10$	OPC paste	10	77	2	479	2
$O_{42}30$	(w/b=0.42)	30	77	2	479	2
$O_{42}40$		40	71-72	2	479	2
$O_{42}70$		70	77	2	479	2
$O_{32}10$	OPC paste	10	77	2	479	2
$O_{32}20$	(w/b=0.32)	20	77	2	479	2
$O_{32}30$		30	77	2	479	2
$O_{32}40$		40	71-72	2	479	2
$P_{42}10$	PFA+OPC	10	77	2	479	2
$P_{42}30$	paste	30	77	2	479	2
$P_{42}40$	(w/b=0.42)	40	72	2	479	2
$P_{42}70$		70	77	2	479	2
$P_{32}10$	PFA+OPC	10	77	2	479	2
$P_{32}20$	paste	20	77	2	479	2
$P_{32}30$	(w/b=0.32)	30	77	2	479	2
$P_{32}40$		40	71-73	2	479	2

TABLE 7.3: Mortars and concretes: experimental programme and test specimens of the investigation into the effect of age on saturated specimens.

Test/ Spec.	Material Composition	Interaction time (s)	Age (days)	No. of Repeats	Age (days)	No. of Repeats
Mortars and concretes			8 months		22 months	
Mp10	Mortar	10	232	3	640	3
Mp30	(PFA+OPC	30	234	3	640	3
Mp50	binder)	50	238	2	640	3
Mp70		70	238	1	640	3
Mo10	Mortar	10	232	3	641	3
Mo30	(OPC binder)	30	234	3	641	3
Mo50		50	238	2	641	3
Mo70		70	238	1	641	3
$Bp_{10}10$	Basalt	10	220	3	627	2
$Bp_{10}20$	Concrete	20	220	3	627	3
$Bp_{10}30$	(PFA+OPC	30	220	3	627	3
$Bp_{10}40$	binder)	40	218-220	3	627	2
$Bo_{10}10$	Basalt	10	220	3	626	3
$Bo_{10}20$	Concrete	20	220	3	626	3
$Bo_{10}30$	(OPC binder)	30	220	3	626	3
$Bo_{10}40$		40	219-220	3	626	3
$Lp_{10}10$	Limestone	10	207	3	612	3
$Lp_{10}20$	Concrete	20	207	3	612	3
$Lp_{10}30$	(PFA+OPC	30	207	3	612	3
$Lp_{10}40$	binder)	40	204-210	3	612	3
$Lo_{10}10$	Limestone	10	207	3	612	4
$Lo_{10}20$	Concrete	20	207	3	612	2
$Lo_{10}30$	(OPC binder)	30	207	3	612	3
$Lo_{10}40$		40	204-211	5	612	3

7.3.2 Test results of saturated specimens

The volume removal and average surface temperature results of saturated hardened cement pastes tested at the age of 3 months (71–77 days) and 17 months (479 days) are presented in Figure 7.1 for OPC specimens and Figure 7.3 for PFA+OPC specimens.

Figure 7.1a shows that the OPC pastes of both w/b ratios (0.32 and 0.42) experienced reduced volume removals when tested at 17 months compared to those tested at 3 months (up to around 40% drop for OPC_{32}, and 30% for OPC_{42}). At interaction times below

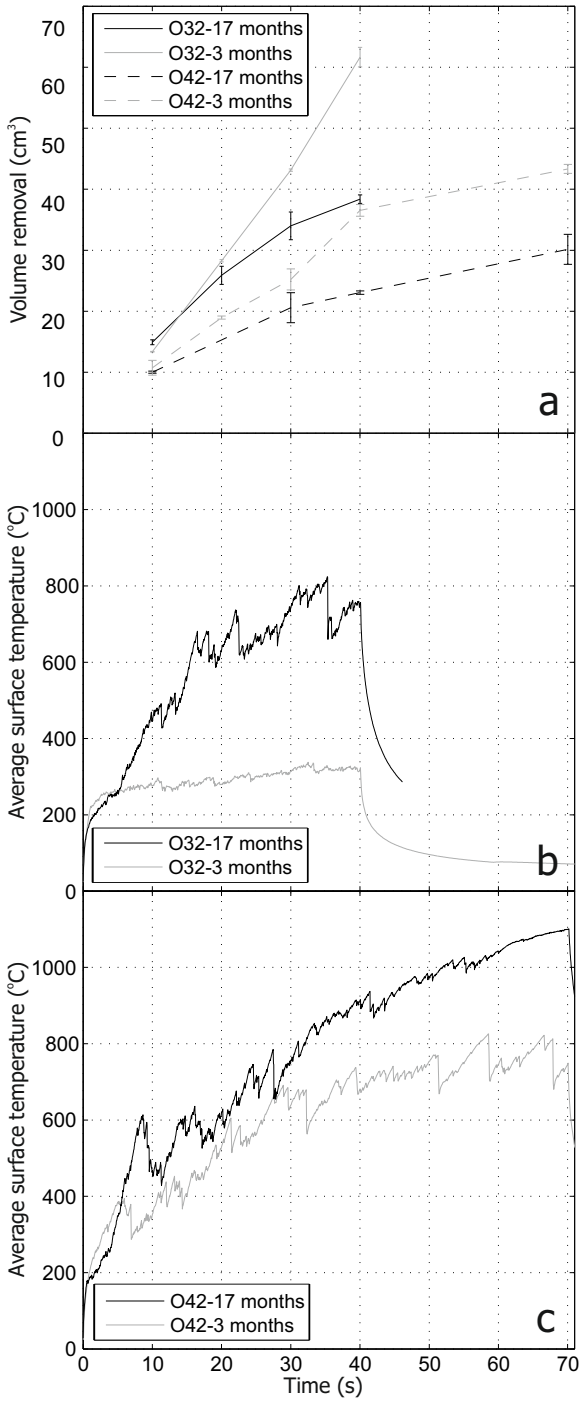

FIGURE 7.1: Saturated OPC paste results: (a) volume removal, (b) average surface temperature results for OPC_{32} pastes and (c) average surface temperature results for OPC_{42} pastes.

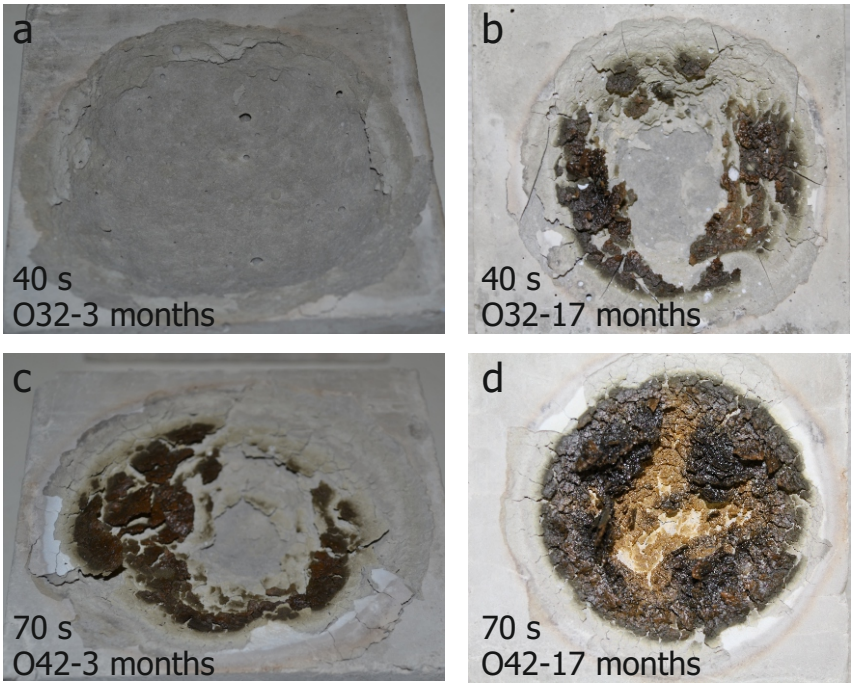

FIGURE 7.2: Photographs illustrating different extents of vitrification in OPC paste specimens: OPC_{32} paste after 40 s at (a) 3 months and (b) 17 months, OPC_{42} paste after 70 s at (c) 3 months and (d) 17 months.

40 s, the younger OPC_{42} paste experienced a higher rate of volume removal (around 0.9 cm^3/s) than the older OPC_{42} paste (around 0.4 cm^3/s), but between 40 s and 70 s both ages showed similar rates of volume removal (around 0.2 cm^3/s). The younger OPC_{32} paste shows a much higher rate of volume removal throughout the interaction times tested (1.6 cm^3/s), compared to the older OPC_{32} paste (1.1 cm^3/s initially, reducing to 0.4 cm^3/s). OPC pastes with lower volume removals exhibit higher average surface temperatures (Figure 7.1b and c); as material is removed less frequently, the surface is exposed to prolonged laser interaction and heated to a greater extent, inducing more extensive vitrification (Figure 7.2).

Figure 7.3 suggests that the age difference of the PFA+OPC paste specimens made little difference to the volume removal during laser scabbling.

The volume removal and average surface temperature results of the saturated mortars and saturated concretes tested at 8 months (207–238 days) and 22 months (612–640 days) are presented in Figures 7.4, 7.5 and 7.6.

Figure 7.4 shows that age had little effect on scabbling of mortars (Mo and Mp), with the same compositions exhibiting similar volume removal.

Figures 7.5a and 7.6a show that the volume removal of older concretes is up to 25% higher than that of the younger concretes. The average surface temperature behaviour

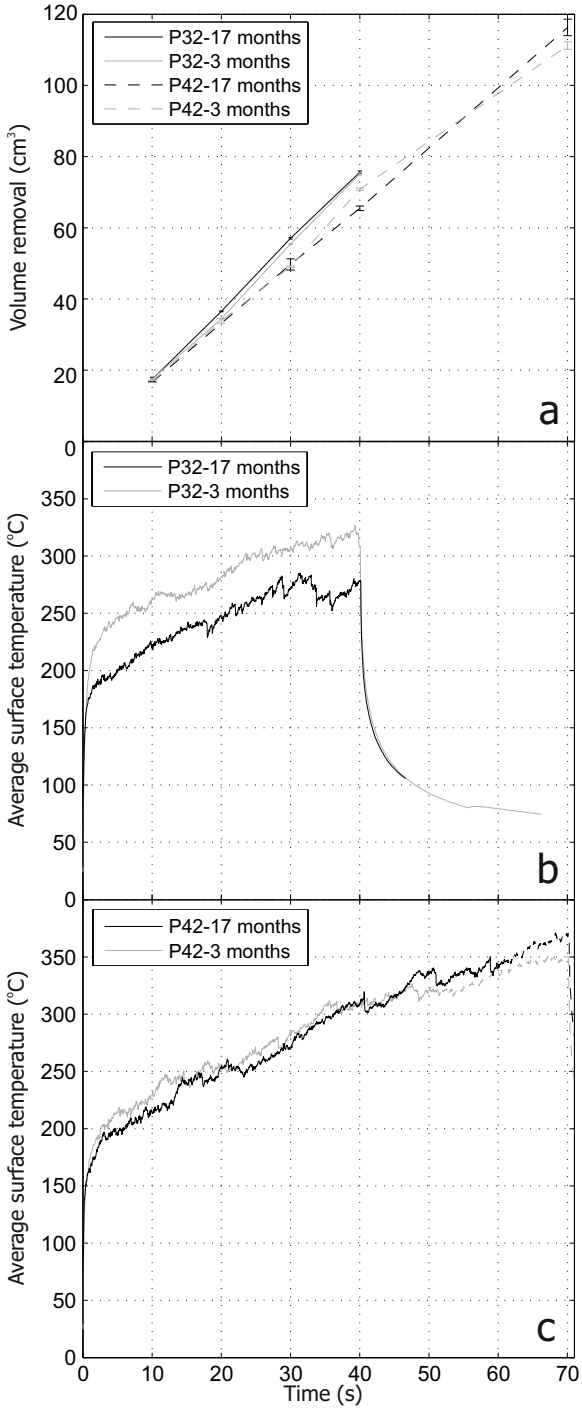

FIGURE 7.3: Saturated PFA+OPC pastes: (a) volume removal, (b) average surface temperature results for $(PFA+OPC)_{32}$ pastes and (c) average surface temperature results for $(PFA+OPC)_{42}$ pastes.

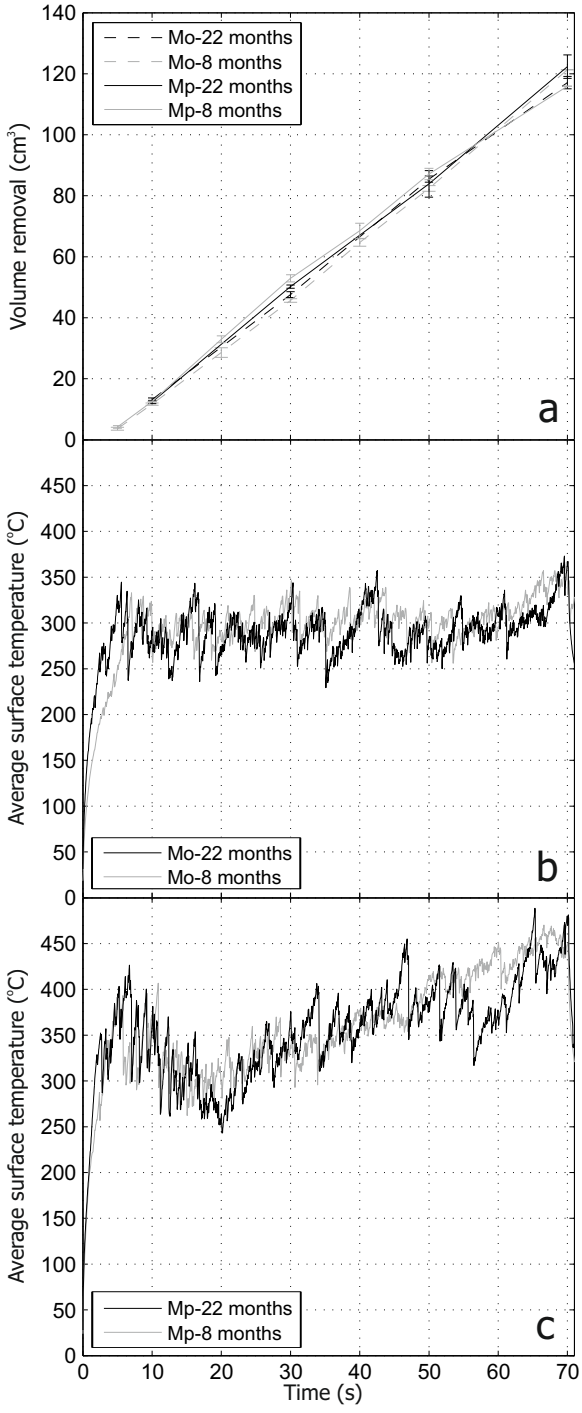

FIGURE 7.4: Saturated mortar results: (a) volume removal, (b) average surface temperature results for OPC mortars (Mo) and (c) average surface temperature results for PFA+OPC mortars (Mp).

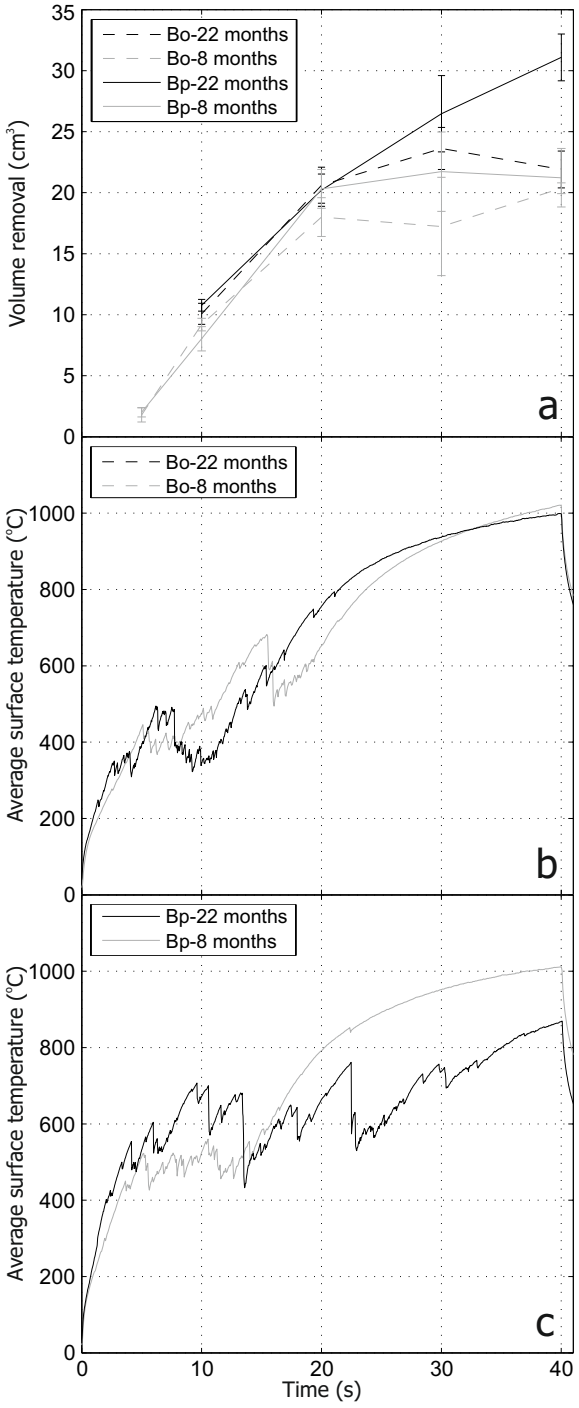

FIGURE 7.5: Saturated basalt concrete results: (a) volume removal, (b) average surface temperature results for OPC basalt concretes (Bo) and (c) average surface temperature results for PFA+OPC basalt concretes (Bp).

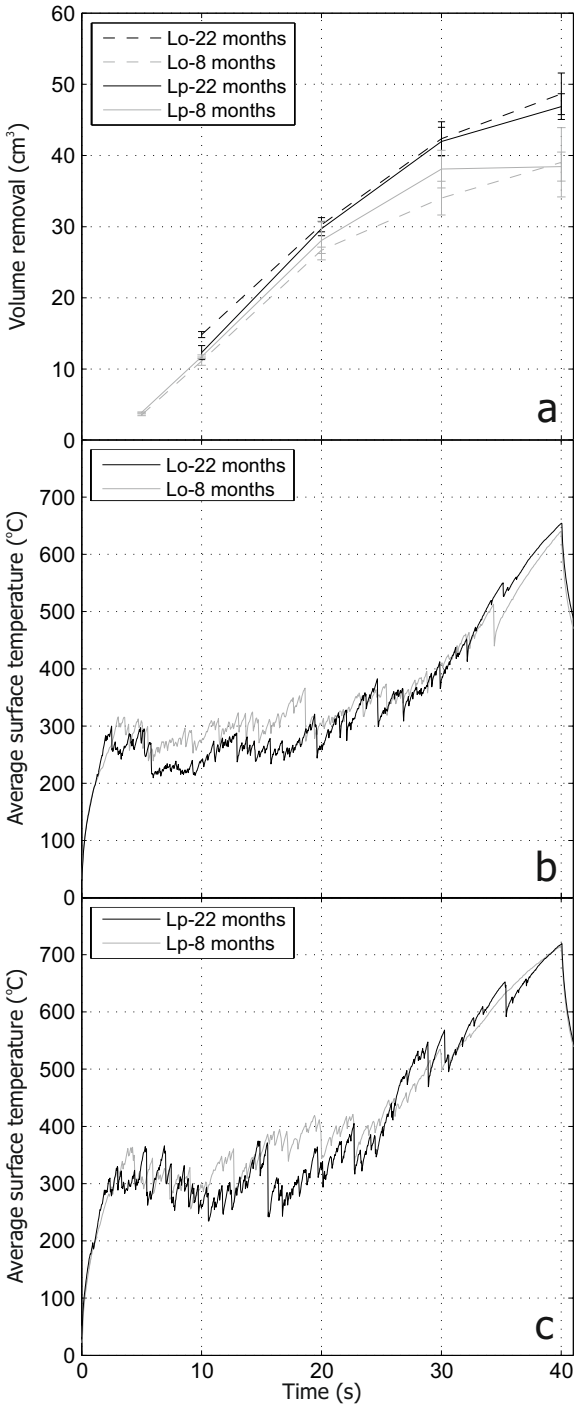

FIGURE 7.6: Saturated limestone concrete results: (a) volume removal, (b) average surface temperature results for OPC limestone concretes (Lo) and (c) average surface temperature results for PFA+OPC limestone concretes (Lp).

of the limestone concretes (Lo and Lp) and the OPC basalt concrete (Bo) is similar for the two ages (Figures 7.6b, 7.6c and 7.5b). However, the older PFA+OPC basalt concrete (Bp) did not experience the same reduction in the rate of volume removal as the younger PFA+OPC basalt concrete. It can be seen in Figure 7.5c, that temperature fluctuations stop at around 15 s in the younger PFA+OPC basalt concrete, whereas the temperature fluctuations continue in the older PFA+OPC basalt concrete until around 30 s laser interaction, which corresponds with greater volume removals in the older concrete (Figure 7.5a).

7.3.3 Discussion of saturated specimens

The results of the age investigation on saturated specimens, suggests that age had little effect on scabbling of saturated mortars or saturated PFA+OPC pastes.

Volume removal of the saturated OPC pastes reduces with age. The older OPC_{32} paste shows similar scabbling behaviour to the OPC pastes of a higher w/b ratio (OPC_{42}, both ages), exhibiting a reduced rate of volume removal and much higher average surface temperatures with larger and less frequent ejections compared to the younger OPC_{32} pastes. Potentially, this is due to the balance between pore pressures and strength. It is assumed that the strength of the OPC pastes will increase from 3 months to 17 months, meaning higher pore pressures are required for scabbling. However, pore pressures developed are not high enough to overcome the higher strength of the older OPC_{32} paste and induce frequent scabbling, causing temperatures to rise and larger fragments to be ejected.

Saturated concretes show an increase in volume removal with age. The reasons for this is unclear but this could be a result of greater saturation of the aggregates.

In conclusion, the results of the investigation into the effect of age on saturated specimens suggests saturated OPC pastes scabble more successfully when of a lower age, saturated PFA+OPC pastes and mortars are unaffected by age, and saturated concretes scabble more successfully at higher age.

7.4 The effect of prolonged drying

7.4.1 Test programme of the prolonged drying investigation

In the first test series (Chapter 4), air dried and saturated specimens were tested. All specimens were kept in a mist room (≈20 °C, ≈95% relative humidity) after casting.

TABLE 7.4: Effect of drying with age: Experimental programme and test specimens. (Las. Int. = laser interaction time, MC = moisture content, SR = degree of saturation)

		4 months				30 months			
Test/ Spec.	Las. Int. (s)	Age (days)	Repeats	MC (%)	SR (%)	Age (days)	Repeats	MC (%)	SR (%)
OS	40	100	1	19.8	102.8	837	2		
OA	40	99	1	14.9	70.4	837	2	7.9	39.9
PS	40	100	1	21.9	96	837	2		
PA	40	99	1	18.2	79.0	837	2	8.2	37.5
MS	40	100	1	9.7	97.7	837	2		
MA	40	99	1	8.0	77.9	837	2	5.0	51.2
BCS	40	114	1	4.5	98.5	851	2		
BCA	40	113	1	3.2	71.2	851	2	2.6	57.4
LCS	40	114	1	4.6	98.7	851	2		
LCA	40	113	1	3.0	67.3	851	2	2.3	50.6

Saturated specimens were kept in the mist room until testing, whereas, the air dried specimens were moved to ambient conditions (≈20 °C, ≈95% relative humidity) at an age of around 50 days for air drying until testing. The specimens were tested at 4 months (≈50 days drying) and 30 months (≈800 days drying), which means the air dried specimens tested at 30 months have undergone a much longer period of drying than those tested at 4 months.

The experimental programme (laser interaction times, specimens ages and number of repeats) and specimen range of the investigation into the effect of prolonged drying is detailed in Table 7.4.

7.4.2 Test results of the prolonged drying investigation

Table 7.4 shows the degree of saturation and moisture contents of the specimens from Series 1 at two different ages. It can be seen that the increased drying time (≈50 days for specimens tested at 4 months versus ≈800 days for 30 months) substantially reduced the degree of saturation and moisture content of the specimens.

Volume removal results for air dried and saturated specimens exposed to 40 s laser interaction time are presented in (Figure 7.7). It can be seen that, with the exception of the mortars (M), all compositions exposed to 40 s laser interaction experienced lower volume removal when tested at 30 months compared with 4 months. The reduction in

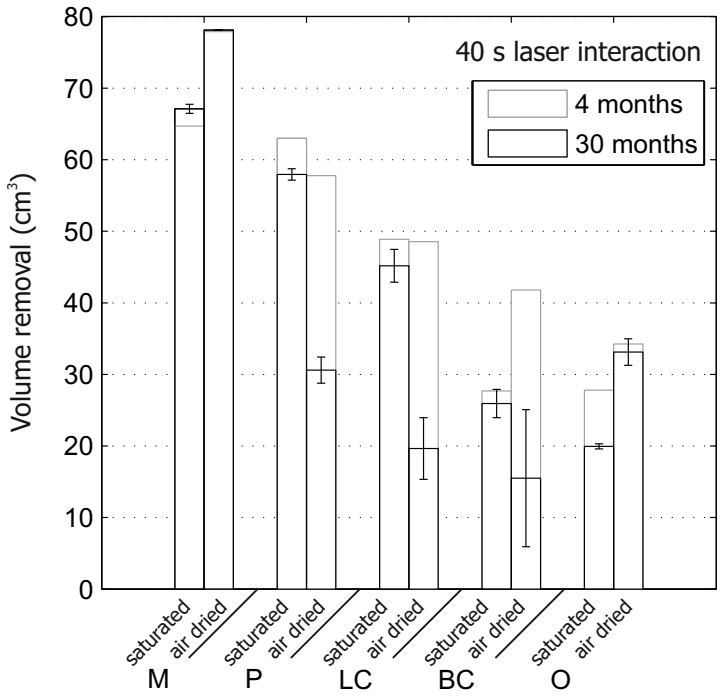

FIGURE 7.7: Volume removal results of specimens tested in the prolonged drying investigation.

volume removal due to age is much larger in the air dried PFA+OPC paste, limestone concrete and basalt concrete specimens than the saturated specimens (shown in brackets): PA = 47% (PS = 8%); LCA = 60% (LCS = 8%); and BCA = 63% (BCS = 7%). It can be seen from Table 7.4 that the reduced degree of saturation of the older air dried specimens may be responsible, reducing the driver necessary for the development of pore pressures.

The OPC paste (O) saw a larger reduction in volume removal in the saturated specimens (28%) due to age, than the air dried (3.4%), which could be a result of strength increase with age.

Age had a negligible effect on the volume removal of mortar specimens (M), but larger volume removals were seen in the air dried specimens compared to saturated.

Average surface temperatures for the concrete and mortar specimens tested at 30 months are presented in Figures 7.8a and b. Unfortunately, due to experimental error, the infra red data for the air dried limestone concrete (LCA) was not recorded. The degree of saturation had little effect on the surface temperature of basalt concrete (BCS and BCA), whereas the saturated mortar (MS) experienced much larger temperature fluctuations compared to the air dried mortar (MA), while remaining at a similar background temperature, and exhibiting similar volume removal rates.

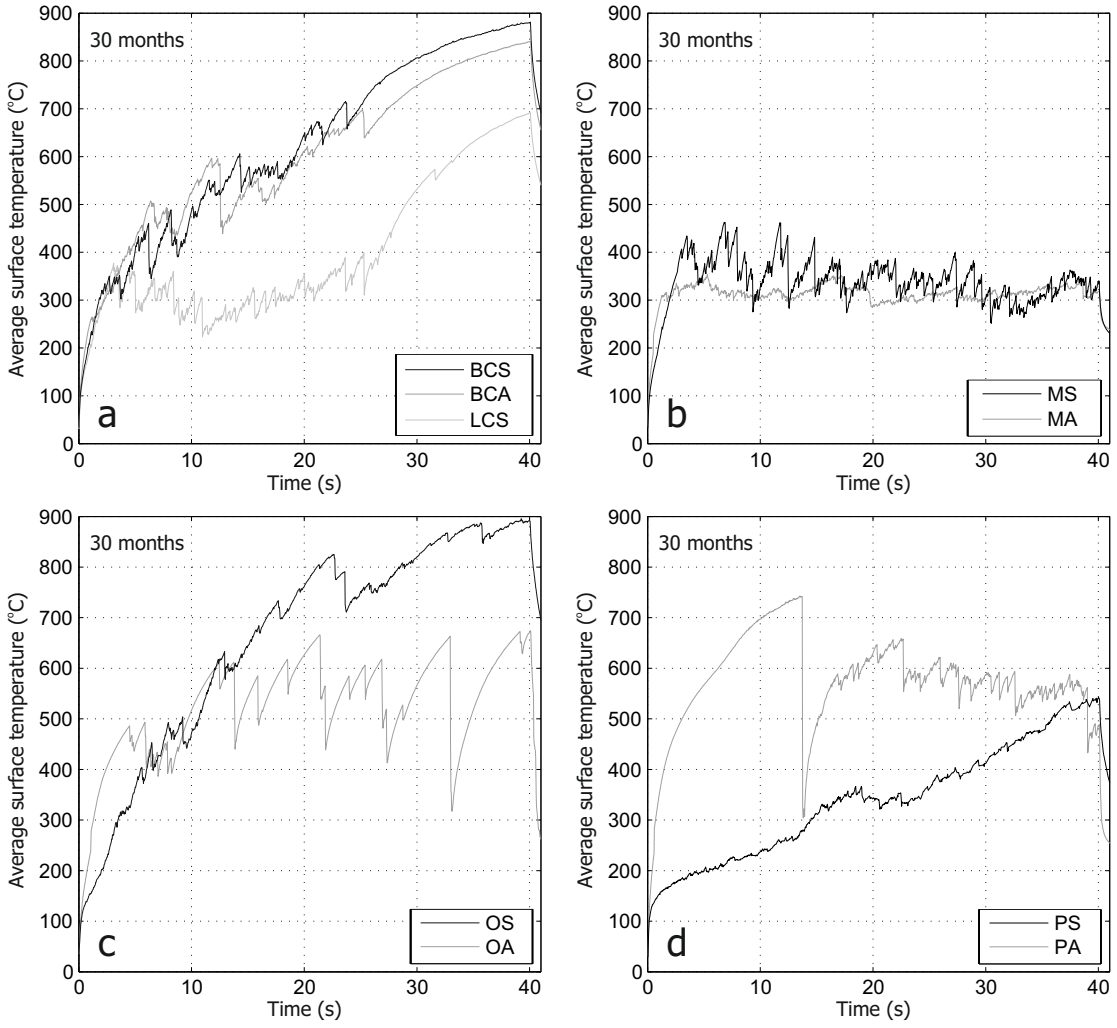

FIGURE 7.8: Average surface temperature results of specimens tested in the prolonged drying investigation: (a) basalt and limestone concretes, (b) mortars, (c) OPC pastes and (d) PFA+OPC pastes.

Average surface temperature results for the hardened cement pastes (Figures 7.8c and d) show very different behaviour between the saturated and air dried specimens. The saturated PFA+OPC paste (PS) undergoes small, frequent temperature fluctuations with a consistent average surface temperature increase of around 10 °C/s. The saturated OPC paste (OS) displays less stable behaviour than the PFA+OPC paste, with temperature fluctuations of up to 90 °C and much higher surface temperatures in general.

The air dried pastes, however, behave in an opposite way, undergoing very large temperature fluctuations (up to 350 °C for air dried OPC paste, OA, and up to 450 °C for the air dried PFA+OPC paste, PA). The more erratic surface temperature behaviour of the air dried specimens corresponds to less volume removal for the air dried PFA+OPC paste compared to the saturated, whereas the volume removal of the air dried OPC paste is greater than the saturated.

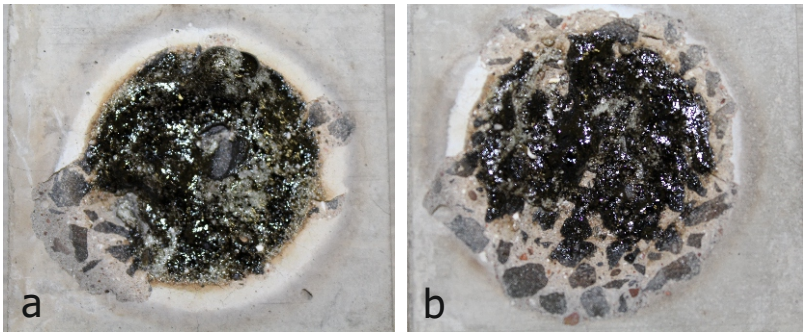

FIGURE 7.9: The two air dried basalt concrete specimens from Series 1 exposed to 40 s laser interaction (BCA); (a) stopped scabbling after 5 s, whereas (b) stopped scabbling after 25 s.

It can be seen in Figure 7.7 that the air dried basalt concrete (BCA) exposed to 40 s laser interaction had a much larger error than the other compositions tested. From inspection of the infra red videos it was seen that one of the two air dried basalt concrete specimens tested did not scabble substantially after 5 s resulting in extensive vitrification and a thick white ring around the heat affected zone (Figure 7.9a). The second specimen scabbled frequently until 25 s, and as a result underwent less vitrification and has only a small part of the white ring (Figure 7.9b).

7.4.3 Discussion of the prolonged drying investigation

The results of the investigation into the effect ofprolonged drying highlights the effect of pore pressure spalling in cement pastes. In the first test series (Chapter 4), the effect of permeability on scabbling of cement pastes led the authors to suggest that pore pressure spalling is the dominant mechanism in laser scabbling of cement pastes. PFA is known to reduce the permeability of a cement paste [28], as a result the permeability of the PFA+OPC paste is low enough for pore pressure spalling to take place in the saturated specimen inducing small, frequent fragment ejections. However, by removing the free water, as a result of prolonged air drying, the driving force for pore pressure spalling is reduced. As pore pressure spalling does not remove the surface, surface temperatures increase causing a severe thermal gradient to develop. This in turn causes large fragments to be ejected as a result of thermal stress spalling, with pore pressures acting in a secondary manner.

The lower volume removal for air dried OPC paste suggests that free water is detrimental to the laser scabbling process in OPC paste. The permeability of the OPC paste is too high for pore pressure spalling to be effective in the saturated specimens and as a result the surface temperature of the OPC paste increases dramatically until temperature gradients are sufficient for thermal stress spalling to occur. The reduced moisture content

in the air dried OPC paste specimens at 30 months (Table 7.4) means less energy is lost from the system due to evaporation, allowing thermal stress spalling to occur more efficiently.

The larger reduction in volume removal due to age in the air dried concretes compared to the saturated concretes, suggests that the free water aides the scabbling process in concretes. The moisture content of the air dried specimens (2.3% and 2.6%) at 30 months may be below a threshold value that was not reached when tested at 4 months (3.0% and 3.2%). Eurocode 2 suggests a moisture content of 3% is necessary for spalling to take place [39]. The fact that air dried mortars tested at 30 months (with moisture content of 5.0%) did not experience a reduction in volume removal compared to the 4 month specimens (8.2%), suggests the greater cement paste content of mortars compared to concretes means mortars have more free water to loose, and as a result, both the saturated and the air dried mortars (at 30 months) are above the scabbling moisture content threshold. Results presented in (Chapter 6) shows that oven drying PFA+OPC mortar ($w/b = 0.42$) to a moisture content of 0%, will reduce scabbling to zero.

Results for the mortar shows that the saturated specimen has a reduced volume removal and larger fragment sizes compared to the air dried specimen. Similar results are reported in (Chapter 6). A possible explanation for this lies in the effect saturation has on thermal conductivity: as water is more conductive than air, heat will transfer through a saturated specimen easier [30]. This will cause heat (and consequently pore pressures) to spread out deeper within the specimen and over a larger area, during laser interaction. This means that temperatures (and pressures) necessary for scabbling must occur over a larger area, causing larger and thicker fragments to be ejected. The lower thermal conductivity of the air dried specimen, on the other hand, allows localised areas of high temperature (and pressure) allowing smaller, thinner fragments to be ejected at a higher rate.

7.5 Stochastic behaviour

This investigation has given an indication that there may be some stochastic behaviour present in the laser scabbling of concretes as reported in [2, 3, 16, 19]. All PFA+OPC basalt concretes reported here have displayed unpredictable behaviour. The PFA+OPC basalt concrete from Series 2 (Section 7.3) tested at 22 months (Figure 7.5c) shows quite different behaviour and large margins of error compared to the specimens tested at 8 months, something that is not seen in the OPC basalt concrete or either of the limestone concretes. The air dried basalt concrete from Series 1 (Section 7.4) tested at 30 months (Figure 7.7) shows a much larger margin of error in volume removal compared

to any other composition. The two air dried basalt concrete specimens also displayed different behaviour in the infra red recordings (Figure 7.8a) and different extents of vitrification after 40 s laser interaction (Figure 7.9). The results suggest that stochastic behaviour may increase with age for PFA+OPC basalt concrete. Alternatively, this could be a combination of the natural variability of concrete and the high sensitivity of laser scabbling to basalt aggregates (Chapter 5).

7.6 Conclusions

(I). The biggest effect of concrete age on laser scabbling is due to the reduction in the degree of saturation caused by drying. Results suggest that the effect of drying on laser scabbling is dependant on composition, with drying reducing laser scabbling in concretes. This is of the utmost importance when considering the use of laser scabbling in situ on structures liable to drying during their operational use.

(II). The effect of ageing on saturated specimens is generally small: saturated OPC pastes scabble more successfully when of a lower age, saturated mortars are unaffected by age, and saturated concretes scabble more successfully at higher age.

(III). The effect of saturation on thermal conductivity may cause saturated mortars to experience different scabbling behaviour to that of the air dried.

(IV). This investigation has given an indication of a stochastic relationship between age and scabbling behaviour.

Chapter 8

Summary of results and discussion on laser scabbling

In this chapter, the results of all test series (Chapters 4, 5, 6 and 7) are summarised and discussed in relation to the mechanism(s) responsible for laser scabbling and the practical application of laser scabbling in nuclear decommissioning.

8.1 The experimental methodology

The main aim of this study was to investigate the mechanism responsible for laser scabbling. Previous research on laser scabbling was limited to concretes with largely unknown compositions. To account for this, the preliminary test series (Chapter 4) was designed to establish an experimental methodology and identify the key factors influencing laser scabbling, to be focused on in subsequent experimental programmes. The main finding was the strong influence of material composition on laser scabbling, which was then chosen as the focus of the second test series (Chapters 5). The first and second test series identified that the mortar was responsible for the driving force in laser scabbling of concretes. The results suggested that scabbling occurred as a result of two main mechanisms: development of pore pressures in the hardened cement paste and interactions between the cement paste and the fine aggregates. The addition of coarse aggregates generally impeded scabbling. The third test series (Chapters 6) therefore focused on an investigation into the parameters influencing laser scabbling of mortars. An investigation into the effect of age (Chapter 7) was carried out in the third test series, on specimens cast for the first and second test series.

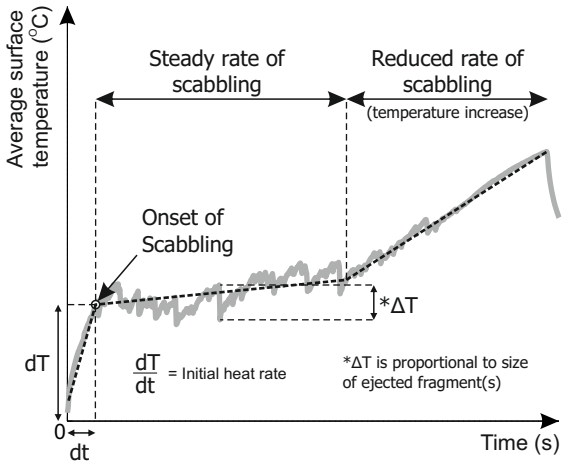

FIGURE 8.1: Example average surface temperature graph, showing trilinear behaviour with different stages of scabbling behaviour highlighted.

Throughout the study, infra red recordings were used to quantify laser scabbling behaviour of the various material compositions. The average surface temperature was calculated from the infra red recordings and plotted against interaction time. Figure 8.1 illustrates the different scabbling behaviour that can be identified from the average surface temperature-time histories. The initial heat rate can be identified, which is followed by a sudden drop in the average surface temperature. The temperature at which this occurs is defined as the temperature at the onset of scabbling. Any drop in the average surface temperature is a result of hot material being removed from the surface, revealing the cooler material beneath, i.e. scabbling. The magnitude of the average surface temperature fluctuations indicates the size (area and thickness) of the fragments ejected. A steady rate of scabbling is characterised by low rate of increase in surface temperature. This can happen with a high frequency of small temperature fluctuations, which indicates frequent ejection of small fragments or, if the scabbling is delayed, a rise of temperature until stresses (due to pore pressure and/or steep thermal stress gradients build up) reaches the tensile strength of the material, resulting in less frequent ejection of larger fragments, and consequently larger drops in surface temperature. Both cases are characterised by a low rate of increase in average temperature, as a result of increase in the background temperature. When the temperature fluctuations reduce or stop, this shows that scabbling has reduced or stopped. Once scabbling stops and material is no longer being removed from the surface, the surface of the specimen is exposed to the laser for a longer period, which induces a sharp increase in the average surface temperature, resulting in decarbonation of coarse limestone aggregate, and vitrification of quartz sand in mortars and coarse basalt aggregate in concretes.

The time histories of the average surface temperature and the volume removal due to laser interaction have been the main parameters used for analysis of the test data in this

study.

8.2 The source of the driving force and the effect of coarse aggregates

The comparison between the response of hardened cement paste, mortar and concrete (identified in the preliminary study and investigated in more detail in the second test series) indicated that the source of the driving force of laser scabbling in concretes is in the mortar, rather than the coarse aggregates or the mortar-aggregate interface. It can be seen from Figure 8.2a that the mortars experienced more volume removal than limestone concrete, and the limestone rock exhibited a negligible amount of volume removal. In simplistic terms the limestone concrete is a combination of limestone rock and mortar. As the rock does not scabble, but the mortar does scabble (more than the concrete), it follows that the driving force of laser scabbling in concretes originates in the

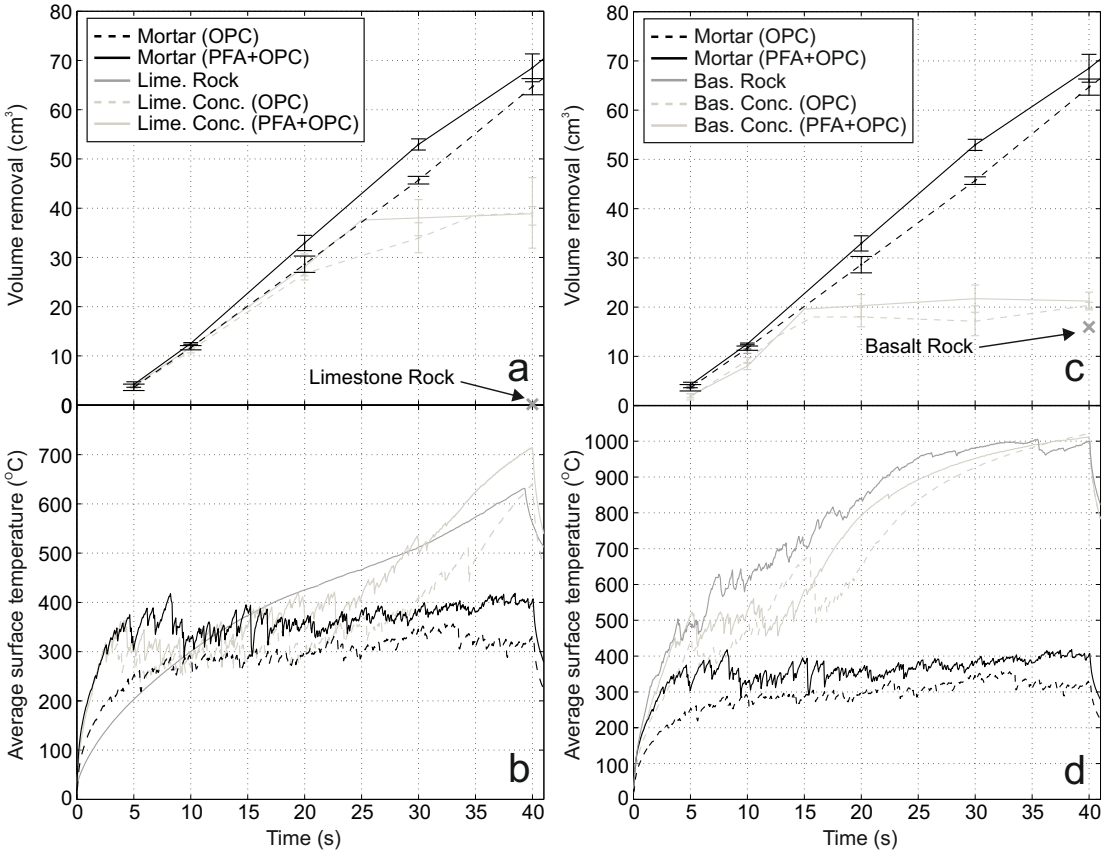

FIGURE 8.2: Results highlighting the origin of the driving force in laser scabbling of concretes, taken from the second test series (Chapter 5), : (a) Volume removal and (b) average surface temperatures of the mortars, limestone concretes, and limestone rock specimens; (c) volume removal and (d) average surface temperatures of the mortars, basalt concretes, and basalt rock specimens.

mortar, and that the limestone aggregate acts as reinforcement in the mortar matrix, reducing the scabbling.

The behaviour of limestone rock compared to limestone concrete (discussed in Chapter 5), and the fact that mortars and pastes scabbled more successfully than limestone concrete proves that the decarbonation of calcium carbonate in the aggregate is not responsible for laser scabbling, contrary to what was suggested by Blair [17].

The same logic can be applied to the basalt concrete (Figure 8.2c). The mortar scabbles more than the basalt concrete, which scabbles more than the basalt rock. As the basalt rock experiences some scabbling it could be assumed that the basalt rock aides the scabbling process. The basalt rock, however, introduces another mechanism: reinforcement of the mortar matrix, which hinders laser scabbling, leading to increase in surface temperature which then leads to vitrification of the basalt (and mortar) and prevents further scabbling. Overall it can be concluded that the mortar supplies the primary driving force, with the basalt aggregate providing some secondary mechanisms.

MacCallum and Norris [19] suggested that the build up of strain in the interfacial transition zone between the cement paste and aggregates was responsible for laser scabbling. This may be true for the mortars but the fact that pastes scabbled so successfully, and that moisture content and permeability are key factors suggests that this is not the only mechanism, and not even the primary mechanism.

There are two factors that could be responsible for the reduced rate of volume removal in concretes, compared to the linear rate of volume removal in mortars.

(i) Replacing the mortar with coarse aggregates in concretes directly reduces the primary driving force available, reducing scabbling. There is a higher proportion of mortar than coarse aggregate at the surface, and as a result, the scabbling behaviour of concretes is similar to that of the mortar at low interaction times. This is illustrated by the average surface temperature behaviour (Figure 8.2b and d). As the surface is removed, the coarse aggregate proportion increases, and the scabbling behaviour resembles that of the rock.

(ii) As more coarse aggregate is exposed, laser interaction with the coarse aggregates causes detrimental mechanisms to take place, such as calcium carbonate decarbonation or vitrification. Basalt readily vitrifies forming a vitrified layer that prevents further scabbling (Chapter 5). The short trials with a pulsed laser beam (Appendix G), have indicated that changing the laser configuration could overcome the problems of vitrification. However, this was only a short trial, and more work is needed to confirm this finding.

8.3 Pore pressure spalling

The results of tests involving different degrees of saturation and materials of different permeabilities, suggest that pore pressure spalling is the dominant mechanism responsible for providing the driving force of laser scabbling. This supports Li's [18] suggestion that laser scabbling occurs as a result of vaporisation of free water.

8.3.1 Effect of the degree of saturation

The results from the investigation into the effect of free water on laser scabbling of mortars (Chapter 6) are presented in Figures 8.3a–c. The difference in volume removal between the specimens oven dried at 105 °C and the non oven dried specimens (and the oven dried at 50 °C), suggests that the absence of free water hinders scabbling of mortars. The fact that the volume removal of the resaturated specimen was similar to that of the saturated specimen, after 10 s laser interaction, suggests that damage which occurred during oven drying did not affect scabbling, contrary to what was suggested by Dowden [70]. The resaturated specimen did not continue scabbling after 8 s laser interaction (Figures 8.3b) because of the limited depth of saturation, after 48 hours submersion in water (Figure 8.3d).

Figure 8.3f shows the volume removal results from the prolonged drying investigation reported in Chapter 7. It shows that the PFA+OPC paste (P), limestone concrete (LC) and basalt concrete (BC) specimens experienced large reductions in volume removal as a result of prolonged drying. This shows that a reduction in free water reduces scabbling in concretes.

Figure 8.4a displays the volume removal results of the prolonged drying investigation (Figure 8.3f), and the investigation into the effect of free water content in mortars (Figure 8.3a), after 40 s laser interaction, plotted against the initial degree of saturation. Although there are only three data points for each composition from the prolonged drying investigation, the higher volume removal for lower degrees of saturation in some compositions (basalt concrete, BC; OPC paste, O; and the mortar, M) suggests that an optimum initial degree of saturation exists below 100%.

The results of the investigation into the effect of free water content in mortars presented in Figure 8.4a (triangles), where there are more data points, identifies that an optimum degree of saturation for the PFA+OPC mortar composition exists between 63 and 78% (shaded area). For 10 s laser interaction it can be seen that an optimum degree of saturation exists between 57 and 67% (shaded area in Figures 8.4b). Figure 8.4a suggests that the resaturated specimen (black triangle) does not follow the degree of

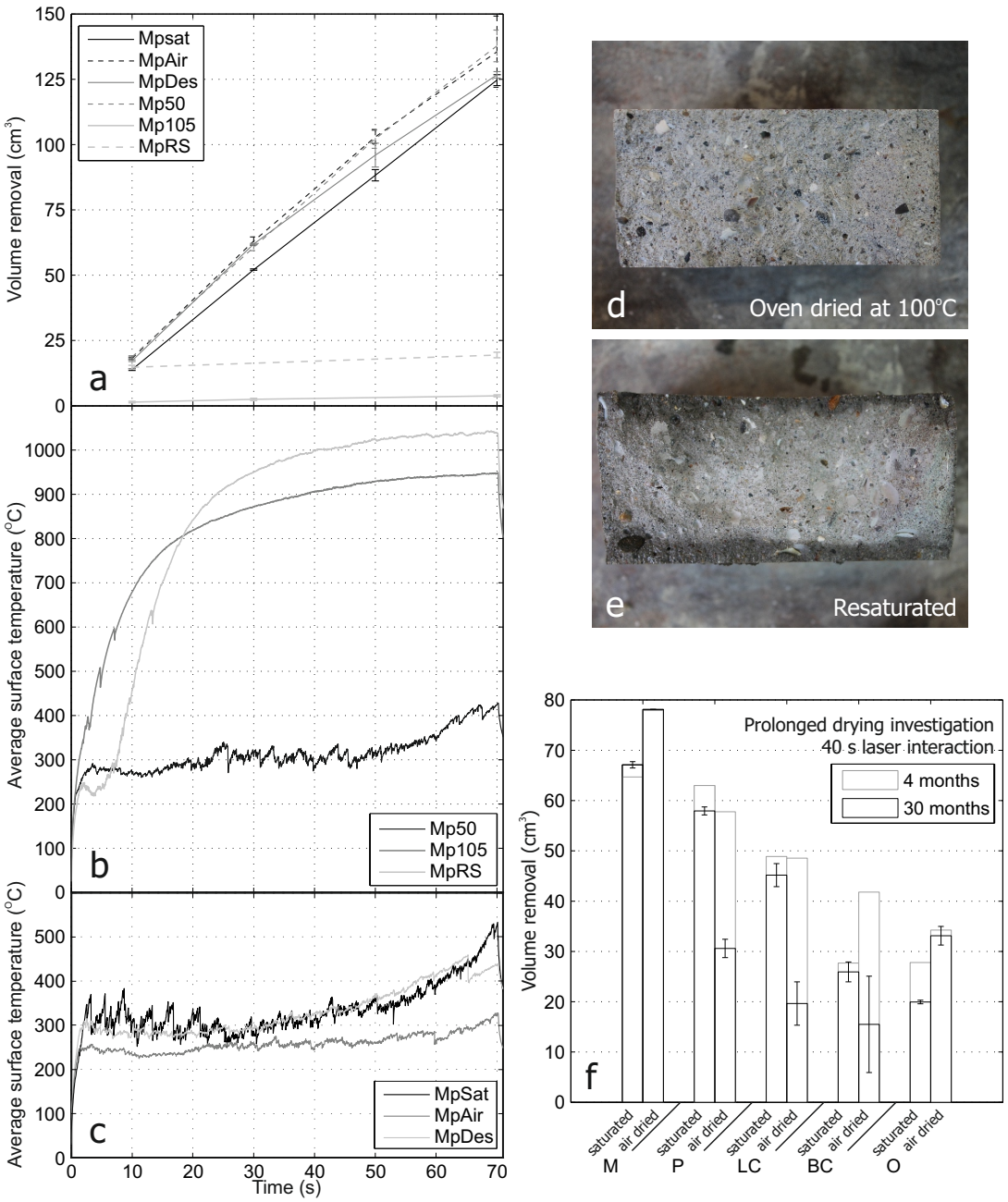

FIGURE 8.3: Results highlighting the role of degree of saturation in laser scabbling. (a–c) Results of the free water investigation (Chapter 6): (a) volume removal; (b) average surface temperatures of specimens oven dried at 50 °C (Mp50) and 105 °C (Mp105), and those resaturated after being oven dried at 105 °C (MpRS); (c) average surface temperature results of the saturated (MpSat), air dried (MpAir) and dessicated specimens (MpDes). (d-e) Cross sections of the specimens (d) oven dried at 105 °C and (e) resaturated. (f) Volume removal results of the prolonged drying investigation (Chapter 7). M in (f) is the same composition (Mp) as in (a–e).

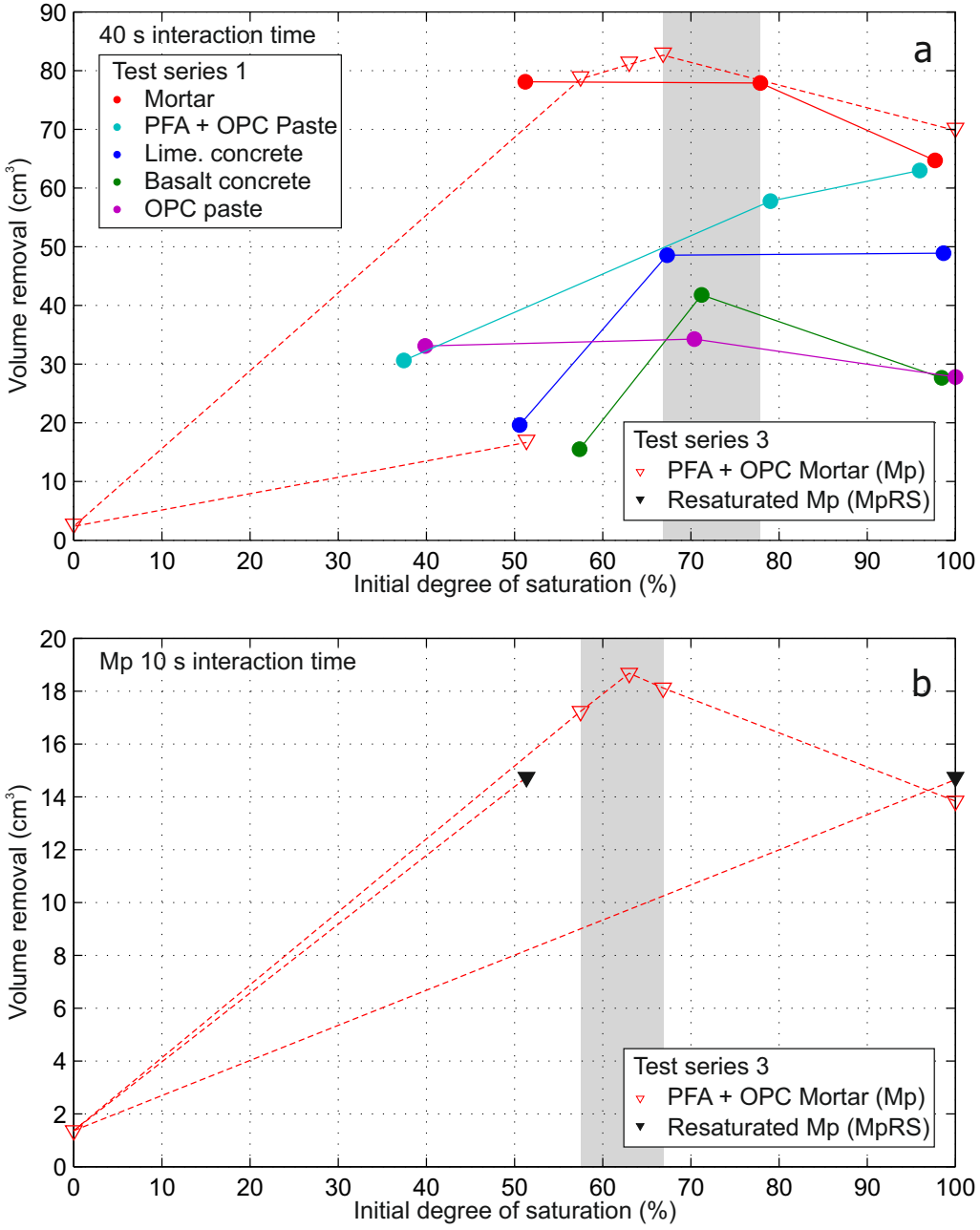

FIGURE 8.4: Volume removal results of specimens with different degrees of saturation (from Chapters 6 and 7) plotted against degree of saturation: (a) after 40 s interaction time (only the older/30 month saturated results are presented), and (b) 10 s laser interaction time results from free water content investigation (Chapter 6). Shaded areas identify the optimum degree of saturations.

saturation–volume removal relationship. The reason for this is that the resaturated specimen stopped scabbling after 8 s (Figures 8.3b), the time at which the saturated surface layer was removed. Figure 8.4b presents the volume removal results after 10 s plotted against the initial degree of saturation. The volume removal of the resaturated specimen is plotted at a degree of saturation of both 51% (average degree of saturation of the whole specimen) and 100% (the estimated degree of saturation of the surface layer, as seen in Figure 8.3d, that was removed in the first 8 s of laser interaction). If the volume removal of the resaturated specimen is assumed to be at a degree of saturation of 100% it suggests that any thermal damage, due to oven drying at 105 °C, did not affect scabbling.

Figure 8.5 shows the average surface temperature results of the prolonged drying investigation (Chapter 7). It can be seen that the effects of prolonged drying on scabbling behaviour vary depending on the composition, although it should be noted that the degree of saturations also vary between the compositions.

Prolonged drying has little effect on the average surface temperatures of the basalt concretes (Figure 8.5a), however, due to the poor repeatability of the results for PFA+OPC basalt concrete (discussed in Section 7.5) the temperature-time history presented here for air dried specimens experienced similar volume removal to the saturated specimens.

The saturated mortar undergoes much larger, less frequent temperature fluctuations compared to the air dried, with lower volume removal. It is suggested in Section 6.4.4 that this is a result of the increased thermal conductivity of the saturated specimens, meaning the driving force required for scabbling forms over a larger area and a longer timescale.

Prolonged drying causes the hardened cement pastes to scabble in much larger fragments compared to the behaviour of the saturated specimens. While this behaviour reduces the volume removal of the PFA+OPC paste, it increases the volume removal of the OPC paste, suggesting scabbling of the two pastes is governed by different mechanisms. The low permeability of the PFA+OPC pastes allows pore pressure build up, causing spalling to occur. The reduction in the degree of saturation reduced the driving force in the specimen, reducing the volume removal and increasing the surface temperatures. The high permeability of the OPC paste, however, means pore pressure spalling is far less effective, and that scabbling of OPC pastes is less sensitive to the degree of saturation.

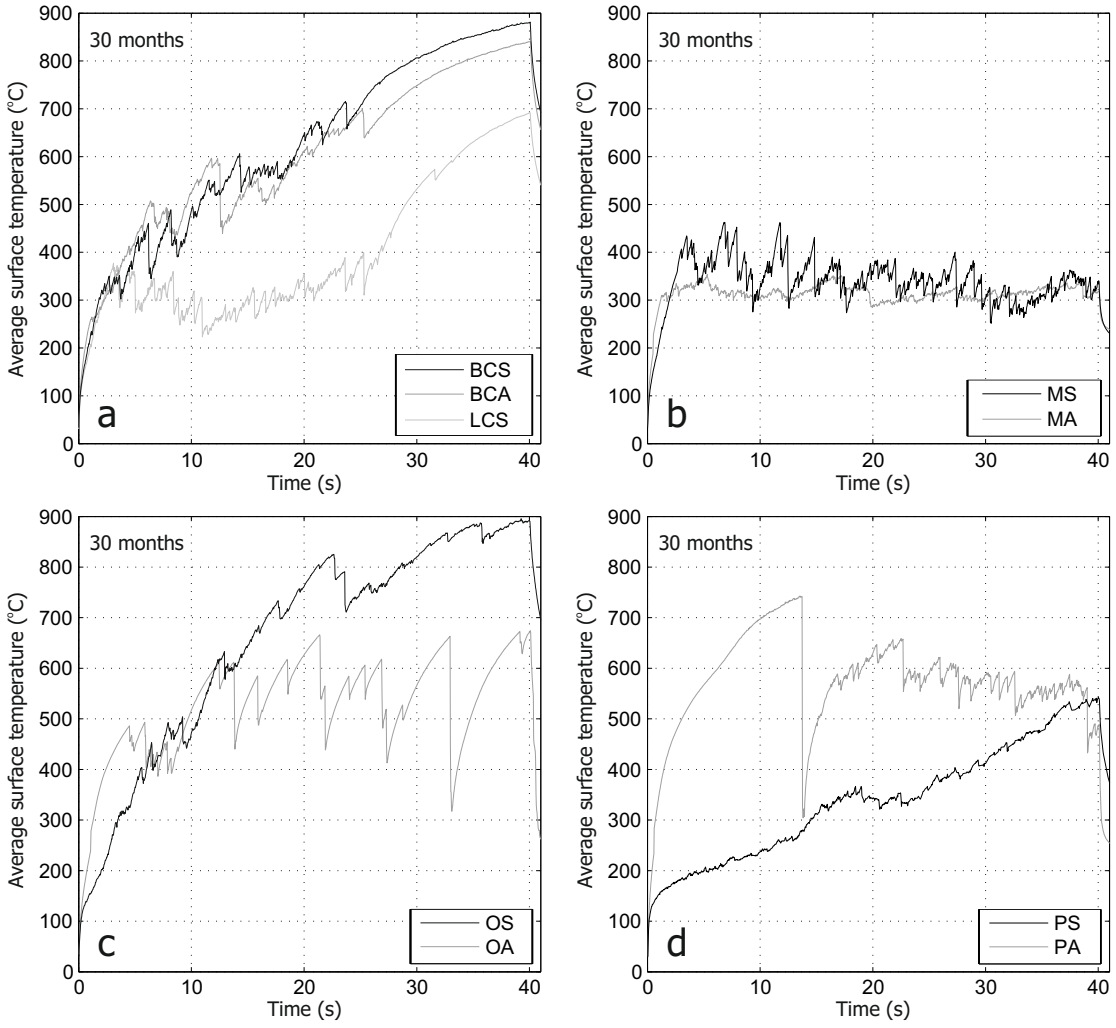

FIGURE 8.5: Average surface temperature results of specimens tested in the prolonged drying investigation (Chapter 7): (a) basalt and limestone concretes, (b) mortars, (c) OPC pastes and (d) PFA+OPC pastes.

8.3.2 Effect of permeability

Permeability is a key factor in pore pressure development and consequently in laser scabbling. Permeability is a measure of the interconnectivity of pores, which controls how easily a fluid can flow through a material. In terms of laser scabbling, the movement of water vapour is of primary concern.

A material of low permeability will restrict the movement of water vapour, allowing pore pressures to build more quickly causing fragments to be ejected more often and at lower temperatures. Higher permeability, on the other hand, allows water vapour to escape more easily, reducing pore pressures and reducing the efficiency of laser scabbling. As the rate of scabbling is lower in a material of high permeability, the surface is removed less often allowing a rise in surface temperatures. This causes more water vapour to

be liberated from greater depths, eventually leading to rise of pore pressures to levels required for scabbling to occur, albeit in less frequent and larger fragments.

The effect of permeability has been investigated throughout the study, by using 25% PFA replacement and altering the w/b ratio. It is well known that using PFA and reducing the w/b ratio in cementitious materials will reduce permeability [28]. It should be noted that reducing the w/b ratio also increases the strength, which in relation to laser scabbling, maintains low permeability, by delaying crack formation, and increases the tensile strain energy, important for the explosive nature of the process.

The effect of w/b ratio on laser scabbling of cement pastes was investigated in the second test series (Chapter 5 and Figures 8.6a and b) and on scabbling of mortars in the third test series (Chapter 6 and Figures 8.6c–e). The results of changing the w/b ratio were consistent throughout the study: a higher w/b ratio resulted in lower volume removals, higher average surface temperatures and larger, less frequent fragments (i.e. larger and less frequent temperature fluctuations).

The effect of 25% PFA replacement was investigated in all three test series. It was tested for cement pastes in the first and second test series (Chapters 4 and 5), for mortars in the second and third test series (Chapters 5 and 6) and for concretes in the second test series (Chapters 5). For all compositions the volume removal due to scabbling is higher in specimens that include PFA (Figures 8.6a and c, and Figures 8.2a and c), but the effect of PFA on the average surface temperature behaviour is not as straight forward. For the pastes, the absence of PFA resulted in lower volume removals, higher average surface temperatures and larger, less frequent temperature fluctuations (Figures 8.6a and b). In mortars (Figures 8.6c–e) and concretes (Figures 8.2a–d), PFA causes slightly higher average surface temperatures, including higher temperatures at the onset of scabbling, and larger temperature fluctuations. This suggests that mortars and concretes with PFA scabble in larger fragments, which ultimately results in larger volume removals, whereas, the PFA+OPC pastes scabble more frequently with smaller fragments, resulting in greater volume removal compared to the OPC pastes.

8.4 The reinforcement effect

The influence of fine aggregate on laser scabbling has been highlighted in each test series. In the first test series (Chapter 4) the mortar (MA and MS, air-dried and saturated) experienced higher volume removal than the PFA+OPC pastes (PA and PS). In the second test series (Chapter 5) differences in the average surface temperature behaviour

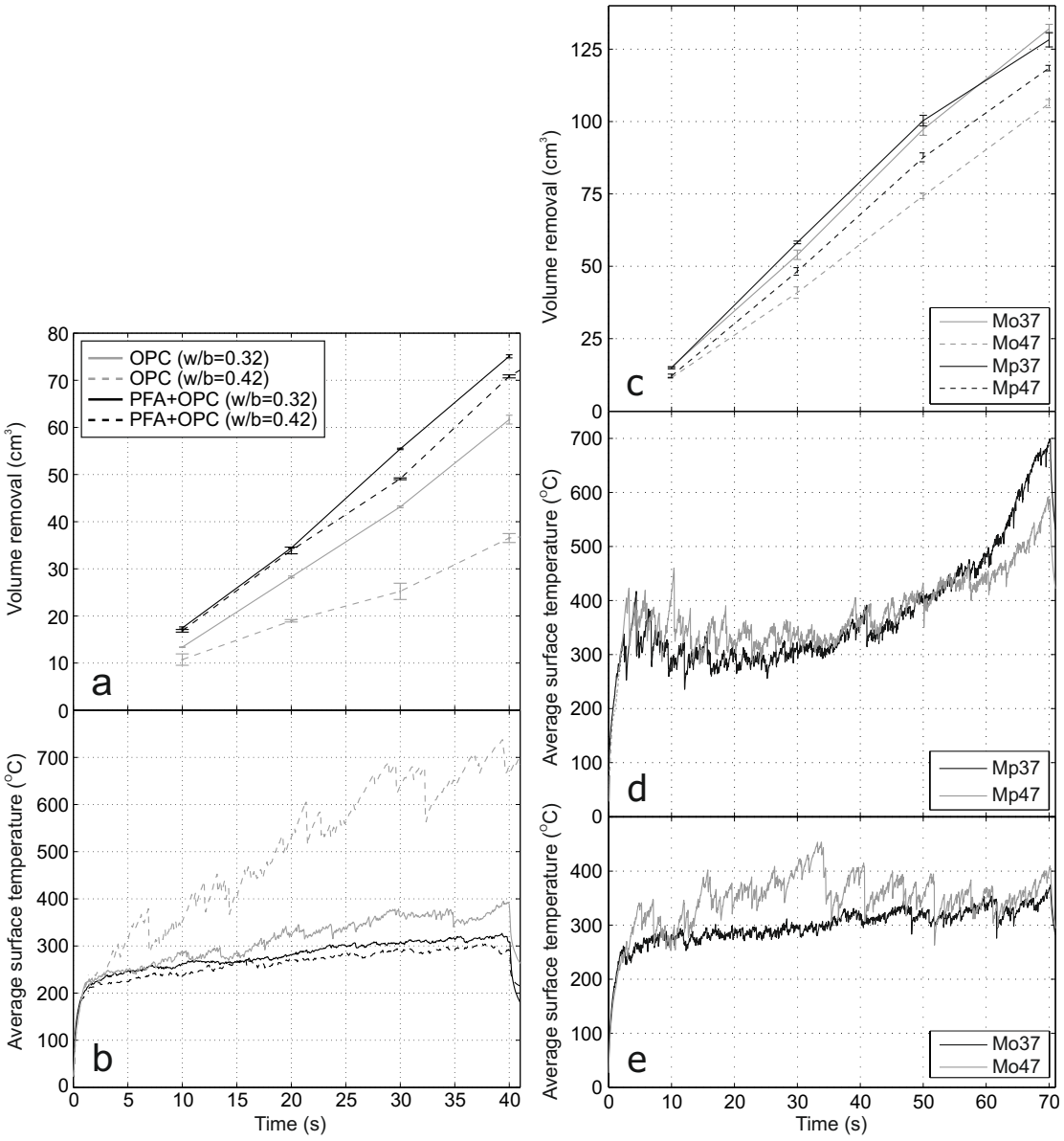

FIGURE 8.6: Results highlighting the effect of permeability on laser scabbling: (a) volume removal results and (b) average surface temperature results of cement pastes tested in the second test series (Chapter 5); (c–e) results of the water/binder ratio investigation in test series 3 (Chapter 6); (c) volume removal; (d) average surface temperatures of PFA+OPC mortars with w/b ratios of 0.37 (Mp37) and 0.47 (Mp47); (e) average surface temperature results OPC mortars with w/b ratios of 0.37 (Mo37) and 0.47 (Mo47).

of the PFA+OPC mortars and $(PFA+OPC)_{42}$ ($w/b = 0.42$) pastes were identified (Figure 8.7c). The mortars exhibit higher temperature at the onset of scabbling and larger temperature fluctuations than the pastes. The greatest effect of fine aggregates, in the second test series, was identified by the comparison between the OPC mortar and OPC_{42} paste (Figures 8.7a and b). The results show that the addition of fine aggregates to the OPC paste dramatically increased volume removal and reduced the average surface temperatures and temperature fluctuations to act more like $(PFA+OPC)_{42}$ paste (and PFA+OPC mortar).

In the third test series, the effect of fine aggregate content was investigated in more detail. The results of mortars with different fine aggregate contents (Figures 8.7d–f) show that a higher fine aggregate content increases the temperature at the onset of scabbling and the general average surface temperatures throughout the interaction times tested. Most importantly, the temperature fluctuations increase in size with aggregate content indicating that much larger fragments are ejected.

As the oven dried specimen in the free water content investigation did not scabble despite containing fine aggregates, this suggests that fine aggregate content enhances pore pressure spalling rather than directly contributing to the driving force of laser scabbling. The reason for this enhancement, is the introduction of a reinforcing effect, which increases the tensile strength and the resistance to scabbling. This causes higher temperatures to be reached, which provide more driving force/higher pore pressures, to induce larger fragment ejection and increase volume removal. An additional mechanism contributing to laser scabbling is the effect of increased thermal conductivity due to increased fine aggregate content which was discussed in Section 6.4.4.

8.5 The effect of age

The main effect of ageing was a result of the reduction in the degree of saturation of specimens caused by prolonged drying, as discussed in Section 8.3.

The stand out result of the age investigation on saturated specimens was the reduction in volume removal and change in average surface temperature behaviour of the OPC paste compositions. Figure 8.8 shows that the older OPC paste specimens (both w/b ratios) experienced lower volume removals, higher average surface temperatures and larger temperature fluctuations. The most dramatic change was seen in the OPC_{32} specimen, which at the younger age scabbles successfully in a similar manner to the PFA+OPC pastes.

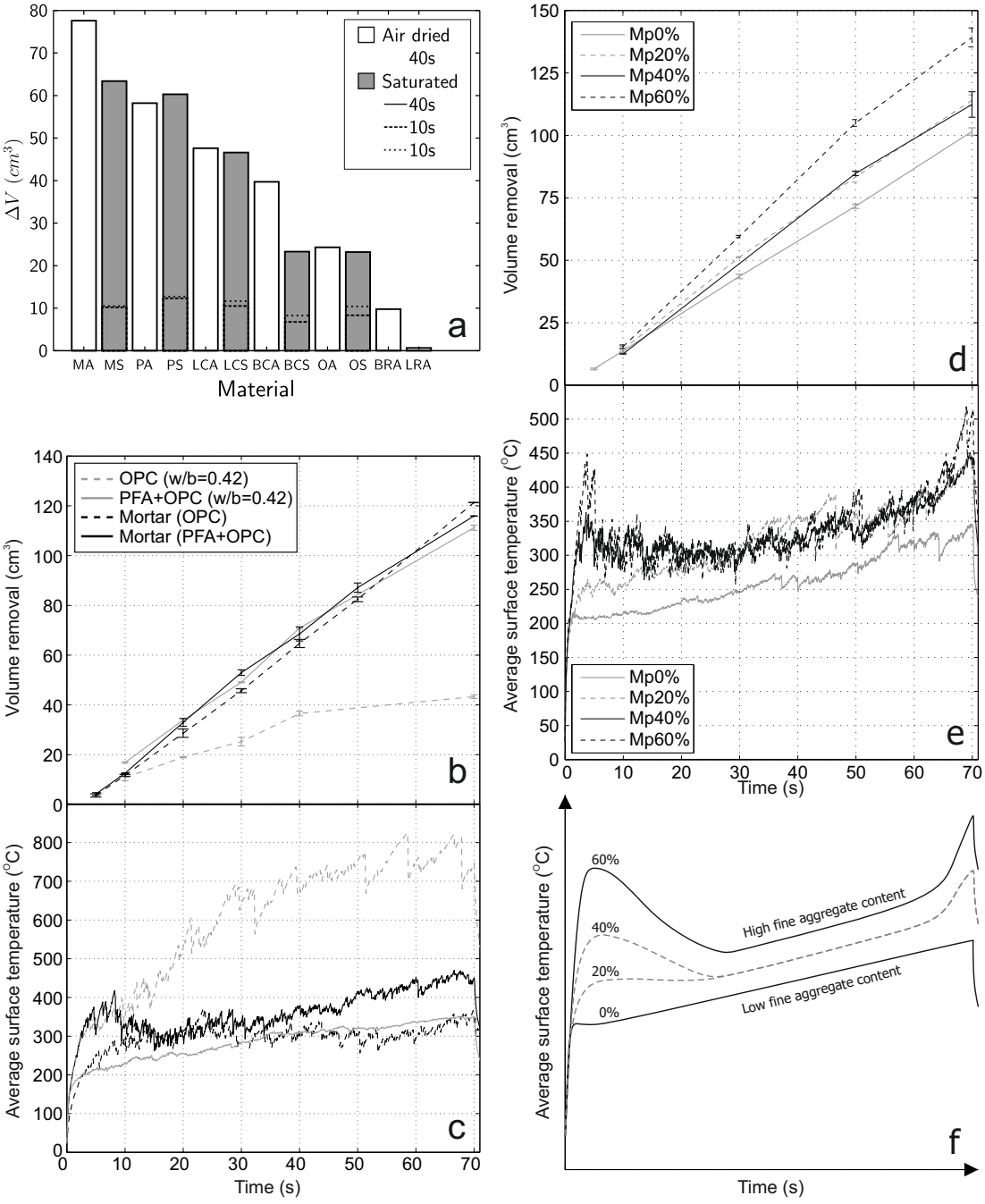

FIGURE 8.7: Results highlighting the reinforcement effect due to fine aggregates: (a) volume removal results from the first test series (Chapter 4); (b) volume removal results and (c) average surface temperature results of pastes and mortars from the second test series (Chapter 5); (d) volume removal results and (e) average surface temperature results of the fine aggregate content investigation, specimens with fine aggregate content ranging from 0% to 60% (Mp0% ,Mp20%, Mp40% and Mp60%), and (f) a simplified graph showing average surface temperature behaviour for mortars of different aggregate contents.

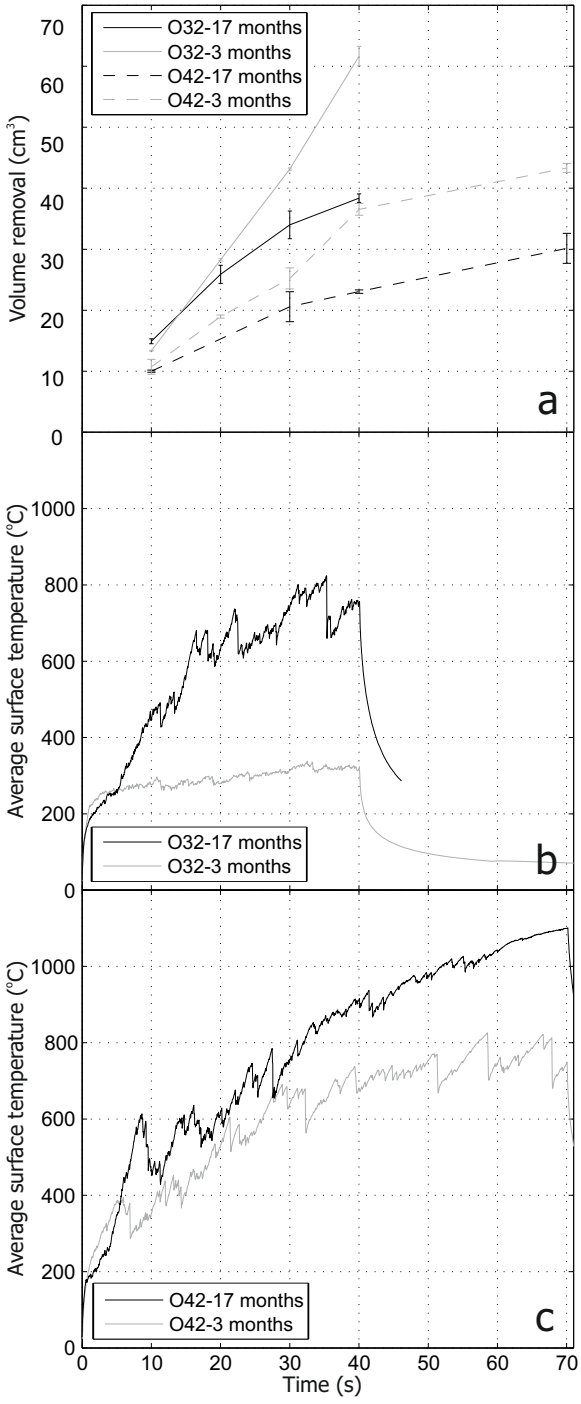

FIGURE 8.8: Saturated OPC paste results from the age investigation (Chapter 7): (a) volume removal, (b) average surface temperature results for OPC_{32} pastes and (c) average surface temperature results for OPC_{42} pastes.

The results of the other compositions in the age investigation on saturated specimens showed that age made little difference, thus validating the results of the first and second test series.

8.6 Repeatability

The first three test series (Chapters 4, 5 and 6) showed no evidence of the stochastic behaviour reported in previous studies [2, 3, 16, 19]. The investigation into the effects of age (Chapter 7), however, indicated that stochastic behaviour may be present in the PFA+OPC basalt concrete composition and that it increases with age, although this requires further investigation due to the limited number of repeats carried out in that part of the study. These results suggest that stochastic behaviour may not be a characteristic of laser scabbling, but a phenomenon that can be restricted, perhaps by reducing variability of materials, especially when the materials are particularly sensitive to laser scabbling, as basalt aggregates are known to be.

8.7 Laser scabbling of existing materials

8.7.1 Degree of saturation

The most important finding from this study, in relation to the practical application of laser scabbling, is the importance of free water within the concrete. The results of the prolonged drying investigation illustrated that 30 months of air drying dramatically reduced the effectiveness of laser scabbling on concretes. While it is true that the small specimen size tested in this study would have accelerated the drying process, it is important to remember that the age of concrete that is to be decommissioned will most likely to be in the range of 80–100 years old.

This suggests that the conditions to which the concrete is exposed during its working life can have a dramatic effect on its susceptibility to laser scabbling. Concrete stored at elevated temperatures (like the concrete taken from a chimney and tested by Nyguen [2]) will experience drying (a reduced degree of saturation) which will reduce scabbling. Before laser scabbling is used, the degree of saturation of the concrete should be determined to assess the susceptibility to laser scabbling.

8.7.2 Resaturation

The results of the investigation into the effect of free water content in mortars suggest that resaturation could be used to overcome the problems of prolonged drying in concrete. However, the same results did indicate the difficulty of resaturating concrete. The use of a high pressure technique may be required to increase the resaturation depth, but this could also drive contamination deeper into the concrete.

8.7.3 Basalt/whinstone aggregate

The largest nuclear site in the UK is Sellafield, Cumbria. The local rock in this area is Whinstone, a type of basalt (and where the basalt used in this study was sourced). As a result a large proportion of the concrete to be decontaminated is made of basalt aggregates. This study has shown that basalt concrete performs badly during scabbling, however, further work on the promising results of the pulsed/modulated trials (Appendix G) may overcome this problem.

8.8 The design of materials to be scabbled

The results of this study have shown that mortars are more susceptible to laser scabbling than the other materials tested, however, mortar is not a structural material. A low permeability (low w/b ratio and including PFA) and high fine aggregate proportion will enhance the scabbling ability of a mortar further. The low permeability will also help reduce water loss (and prevent ingress of contamination). Adding a sacrificial layer of mortar to structural concrete for decontamination purposes, may be a viable option.

In terms of scabbling structural materials, limestone concrete is much more susceptible to laser scabbling than basalt concrete, although the possibilities explored during the pulsed/modulated beam trials may overcome the problem of vitrification in basalt concrete. A mix design that incorporates PFA, a low w/b ratio and a high fine aggregate proportion will enhance the scabbling process.

As free water is necessary for laser scabbling, methods of sealing the surface of concrete should be explored, to try and limit the drying process.

Chapter 9

Conclusions and further work

9.1 Conclusions

(I). Increasing the degree of saturation in cementitious materials (Chapters 6 and 7) and altering the composition in a manner known to reduce the permeability (Chapters 4, 5 and 6), namely by increasing the PFA content or reducing the w/b ratio, results in larger volume removals during laser scabbling. These observations strongly suggest that pore pressure spalling is the predominant mechanism responsible for laser scabbling of cementitious materials.

(II). A comparison between laser scabbling tests on cement pastes, mortars, concretes and solid rock specimens (Chapters 4 and 5) indicates that the driving force responsible for laser scabbling of concretes originates in the cement paste, but it is strongly affected by the addition of fine aggregates (mortar).

(III). A higher content of fine aggregates increases the size of fragments ejected during laser scabbling of mortars which results in greater volume removals (Chapter 6). The results are explained in relation to a reinforcement effect created by the fine aggregates which increases the tensile strength of the mortar, causing scabbling to be delayed until a fracture plane at a deeper position is formed, causing larger fragments to be ejected less frequently, which is more efficient than smaller, more frequent ejections. The reinforcement effect of the larger coarse aggregates, however, reduces the volume removal of scabbling because their larger size results in fracture planes having to pass through coarse aggregates, requiring larger forces to be developed for a similar fragment size and ultimately a similar volume removal (Chapter 5).

(IV). Mechanisms caused by laser interaction with the coarse aggregates, such as vitrification or decarbonation, reduce the volume removal during laser scabbling (Chapters 4, 5 and 6). Different laser configurations (pulsed and/or modulated), however, may overcome the problem of vitrification in basalt concretes (Appendix G).

(V). Results of thermal analysis techniques (DTA/TGA), combined with observations of temperatures recorded during laser scabbling, suggest that calcium carbonate decarbonation and the α-quartz to β-quartz inversion are not the primary mechanisms responsible for laser scabbling, as these processes occur at temperatures that are higher than the temperatures at the onset of scabbling for all materials (Chapter 4).

(VI). The relationship between saturation and volume removal during laser scabbling is not linear; results suggest an optimum degree of saturation for maximum volume removal exists below 100% saturation (Chapters 6 and 7).

(VII). The experimental procedure used throughout this study has demonstrated that infra red recordings can be used to successfully monitor laser scabbling behaviour.

(VIII). Stochastic behaviour reported in previous studies has largely been absent from this study (Chapters 4, 5 and 6), suggesting that it is not a characteristic of laser scabbling but a result of variability in the materials scabbled (Chapter 7) or problems with the experimental procedure used.

(IX). In terms of considerations for the practical application of using laser scabbling on existing materials, the importance of the degree of saturation and the permeability of the concrete has been highlighted (Chapters 6 and 7). As a result, consideration of the conditions to which concrete is exposed to during its working life should be made before laser scabbling is used, with emphasis made on processes related to drying and cracking. Furthermore, this study has noted that basalt aggregate concrete is less susceptible to scabbling than limestone concrete (Chapters 4 and 5). As a result, careful consideration should be made in relation to the type of coarse aggregate used in concretes to be scabbled.

(X). In relation to the design of materials to be scabbled, the results of this study indicate that a low permeability (low w/b ratio and including PFA) and a high proportion of fine aggregate will enhance scabbling (Chapters 4, 5, 6 and 7). It has been noted that the high susceptibility to laser scabbling of mortars makes adding a sacrificial layer of mortar to structural concrete, for decontamination purposes, an attractive option.

9.2 Further work

Prior to this study, research on laser scabbling was sparse. This study investigated some key issues but there are still many aspects of laser scabbling that require further work. In this section some areas in which the research could be continued are suggested.

9.2.1 Pulsed/modulated trials

One of the biggest problems regarding the use of laser scabbling in nuclear decommissioning in Britain is the problem with basalt concrete. The problem of vitrification of basalt concretes during laser scabbling (highlighted in Chapters 4 and 5) must be overcome if laser scabbling is to be used on this type of concrete. Laser scabbling of basalt concrete is of particular interest as much of the concrete at Sellafield, the UK's largest nuclear facility, is likely to be made up of basalt concrete. The preliminary trials on pulsed/modulated beam carried out in this study (Appendix G) suggest that altering the laser configuration may overcome the problem of vitrification in basalt concretes during laser scabbling. A detailed investigation on the effect of different laser configurations on laser scabbling of basalt concretes should be carried out.

9.2.2 Degree of saturation

The investigation into the effect of moisture content carryed out in this study has indicated that there is a different optimum degree of saturation for different compositions. In order to identify these, a detailed investigation should be carried out where small variations of the degree of saturation are tested for different compositions. For example, degrees of saturation ranging from 0–100% with 10% intervals. In a practical sense, it would be highly beneficial to ascertain the upper and lower limits of degree of saturation required for laser scabbling to occur.

9.2.3 Modelling

Modelling of concrete at high temperatures is notoriously difficult as there are so many interconnected chemical-hygro-mechanical processes involved. This study has yielded a wealth of results that could be used to validate models of laser scabbling of concrete in the future.

If a working computer model of laser scabbling of concrete was developed, it could be used in a number of ways. In terms of the fundamental science behind laser scabbling, it

would be useful to model the the development of pore pressures within the concrete and assess the interaction between permeability, degree of saturation and concrete strength. In practical terms, modelling could be used to assess the processing parameters to maximise the efficiency of laser scabbling without carrying out large, costly experimental programmes.

References

[1] E. Johnston and J.T. Spencer. High power nd:yag scabbling of concrete. 1st progress report. Technical report 88277/48/98, TWI Ltd, Granta park, Cambridge, December 1998.

[2] L. Nguyen. Removal of surface concrete with high power yb fibre lasers. Technical report 17800/1/07, TWI Ltd, Granta park, Cambridge, October 2007.

[3] P. Hilton. Scabbling of dry and wet concrete and submerged concrete. Technical report 18039/1/08, TWI Ltd, Granta park, Cambridge, December 2008.

[4] Y. Fu and L. Li. Study on mechanism of thermal spalling in concrete exposed to elevated temperatures. *Materials and structures*, 44(1):361–376, 2011.

[5] G.A. Khoury and Y. Anderberg. Concrete spalling review. Technical report, Swedish national road administration, June 2000.

[6] Z. P. Bazant and G. Cusatis. Concrete creep at high temperature and its interaction with fracture: recent progress. In *Creep, shrinkage and durability of concrete and concrete structures: CONCREEP 7: September 12-14, Nantes, France*, pages 143–149. Laser Institute of America, Hermes Science, 2005.

[7] Y. Sertmehmetoglu. *On a mechanism of spalling concrete under fire conditions.* PhD thesis, University of London, London, July 1977.

[8] R.J. Connolly. *The spalling of concrete in fires.* PhD thesis, Aston University, 1995.

[9] H.F.W. Taylor. *Cement chemistry.* Thomas Telford Publishing, London, 2nd edition, 1997.

[10] B. Peach, M. Petkovski, J. Blackburn, and D.L Engelberg. Laser scabbling for nuclear decommissioning: Effect of concrete composition on volume removal efficiency. *Proceedings of 2nd International Symposium on Cement-based Materials for Nuclear Wastes (NUWCEM, Avignon, France)*, 2014. "to be published".

[11] Nuclear-Energy-Agency. Decontamination and dismantling of radioactive concrete structures. Technical report NEA/RWM/CPD(2010)3, Radioactive waste management committe (RWMC), July 2011.

[12] P.A. Lavdanskij, V.M. Nazarov, N.I. Stefanov, and M.V. Frontasyeva. Neutron activation analysis for determination of induced radioactivity in concrete of nuclear reactor shielding. *Journal of Radioanalytical and nuclear chemistry*, 131(2):261–270, 1989.

[13] DEFRA. Managing radioactive waste safely. proposals for developing a policy for managing solid radioactive waste in the uk. Technical report PB5957, Department for environment, food and rural affairs, London, March 2001.

[14] S.P. Burke. Concrete decontamination - a literature review. Technical report AEEW-R-2609, Winfrith, United Kingdom Atomic Energy Authority, Winfrith, March 1990.

[15] T. Hirabayashi, Y. Kameo, and M. Myodo. Application of a laser to decontamination and decommissioning of nuclear facilities at jaeri. In *Advanced High-Power Lasers and Applications*, pages 94–103. International Society for Optics and Photonics, 2000.

[16] P. Hilton. The potential of high power lasers for concrete scabbling and pipe cutting in nuclear decommissioning. Technical report 19124/1/10, TWI Ltd, Granta park, Cambridge, March 2010.

[17] K.J. Blair. *The interaction of CO_2 lasers with concrete and cement materials.* PhD thesis, University of Liverpool, Liverpool, June 1996.

[18] L. Li, W.M Steen, P.J. Modern, and J.T. Spencer. Laser removal of surface and embedded contaminations on/in building structures. In *Optics for Productivity in Manufacturing*, pages 84–95. International Society for Optics and Photonics, 1994.

[19] D.O.l. MacCallum and J.T. Norris. Laser concrete ablation scaling effects. In *ICALEO : 27th international congress on applications of lasers and electro-optics.*, pages 143–149. Laser Institute of America, 2008.

[20] M. Savina, Z. Xu, Y. Wang, M. Pellin, and K. Leong. Pulsed laser ablation of cement and concrete. *Journal of Laser Applications*, 11:284, 1999.

[21] M. Savina, Z. Xu, Y. Wang, C. Reed, and M. Pellin. Efficiency of concrete removal with a pulsed nd: Yag laser. *Journal of Laser Applications*, 12:200, 2000.

[22] A. Anthofer, W. Lippmann, and A. Hurtado. Development and testing of a laser-based decontamination system. *Optics & Laser Technology*, 48:589–598, 2013.

[23] T. Thomas, E. Johnston, and J.T. Spencer. High power nd:yag scabbling of concrete. 2nd progress report. Technical report 88277/81/02, TWI Ltd, Granta park, Cambridge, April 2002.

[24] M. Gary. Fire tests on reinforced concrete buildings. *Verlag Wilhelm Enst und sohn*, 11, 1916.

[25] S.A. Austin, P.J. Robins, and M.R. Richards. Jetblast temperature-resistant concrete for harrier aircraft pavements. *STRUCTURAL ENGINEER*, 70:427–427, 1992.

[26] Ping Zhang, Erling Nordlund, Ganesh Mainalia, Christine Saiang, Robert Jansson, and Bijan Adl-Zarrabi. Experimental study of thermal spalling of rock blocks exposed to fire. *Bergmekanik I Norden*, pages 9–12, 2010.

[27] M. Sedlenieks. Flame treatment of concrete for finishing and cleaning. *The Aberdeen Group*, 1978.

[28] A.M. Neville. *Properties of concrete. 4th and final ed.* Harlow, UK: Pearson Education Limited, 1997.

[29] Leslie Alan Ashton and SSS Bate. Fire resistance of prestressed concrete beams. In *ACI Journal Proceedings*, volume 57. ACI, 1961.

[30] U. Schneider, U. Diederichs, and C. Ehm. Effect of temperature on steel and concrete for pcrv's. *Nuclear Engineering and Design*, 67(2):245–258, 1982.

[31] K.D. Hertz. Danish investigations on silica fume concretes at elevated temperatures. *ACI Materials journal*, 89(4), 1992.

[32] S.Y.N. Chan, G.-F. Peng, and M. Anson. Fire behavior of high-performance concrete made with silica fume at various moisture contents. *ACI Materials Journal*, 96(3), 1999.

[33] H.L. Malhotra. *Spalling of concrete in fires.* Construction Industry Research and Information Association, 1984.

[34] I.W.J. Copier. The spalling of normalweight and lightweight concrete on exposure to fire. *HERON*, 24(2):1–92, 1979.

[35] Robert Jansson and Lars Boström. The influence of pressure in the pore system on fire spalling of concrete. *Fire technology*, 46(1):217–230, 2010.

[36] Jean-Christophe Mindeguia, Hélène Carré, Pierre Pimienta, and Christian La Borderie. Experimental discussion on the mechanisms behind the fire spalling of concrete. *Fire and Materials (2014)*, 2014.

[37] J.W. Dougill. *The effects of high temperature on the strength of concrete with reference to thermal spalling*. PhD thesis, Imperial College London, 1971.

[38] J. Piasta. Heat deformations of cement paste phases and the microstructure of cement paste. *Matériaux et Construction*, 17(6):415–420, 1984.

[39] British-Standards-Institution. Part 1-1: General rules and rules for buildings. *Eurocode 2: Design of Concrete Structures*, EN 1992-1-1, 2004.

[40] G. Sanjayan and L.J. Stocks. Spalling of high-strength silica fume concrete in fire. *ACI Materials Journal*, 90(2):170–173, 1993.

[41] S.Y.N. Chan, X. Luo, and W. Sun. Effect of high temperature and cooling regimes on the compressive strength and pore properties of high performance concrete. *Construction and Building Materials*, 14(5):261–266, 2000.

[42] L.T. Phan. Pore pressure and explosive spalling in concrete. *Materials and structures*, 41(10):1623–1632, 2008.

[43] Y. Anderberg. Spalling phenomena of hpc and oc. In *Proceedings of the international workshop on fire performance of high-strength concrete, NIST, Gaithersburg*, 1997.

[44] British-Standards-Institution. Code of practice for special circumstances. *Structural use of concrete - Part 2*, BS 8110-2:1985, 1985.

[45] Z. Pan, J.G. Sanjayan, and D.L.Y. Kong. Effect of aggregate size on spalling of geopolymer and portland cement concretes subjected to elevated temperatures. *Construction and Building Materials*, 36:365–372, 2012.

[46] British-Standards-Institution. Density of hardened concrete. *Testing hardened concrete*, BS EN 12390-7:2009, 2009.

[47] ISO. Condition monitoring and diagnostics of machines—Thermography—Part 1: General procedures. ISO 18434-1:2008(E), International Organization for Standardization, Geneva, Switzerland, 2008.

[48] B. Peach, M. Petkovski, J. Blackburn, and D.L Engelberg. An experimental investigation of laser scabbling of concrete. *Construction and Building Materials*, 59: 76–89, 2015.

[49] Jie Zhao, Jian-Jun Zheng, Gai-Fei Peng, and Klaas van Breugel. Prediction of thermal decomposition of hardened cement paste. *Journal of Materials in Civil Engineering*, 24(5):592–598, 2011.

[50] Gai-Fei Peng and Zhi-Shan Huang. Change in microstructure of hardened cement paste subjected to elevated temperatures. *Construction and building materials*, 22 (4):593–599, 2008.

[51] W. Czernin. *Cement chemistry and physics for civil engineers*. Bauverlag, 1980.

[52] ASTM. Standard practice for petrographic examination of hardened concrete. *C856-1995*, 1995.

[53] H.K. Hilsdorf. A method to estimate the water content of concrete shields. *Nuclear Engineering and Design*, 6(3):251–263, 1967.

[54] E.T. Stepkowska, J.M. Blanes, A. Justo, M.A. Aviles, and J.L. Perez-Rodriguez. Thermo xrd-analysis of two aged cement pastes. *Journal of thermal analysis and calorimetry*, 80(1):193–199, 2005.

[55] V. Lilkov, O. Petrov, Y. Tzvetanova, and P. Savov. Mössbauer, dta and xrd study of portland cement blended with fly ash and silica fume. *Construction and Building Materials*, 29:33–41, 2012.

[56] I. Odler and S. Abdul-Maula. Possibilities of quantitative determination of the aft-(ettringite) and afm-(monosulphate) phases in hydrated cement pastes. *Cement and Concrete Research*, 14(1):133 – 141, 1984.

[57] L. Alarcon-Ruiz, G. Platret, E. Massieu, and A. Ehrlacher. The use of thermal analysis in assessing the effect of temperature on a cement paste. *Cement and Concrete Research*, 35(3):609–613, 2005.

[58] T.Z. Harmathy. Thermal properties of concrete at elevated temperatures. *Journal of Materials*, 5(1):47–74, 1970.

[59] G.A. Khoury, B.N. Grainger, and P.J.E. Sullivan. Transient thermal strain of concrete: literature review, conditions within specimen and behaviour of individual constituents. *Magazine of concrete research*, 37(132):131–144, 1985.

[60] W.P.S. Dias, G.A. Khoury, and P.J.E. Sullivan. Mechanical properties of hardened cement paste exposed to temperatures up to 700 c (1292 f). *ACI Materials Journal*, 87(2):160–166, 1990.

[61] A. Palomo, A. Fernández-Jiménez, G. Kovalchuk, L.M. Ordoñez, and M.C. Naranjo. Opc-fly ash cementitious systems: study of gel binders produced during alkaline hydration. *Journal of materials science*, 42(9):2958–2966, 2007.

[62] V.G. Papadakis. Effect of fly ash on portland cement systems: Part i. low-calcium fly ash. *Cement and Concrete Research*, 29(11):1727–1736, 1999.

[63] Wallace Gary Ernst. *Earth materials*. Englewood Cliffs, New Jersey: Prentice Hall, 1969.

[64] B. Peach, M. Petkovski, J. Blackburn, and D.L Engelberg. The effect of concrete composition on laser scabbling. *Construction and Building Materials - under review*, 2015.

[65] Robert Jansson and Lars Boström. The influence of pressure in the pore system on fire spalling of concrete. *Fire technology*, 46(1):217–230, 2010.

[66] B. Lothenbach, K. Scrivener, and R.D. Hooton. Supplementary cementitious materials. *Cement and Concrete Research*, 41(12):1244–1256, 2011.

[67] Idawati Ismail, Susan A Bernal, John L Provis, Sinin Hamdan, and Jannie SJ van Deventer. Drying-induced changes in the structure of alkali-activated pastes. *Journal of Materials Science*, 48(9):3566–3577, 2013.

[68] RC Stein, M Petkovski, DL Engelberg, F Leonard, and PJ Withers. Characterizing the effects of elevated temperature on the air void pore structure of advanced gas-cooled reactor pressure vessel concrete using x-ray computed tomography. In *EPJ Web of Conferences*, volume 56, page 04003. EDP Sciences, 2013.

[69] S.B. Tatro. Thermal properties. *ASTM STP 169D–Significance of Tests and Properties of Concrete & Concrete-making Materials*, pages 226–237, 2006.

[70] John Dowden, Antar Lazizi, Emma Johnston, and Sebastien Nicolas. A thermoelastic analysis of the laser scabbling of concrete. *Journal of Laser Applications*, 13 (4):159–166, 2001.

[71] J. CHEN, L.and HE, J. CHAO, and B. QIN. Swelling and breaking characteristics of limestone under high temperatures. *Mining Science and Technology (China)*, 19 (4):503–507, 2009.

[72] D.L. Fillmore. *Literature Review of the Effects of Radiation and Temperature on the Aging of Concrete*. United States. Department of Energy, 2004.

[73] B. Pomaro, V.A. Salomoni, F. Gramegna, G. Prete, and C.E. Majorana. Radiation damage evaluation on concrete shielding for nuclear physics experiments. *Annals of Solid and Structural Mechanics*, 2(2-4):123–142, 2011.

[74] V.B. Dubrovskii, S. Ibragimov, M.Y. Kulakovskii, A.Y. Ladygin, and B.K. Pergamenshchik. Radiation damage in ordinary concrete. *Atomic Energy*, 23(4):1053–1058, 1967.

[75] F. Vodák, V. Vydra, K. Trtík, and O. Kapičková. Effect of gamma irradiation on properties of hardened cement paste. *Materials and structures*, 44(1):101–107, 2011.

[76] T. Ichikawa and H. Koizumi. Possibility of radiation-induced degradation of concrete by alkali-silica reaction of aggregates. *Journal of Nuclear Science and Technology*, 39(8):880–884, 2002.

[77] T.L. White, R.G. Grubb, L.P. Pugh, D. Foster Jr, and W.D. Box. Removal of contaminated concrete surfaces by microwave heating-phase i results. *WASTE MANAGEMENT-TUCSON-*, pages 745–745, 1992.

[78] L. Objois. Nithrow: A dedicated tool for d&d applications. *Decommissioning challenges ¿ Industrial reality and prospects. Avignon, France*, pages 745–745, 2013.

Appendix A

Concrete contamination

A.1 Contamination types

Burke [14] identified two methods of contamination present at nuclear facilities. The first being dry insoluble contamination such as plutonium dioxide, uranium dioxide or mixed oxide present from fuel manufacture activities. Insolubility of this contamination means contaminant penetration is limited by physical processes, grinding into concrete floors via moving heavy plant around is suggested as a possible method of intrusion. Dry insoluble contamination is generally limited to the first few millimetres of concrete, or if the surface is painted, contamination will be limited to the paint.

The second is soluble contamination; caesium is the principle constituent but in chemical extraction facilities contamination such as plutonium nitrate may be water soluble. Contaminated water is held in the porous network of concrete the same way as uncontaminated water, free or adsorbed. It seems reasonable to assume contamination depth due to soluble contamination is a function of exposure time; the longer concrete is submerged the further contaminants will protrude. A study on cores of the B29 storage pond showed that the concrete is classed as ILW from the surface to a depth of 10 mm and LLW until a depth of 120 mm.

A.2 Neutron flux

Concrete used as biological shielding is exposed to a neutron flux and can become activated, i.e. radioactive (classified as intermediate level waste [14]). Concrete used in a biological shield can become activated at depths up to 1 m from the surface of the concrete; as a result decontamination of biological shields may be beyond the capabilities

TABLE A.1: Radionuclides, and the corresponding half lives and decay modes (β=beta decay and EC=electron capture), present in concrete activated by neutron flux. All values taken from [11] unless marked with '*' which are taken from [12].

Element	Half life	Decay mode
^{41}Ca	1.03 E+05 y	EC
^{59,63}Ni	7.6 E+04 - 100.1 y	β
^{24}Na	15 y*	β
^{152,154,155}Eu	13.5 - 4.76 y	β
^{60}Co	5.27 y	β
^{55}Fe	2.73 y	EC
^{134}Cs	2.1 y	β
^{54}Mn	312 d	β
^{65}Zn	244 d	β
^{182}Ta	115 d*	β
^{46}Sc	83.3 d*	β

of laser scabbling. Elements present in concrete, that are activated by a neutron flux are summarised in Table A.1 in descending order of half lives. It should be noted that some elements may be more abundant in concrete but with relatively short half lives, making some of the trace elements the most problematic.

Lavdanskij et al [12] carried out a neutron activation analysis on portland cement and various aggregate types in search of the long lived nuclides (halflife>2days) produced from neutron activation. Quartz sand samples showed no long lived nuclides after thirteen days cooling. Radionuclides Europium 152 and 154, Cobalt 60 and Caesium 134 were common to limestone, granite and Portland cement samples, with Tantalum 182 and Scandium 46 also being present in Portland cement samples. It is noted that 80–90% of dose is limited to the first 5–10 cm of the concrete. After half a year limestone concrete used as biological shielding would have an activity of 5e–7 Gy/s.

Chen [71] used a combination of experimental and calculational methods to determine Europium, Cobalt and Caesium were the elements responsible for long lived radioactivity in neutron activated concrete. It was determined that after 40 years operation and a 25 year 'cooling off period' the dry well wall of a the Lungmen nuclear power plant could be disposed of as construction waste, whereas the activity of the reactor shield) was greater than the exemption level after 25 years.

A.3 Concrete Condition

Burke [14] identified the importance of the condition of the concrete with relation to contamination depths. Bare concrete walls will allow for much greater penetration than walls clad in stainless steel, or walls with epoxy paint applied. Nuclear grade epoxy paint is now used extensively in the industry and its effectiveness was proved by Three Mile Island studies, but it has not been used in many older facilities such as B29 or B30 at Sellafield are not. Burke also highlighted that good maintenance was required in order to ensure any remediation methods were effective.

The Three Mile Island (TMI) incident gave a unique opportunity to study the depth of water soluble contamination in concrete structures with scratched and unscratched epoxy paint [14]. The basement of the TMI nuclear power plant was left flooded with up to 2.5 m of contaminated water for over 3 years. Contaminant penetration was mainly due to caesium and strontium. Cores were taken and contamination was found to extend up to 8 mm from the surface, however where scratched this increased to several centimetres. Other studies at sites such as the Japanese Power Demonstration Reactor have proved contamination to penetrate to a maximum of 2 cm.

A.4 Environmental factors

Many factors, likely to vary from site to site, can affect the contamination depths in concrete [14]. Acidic water can cause chlorine to leach out of the cement matrix increasing permeability, however this is unlikely to be an issue as alkali conditions are usually encouraged at nuclear facilities to immobilise radionuclides present in spent fuel. The movement of water is likely to affect penetration, with stagnant water causing less penetration than turbulent. In dry conditions the humidity of the facilities will affect penetration.

A.5 Radiation damage in concrete

Radiation damage in concrete may affect the success of laser scabbling. It should be noted that any notable changes to concrete properties are only evident in the extremes of radiation exposure. Radiation can cause damage to concrete in two ways; absorption of radiation energy causing localised heating, or radiation interaction with matter which can break bonds within the concrete microstructure. Both heat and radiation damage yield similar outcomes, which Fillmore [72] found difficult to separate. Fillmore found

that low radiation doses ($< 10^{10} n/cm^3$ or $10^{10} Gy$ of gamma) have an insignificant effect on concrete over a 50 year timescale, above this, a significant reduction in compressive and tensile strengths were reported along with an increase in volume.

Radiation damage in concrete is most prominent in the aggregates. Pomoro et al [73] suggests aggregates undergo volume change as a result of radiation exposure. Fast neutrons induce changes to the lattice structure of minerals present in the aggregates. The extent of damage is dependant upon the bonding within the lattice. Covalent bonding, present in quartz for example, is more susceptible to damage than weak ionic bonding, seen in calcareous aggregates. A neutron flux of 1 x 10^{19} n/cm^2 and a gamma intensity of 10^{10} rad are identified as critical values.

Dubrovskii et al [74] reported the behaviour of an OPC sandstone concrete when exposed to temperature cycling and neutron flux simultaneously. Expansion was noted in all specimens exposed to a neutron flux. An increase in diameter in excess of 6% was noted for samples exposed to neutron fluxes in excess of 2 x 10^{20} n/cm^2. Reduction in weight and dramatic swelling result in significant reductions in density from 3–20%. This effect was accredited to the amorphous transformation of quartz present in the sandstone aggregate. Extensive damage to the concrete structure unsurprisingly led to a decrease in thermal expansion and conductivity properties. A threshold neutron flux of 5 x 10^{19} n/cm^2 is suggested, above which structural properties of concrete should not be relied upon.

Vodak [75] investigated the effect of gamma radiation, up to 1 MGy, on hardened cement paste. It was found that radiation induced carbonation, or at least increased the rate of natural carbonation. It was suggested that hydrogen peroxide produced from water radiolysis reacts with calcium hydroxide to form calcium peroxide, which in the presence of carbon dioxide, decomposes to form calcium carbonate (calcite). It is suggested that the carbon dioxide may be formed from oxidation of carbon present in PFA, but equally it may be present due to diffusion. The calcite content of concrete was seen to increase after just 0.1 MGy of radiation. Natural carbonation is known to destroy CSH gel to form hydrous silica [9].

Ichikawa [76] found that silica, present in silica-rich aggregate, increased in reactivity after radiation exposure. A positive correlation between reactivity and radiation dose was identified. The first 20 cm of a biological shield, over a 60 year lifetime, was found to be exposed to the critical dose rate due to fast neutrons, as a result, severe damage could be done to the concrete due to extensive alkali-silica reaction, possibly rendering it too damaged to scabble.

Appendix B

Comparison of contaminated concrete removal techniques

Many techniques have been investigated with the aim of removing the contaminated surface of concrete; this appendix explains the advantages and disadvantages of each.

B.1 Laser surface removal

Laser scabbling [16] - On application of a high power near infra red laser beam, with relatively low power density, to a concrete surface the explosive ejection of concrete fragments occurs. The process is thought to be a function of rapidly developed pore pressures within the concrete coupled with severe thermal gradients induced from laser interaction. The most extensive and recent research, prior to this study, was carried out by TWI Ltd (described in Section 2.1). Removal rates of 0.75 m^2/h, 5 mm depth, were reported but the depth can be altered (up to 20 mm) by differing laser parameters. The process is dependant upon concrete composition which may result in stochastic behaviour. This aspect was addressed in the present study. Laser power can be transmitted down an optical fibre several hundred metres and received by a relatively light weight process head which enables efficient remote handling.

Laser ablation [22]- Laser ablation has been extensively studied on surface decontamination of metals and coating removals, but relatively little has been done concerning decontamination of concrete. Recent work on concrete involves using near infra red, high power lasers to melt the surface while a high pressure air jet dislodges the molten material. A suction device collects the debris which cools into glassy sphere suitable for

direct disposal. Similar to laser scabbling, this technique is viable for remote handling. Anthofer reported optimum removal rates of 2 m^2/h with depths up to 5 mm.

Microwave [77] - The use of microwaves as a decontamination technique is similar to laser scabbling, except a different wavelength of electromagnetic radiation is used. Microwaves are used to heat the concrete surface non-uniformly inducing temperature gradients and high pore pressures. The wavelength of microwave radiation favours absorption of water molecules limiting the effects of concrete thermal properties and thereby peak temperatures exist within the concrete rather than the surface. Removal rates of 10.4 m^2/h with depths of 4 mm were reported. Microwave decontamination yields similar remote handling benefits to the other laser based processes.

B.2 Physical surface abrasion

There are many methods in which mechanical means are utilised to remove multiple layers of contaminated concrete until the surface is deemed uncontaminated.

Needle scaling [11] - Diamond tipped pins of different diameters and tip shapes are pneumatically driven in a reciprocating manner to chip away material. A vacuum is attached to collect debris. The slow removal rate (0.1 m^2/h, 1-2 mm depth) and high vibration exposure to workers of this technique limits its use to hard to access areas, to complement other more extensive methods.

Mechanical scabbling [11] - A surface preparation technique that has long been used in civil engineering. Pneumatic piston heads chip away at the surface, typically several are attached to a wheeled chassis to allow for manoeuvrability. A variety of sizes are commercially available, hand held or remotely controlled. The lifespan of the piston heads depends largely on their composition and the concrete composition. Scabbling generally can't be used for corners and an alternative technique, such as needle scaling, is required. Debris collection devices are attached to the machines to contain contamination. Large vibration forces make this an unpleasant task for the operator and remote handling is difficult due to large size and weight of equipment.

Shaving/milling [11] - Rotating milling drums housed in a metal box to restrict debris release are run along the concrete surface. Working depths can be adjusted with great accuracy up to a maximum depth of 5 mm and removal rates of up to 25 m^2/h. It results in very smooth surface finish. A plane surface is required for this technique and any reinforcement present will drastically reduce the lifespan of milling cutters. Different tool shapes are required for different material hardnesses. The large weight of these devices means deployment systems required can be extensive, especially for wall

or ceiling decontamination. Hand held shavers are also available with relatively low vibration exposures.

B.3 Alternative methods

High pressure water jet [11] - HPWJ has been used successfully in civil engineering applications and can remove several centimetres of concrete in one pass. The use of high pressure water can drive contamination further into the concrete matrix through pores or cracks (known as the hammering effect). Also, it is costly to treat, and difficult to contain secondary wastes, as it results in large volumes of contaminated water and aerosols.

Abrasive blasting [11] - The method of accelerating an abrasive medium towards a surface, via a rotating turbine. Traditionally used to remove a contaminant or prepare a surface for coating, the technique has been used since the 1800's and is commercially available. Different abrasive mediums can be used for different applications in the same machine giving a certain flexibility to the process. Steel grit yields a concrete removal rate of up to 2 m^2/h at a depth of 4-5 mm. Blasting can take place openly with no confinement meaning the operator requires protective clothing and post processing particle collection (useful for hard to reach areas), or a closed system can be used in which abrasives are collected and reused at the source. Wet abrasive blasting is deemed unsuitable for decontamination for radioactive surfaces for the same disadvantages as that of HPWJ. Abrasive blasting creates a very fine dust which must be confined to avoid contamination, also the abrasive medium will be radioactively contaminated creating a secondary waste. Sponge blasting is an specific abrasive medium which involves a sponge embedded with an abrasive material. The expansion and contraction of the sponge on impact has a scrubbing effect, and the loss of energy on impact means the operator does not require protective clothing.

High pressure liquid nitrogen [78] - Areva have developed a method of decontamination, scabbling and cutting using the projection of high pressure (3500 bar), supercooled (-140°C) liquid nitrogen. The liquid nitrogen has a threefold effect on the concrete: a thermal effect whereby the temperature drop causes embrittlement and decohesion of the concrete, a mechanical effect caused by kinetic energy dissipated on the material due to the high velocity of the jet, and finally, a blast effect which arises from the explosive force due to rapid expansion (by a factor of 800) as the liquid nitrogen changes state. Excellent removal rates have been reported and can be tailored to large depth removal and low rate (1 m^2/h, 30 mm) or vice versa (6 m^2/h, 5 mm). A vacuum system is used to ensure there is limited contamination release. The high pressure and low temperature

does introduce engineering challenges of containment and delivery systems, however, remotely handled tests have been carried out successfully.

TABLE B.1: A comparison of concrete decontamination techniques.

Technique	Removal rate	Benefits	Downfalls
Laser scabbling	0.75 m^2/h, 5 mm	Remote handling.	Introduction of thermal effects.
		Same technology used for alternative decommissioning activities	Stochastic behaviour.
Laser ablation	2 m^2/h, 5 mm	Remote handling.	Unlikely to work for calcareous aggregates.
		Debris ready for direct disposal.	
Microwave	10.4 m^2/h, 4 mm	Avoids thermal effects of concrete.	Large wavelength may make remote handling difficult.
Scabbling	1 m^2/h, 3 mm	Commercially available.	High vibration exposure.
		Vast knowledge base.	Alternative method required for corners.
			Remote handling difficult.
Needle scaling	0.1 m^2/h, 2 mm	Access hard-to-reach areas	Manual, high vibration exposure.
			Slow process.
Shaving/milling	25 m^2/h, 3 mm	Extensive knowledge base.	Remote handling difficult.
		Very smooth finish.	
		Accurate removal depths.	
HPWJ	Several cm in a single pass	Extensive knowledge base.	Secondary wastes.
		Large removal rates.	
Abrasive blasting	2 m^2/h, 5 mm	Extensive knowledge base.	Secondary wastes.
			Fine dust creation.
NiThrow	6 m^2/h, 5 mm	Excellent removal rate.	Engineering challenges of high pressure, low temperature medium.
	1 m^2/h, 30 mm	Remote handling.	
		Same technology used for alternative decommissioning activities.	

Appendix C

Volume removal measurements

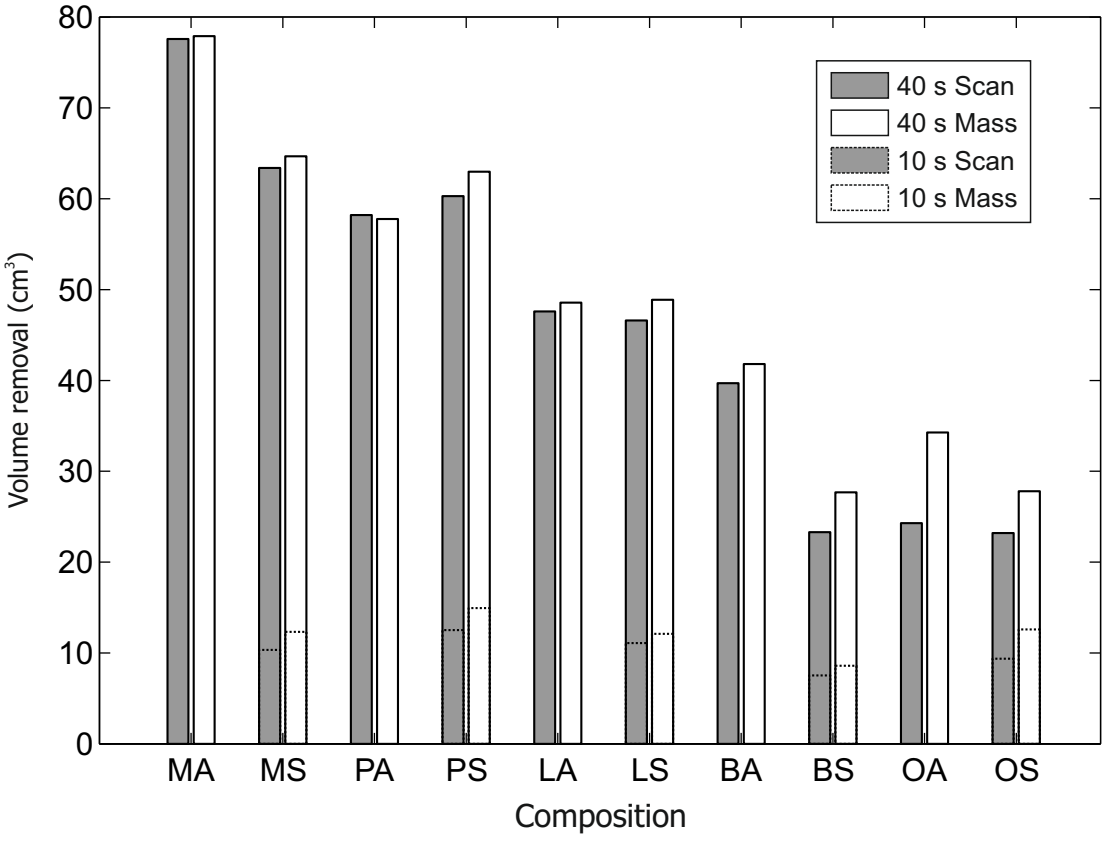

FIGURE C.1: Volume removal after 10s and 40s laser interaction time for two methods of volume measurement.

After the preliminary trials it was deemed appropriate to test the accuracy of the volume loss calculated from the mass loss of the specimen and the density of control specimens (as described in Section 3.4.2). Volume removal due to scabbling after 10 s and 40 s laser interaction was obtained using a 3D scanner (Geomagic Faro ScanArm 3D scanner) to detect the surface profile of specimens after the tests. The removed volume was calculated using Geomagic Studio software.

Figure C.1 compares the results of the two methods of volume measurement. It can be seen that the difference between the two methods is small in all specimens except those that experienced vitrification. The laser scanner on the 3D scanner did not pick up the vitrified area and therefore these had to be reconstructed using the mesh GeoMagic software.

Appendix D

Determination of infra red parameters

D.1 Emissivity

Different materials emit different amounts of infra red light when they are at the same temperature. The factor that normalises materials is known as the emissivity, this must be applied to infra red data. The Reference Emissivity Material Method detailed in ISO 18434-1 was used to determine the emissivities of the different materials. The method used in this study was as follows:

(I). Recreate experimental set up, i.e. distance between the infra red (IR) camera and the target specimen (Figure D.1).

(II). Apply surface modifying material on the target specimen (in this case scotch electrical tape was used as suggested in the IR camera's user manual.

(III). Heat specimen in the oven (to temperature discussed in Section D.3).

(IV). Enter known emissivity of the surface modifying material into camera settings.

(V). Focus IR camera on the specimen and capture a still image.

(VI). Note down the recorded temperature of the surface modifying material, Temperature A, and the temperature of the target specimen immediately adjacent to the surface modifying material, Temperature B.

(VII). Adjust the emissivity setting until the temperature of the adjacent area is the same as Temperature A, this new emissivity is the emissivity of the target specimen.

TABLE D.1: Emissivity test parameters used in the setup detailed in Figure D.1

	d_w	d_s
Preliminary study	400mm	700mm
Effect of composition	10mm	340mm

(VIII). Repeat this four times, and take an average of the four values. Emissivity values are detailed in Table D.2.

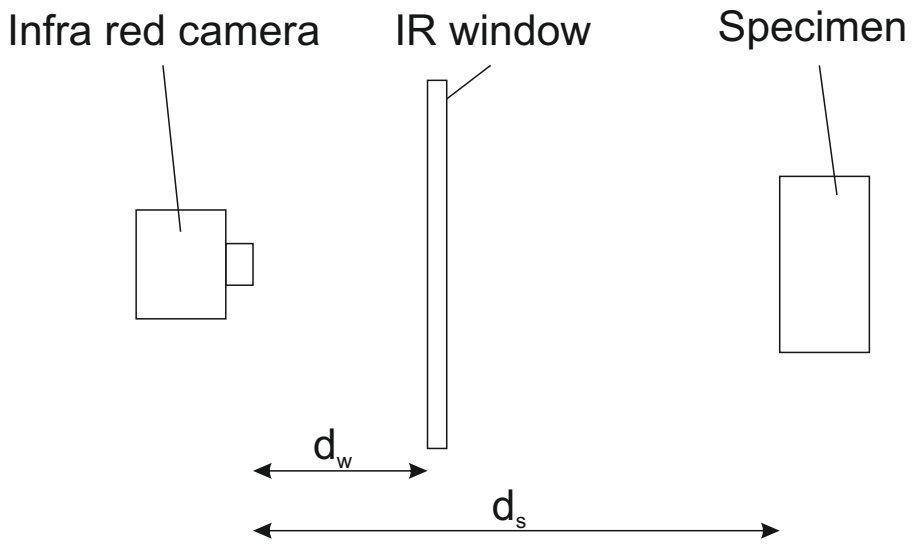

FIGURE D.1: Experimental setup recreated in the emissivity and transmission tests.

D.2 Transmission

In order to protect the infra red camera from any damage from flying debris, a translucent infra red (IR) window supplied by Edmund Optics was used. The transmission of this window (the amount of infra red radiation that passes through the window) is needed to correct recorded data. The following method was used to determine the transmission factor of the IR window.

(I). Recreate the experimental set up, i.e. distance between IR camera, IR window and target specimen (Figure D.1).

(II). Heat the target specimen in the oven (to temperature discussed in Section D.3).

(III). Capture an image of the target specimen without the IR window; Image A.

(IV). Capture an image of the target specimen with the IR window in place; Image B.

TABLE D.2: Emissivity values determined in the emissivity tests during the first and second test series (Chapters 4 and 5). Test series 2= the effect of concrete composition.

Preliminary studies		Test series 2*	
LC (Lp)	0.966	Lp	0.966
		Lo	0.966
BC (Bp)	0.978	Bp	0.966
		Bo	0.966
M (Mp)	0.990	Mp	0.958
		Mo	0.969
		O32	0.971
O (O42)	0.975	O42	0.975
		P32	0.960
P (P42)	0.978	P42	0.964

(V). Capture an image of the target specimen without the IR window; Image C.

(VI). Take an average of the target specimen temperatures in Image A and Image C; Temperature 1.

(VII). Adjust the transmission setting on the IR camera until the specimen temperature in image B is equal to Temperature 1. The new transmission value is the transmission factor for the IR window.

(VIII). Repeat this three times, take an average of the three values.

An average transmission factor for the IR window over all the compositions was taken and a transmission of 0.583 +/− 0.005 was determined. Edmund Optics supply the graph shown in Figure D.2, which complies with the value determined by the method described here.

D.3 Oven temperature used in emissivity and transmission factor tests

The temperature used in the emissivity and transmission factor tests for the preliminary studies (Chapter 4) was 80°C. For the second experimental programme (the effect of concrete composition, Chapter 5) three temperatures were planned 50°C, 100°C and 150°C, but at 100°C moisture loss from the concrete caused bubbles to form in the

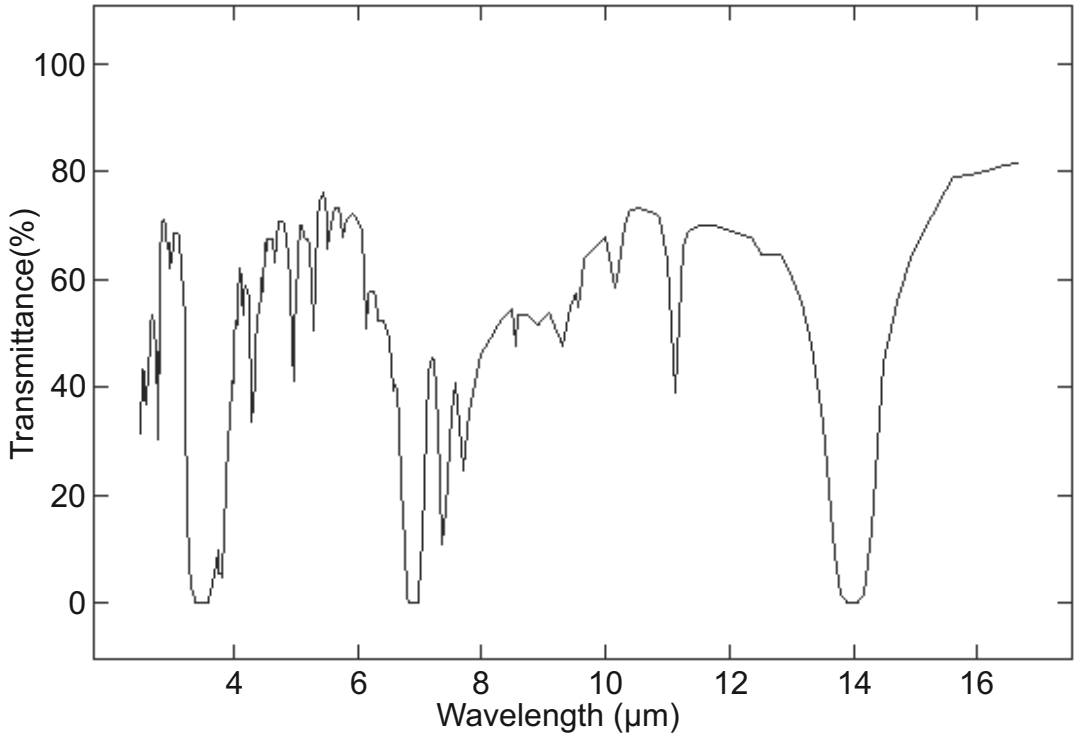

FIGURE D.2: Graph of the IR window transmission supplied by Edmund Optics. The spectral range of the IR camera is included on the graph.

scotch tape and the tests were deemed inaccurate, as a result the results from the 50°C were used.

Appendix E

Surface temperature analysis

In this section, the method used to analyse the surface temperature data is discussed.

The aim of the infra red thermography was to determine the thermal characteristics of laser scabbling. This required a method of presenting the thermal data against interaction time in a way that was representative of the whole area under laser application. The scabbling process was recorded with the infra red camera at 1/15 or 1/30 fps (depending on the camera's functionability). Each frame that was recorded consisted of a 2D grid of temperature values. The average surface temperature and maximum surface temperature are functions programmed into the Thermacam Researcher software, and were used to present the temperature data against the interaction time.

Figure E.1-b shows the average and maximum surface temperature-time histories for results of the preliminary studies (Chapter 4). It can be seen that the average surface temperatures are far lower than the maximum surface temperatures. The problem with the maximum surface temperatures is that this value is not related to size in any way: the maximum surface temperature is the single highest temperature value recorded in each frame. The nature of scabbling means this could be some debris that has already been scabbled rather than contributing to scabbling, obscuring the maximum surface temperature measurements. As a result, the maximum surface temperature is not representative of the temperature that is causing laser scabbling to occur or of the scabbling behaviour of the whole surface.

Figure E.1-a shows the average surface temperature-time histories for results of the preliminary studies (Chapter 4) using both temperature ranges. It can be seen that the the average surface temperatures for both temperature ranges are similar, for all compositions. As the 0–550 °C range will take any value above 550 °C as 550 °C, and the 200–2000 °C range takes any value under 200 °C as 200 °C, the fact that

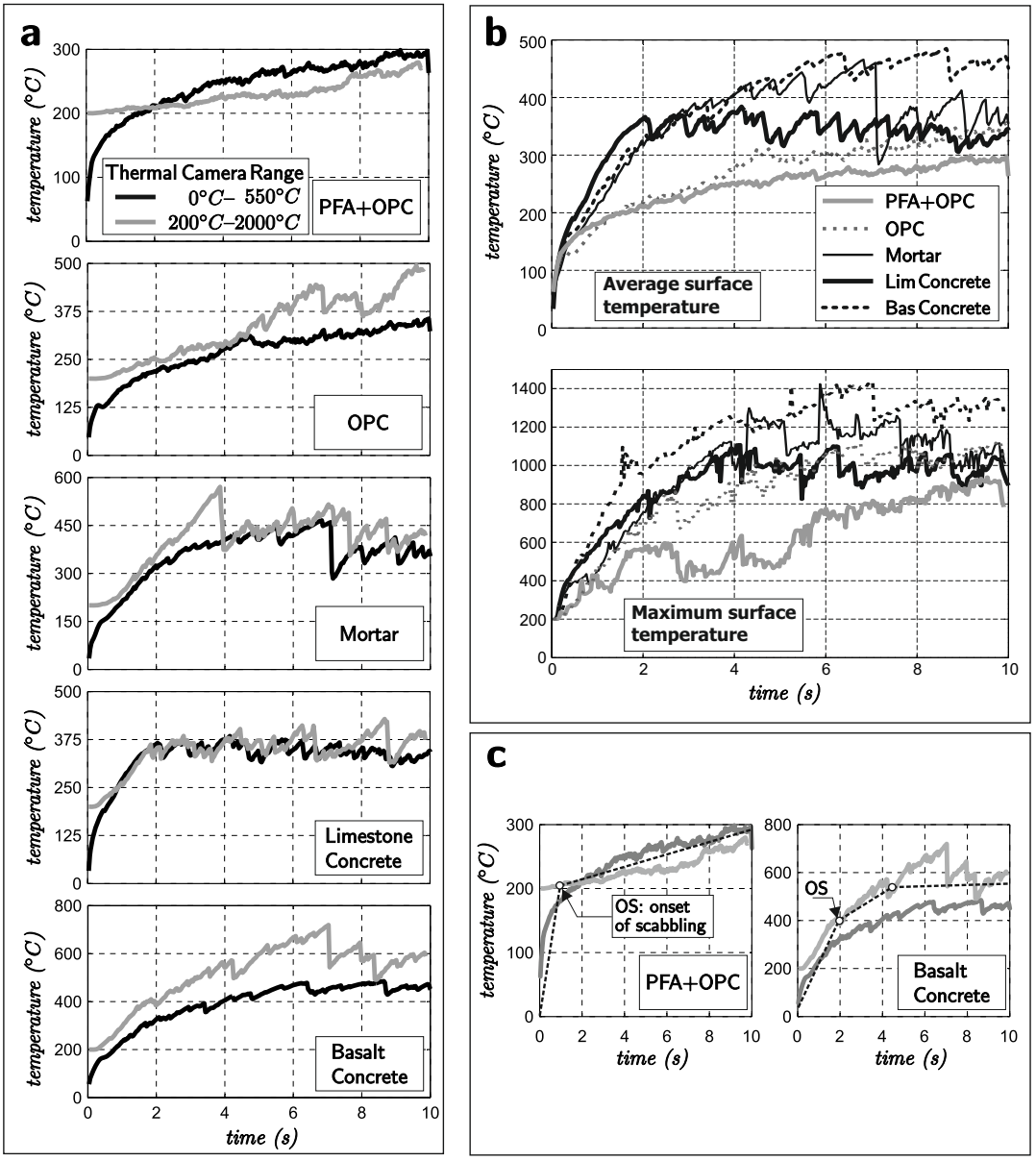

FIGURE E.1: (a) Time histories of average surface temperatures for each material (saturated) recorded in two tests using two different thermal camera settings, 0-550 and 200-2000, (b) comparison of time histories of maximum and average surface temperatures all compositions used in the preliminary studies, and (c) detection of phases in scabbling behaviour: onset of scabbling and onset of steady state phase.

the average surface temperatures are similar for each range suggests that the surface temperatures are mostly between 200 °C and 550 °C. As a result this makes the average surface temperatures much more representative of the temperature of the surface over the whole area of laser application, than the maximum surface temperatures. The largest variation between the two temperature ranges was identified in the basalt concrete as a result of vitrification of the basalt aggregates.

A single temperature was required for each composition to relate to the DTA/TGA analysis to identify which thermal reactions were taking place and potentially causing laser scabbling to occur. The obvious choice was to use the maximum surface temperature as this is the highest temperature reached during the trial, and as a result any thermal reactions which occur below this temperature would take place to some extent. While this is true, it was deemed inappropriate for the reasons described above. The median of the average surface temperature over the 10 s interaction time was looked at briefly, but from inspection of the average surface temperature time histories, it became apparent that key characteristics could be identified from the shapes of the graphs themselves.

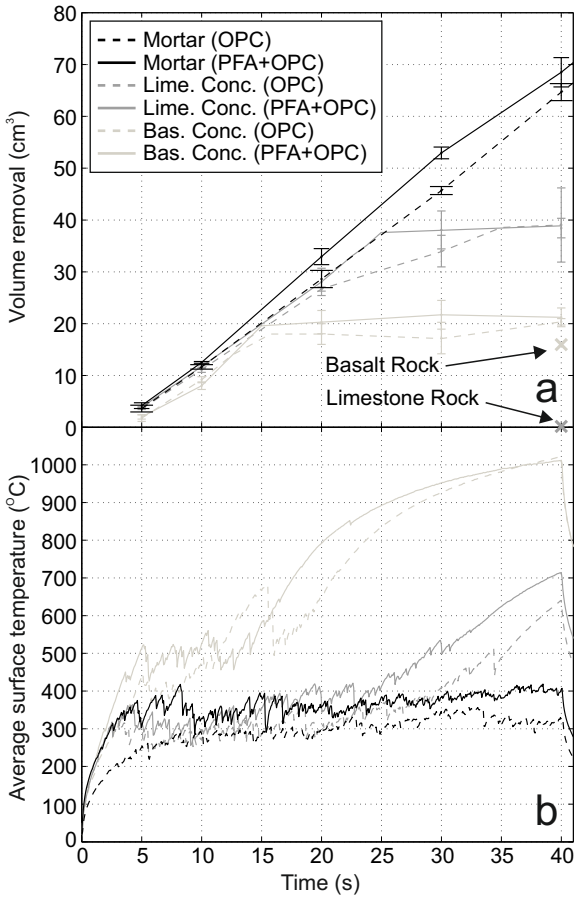

FIGURE E.2: (a) Volume removal and (b) time histories of average surface temperatures for mortar, limestone concrete and basalt concrete compositions using both OPC_{42} and $(PFA+OPC)_{42}$ binder compositions. Concretes made with 10mm coarse aggregates.

Figure E.1-c illustrates the key characteristics which can be detected from the average surface temperature-time histories. It can be seen that the surface temperature behaviour can be separated into separate periods. Firstly there is a heating period, which generally lasts for less than 1–2 s and is a similar rate for most compositions (although this is not the case for the OPC mortar presented in Section 5.3.2). Following this there is a reduction in surface heating identified by a reduction in the gradient of the average surface temperature-time histories. The temperature where this occurs has

been labelled as the temperature at the onset of scabbling. As reported in Section 3.4.3, the temperatures at the onset of scabbling occur at different times and vary for different compositions. After the onset, the PFA+OPC paste (w/b=0.42) and the mortar (PFA) show a consistent rate of background heating, coinciding with consistent volume removal, whereas the rate of background heating of the concretes (PFA) and OPC paste (w/b=0.42) reduce further. Results from the second experimental programme (Section 5.3.3) showed a sharp increase in the average surface temperature after 20–30 s during laser scabbling of concretes, coinciding with a reduction of volume removal (Figure E.2).

E.1 Average surface temperature drops

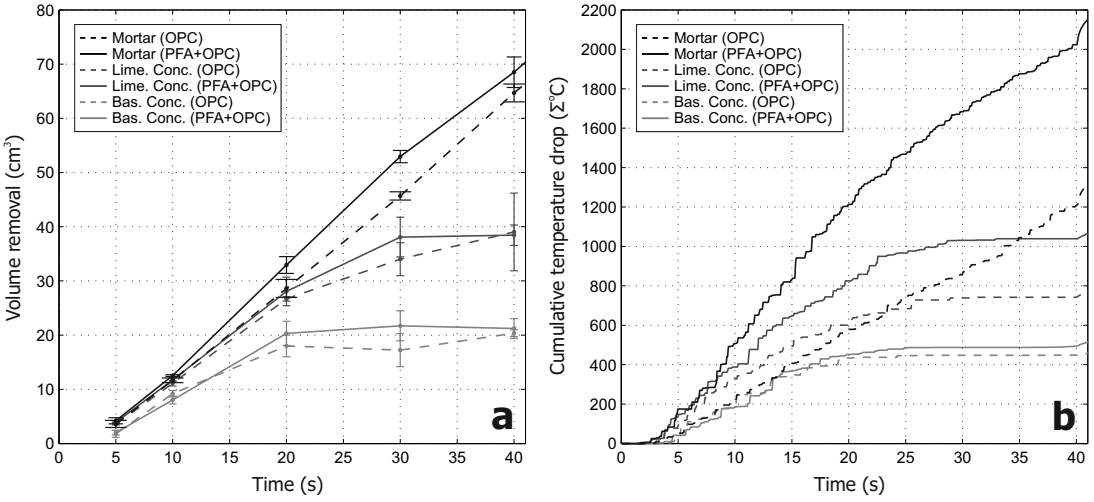

FIGURE E.3: (a) Volume removal and (b) cumulative average surface temperature drops for mortar and concrete compositions from the preliminary studies.

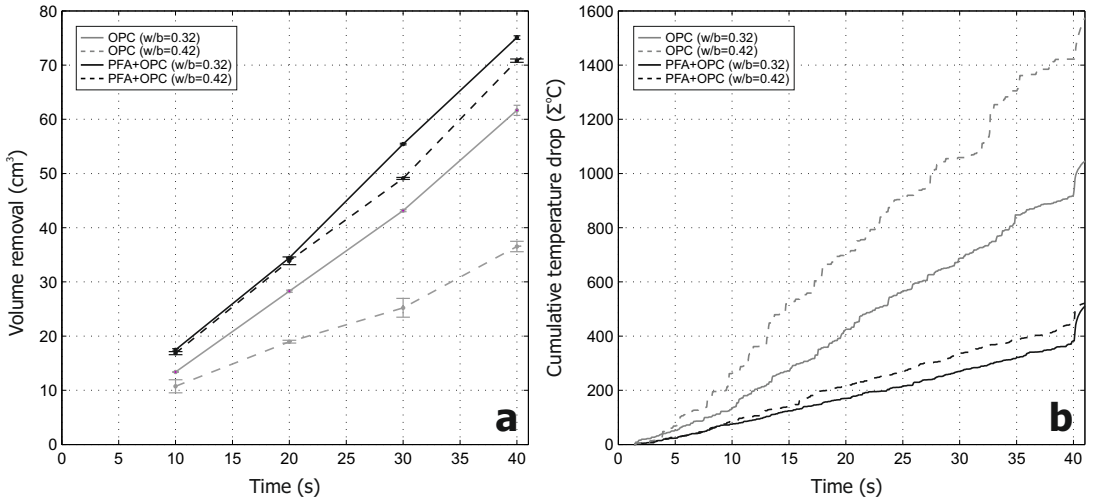

FIGURE E.4: (a) Volume removal and (b) cumulative average surface temperature drops for cement paste compositions from the preliminary studies.

Distinct fluctuations can be seen in the time histories of the average surface temperatures (Figure E.1) which represent the ejection of material. A larger temperature drop equates to a larger fragment, in either surface area or depth. A fragment of a larger area would result in more temperature values reducing, whereas a thicker fragment would reveal cooler material reducing individual temperature values more, both of which would cause a sudden drop in the average surface temperature. In the second test series (Chapter 5), the temperature drops from the average surface temperature-time histories were isolated and plotted with the volume removal. Figure E.3 shows good correlation between the cumulative temperature drops and the volume removal for the mortars and concretes. The volume of removal in cement pastes however is inversely proportional to the temperature drops (Figure E.4), indicating that the mechanism of scabbling differs between scabbling of pastes and compositions including aggregates.

Appendix F

The repeatability of the average surface temperature data

To present the repeatability of the average surface temperature data presented in the relevant Chapters (4, 5, 6 and 7), all infra red data that was collected during the project is grouped by composition below. It can be seen that where repeats have been carried out, the repeatability of the average surface temperature–time histories was good.

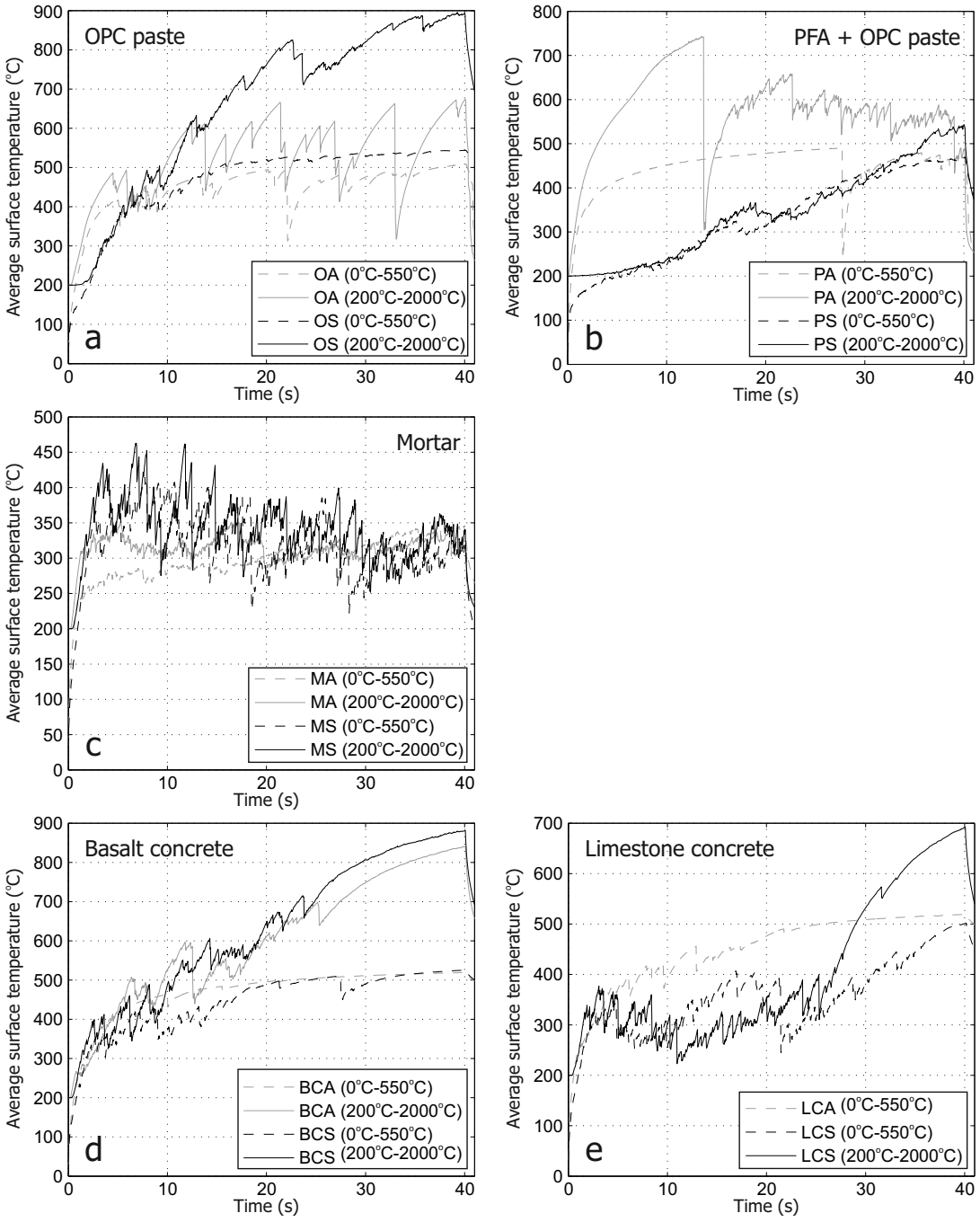

FIGURE F.1: All infra red data collected during the age investigation for Series 1 specimens.

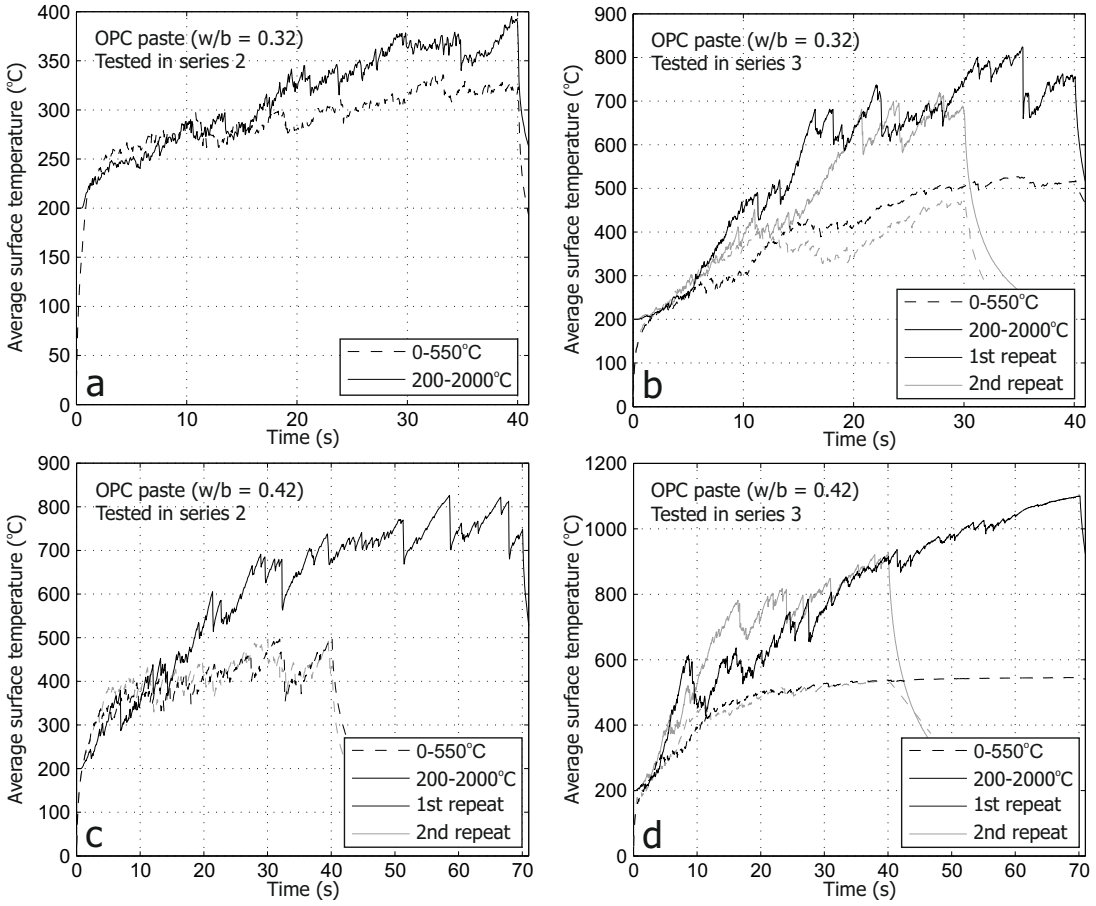

FIGURE F.2: All infra red data collected during Series 2 and the age investigation for Series 2 OPC paste specimens.

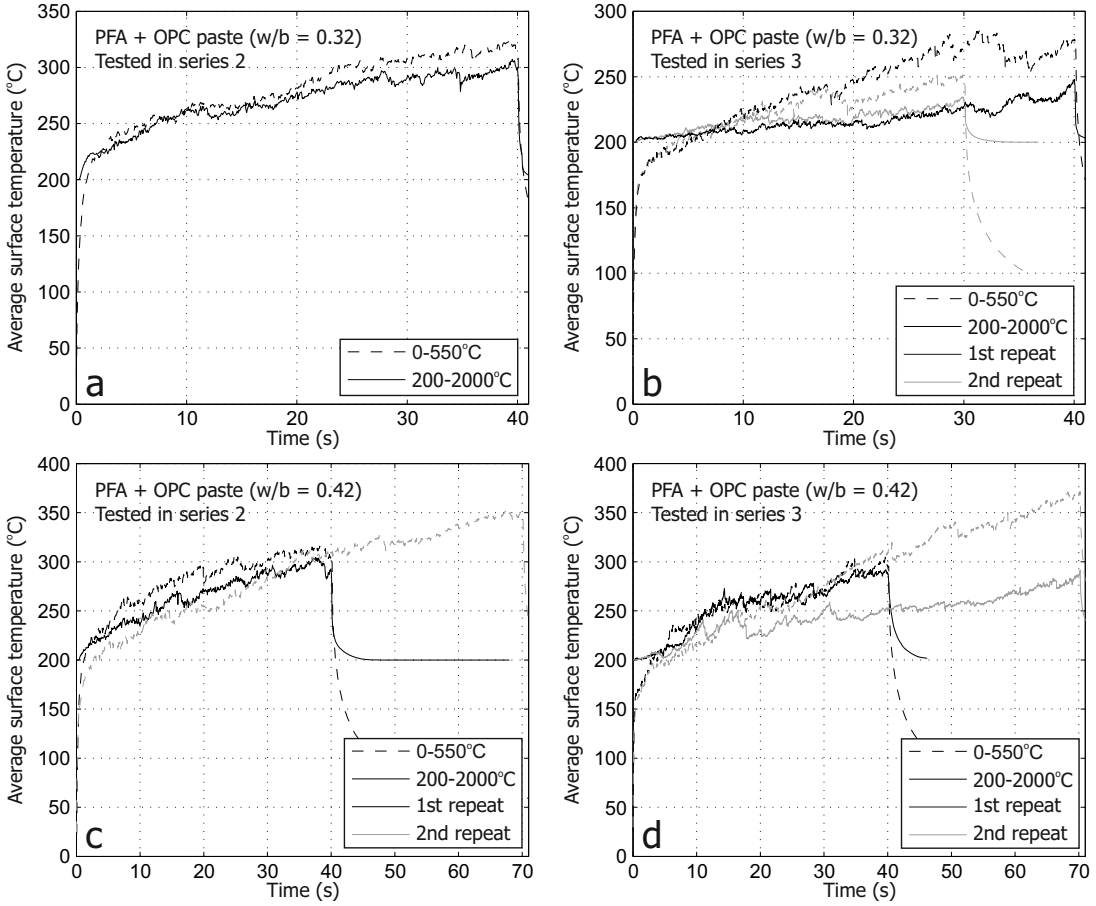

FIGURE F.3: All infra red data collected during Series 2 and the age investigation for Series 2 PFA + OPC paste specimens.

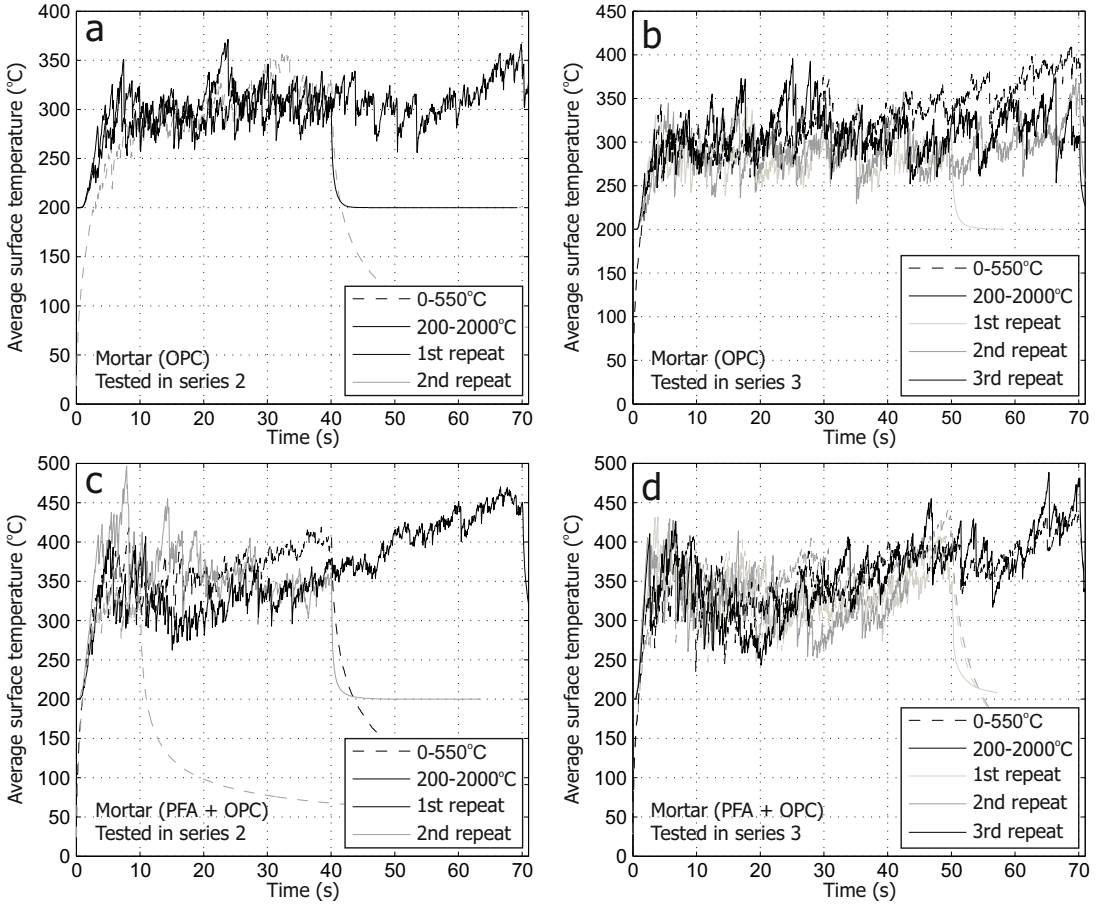

FIGURE F.4: All infra red data collected during Series 2 and the age investigation for Series 2 mortar specimens.

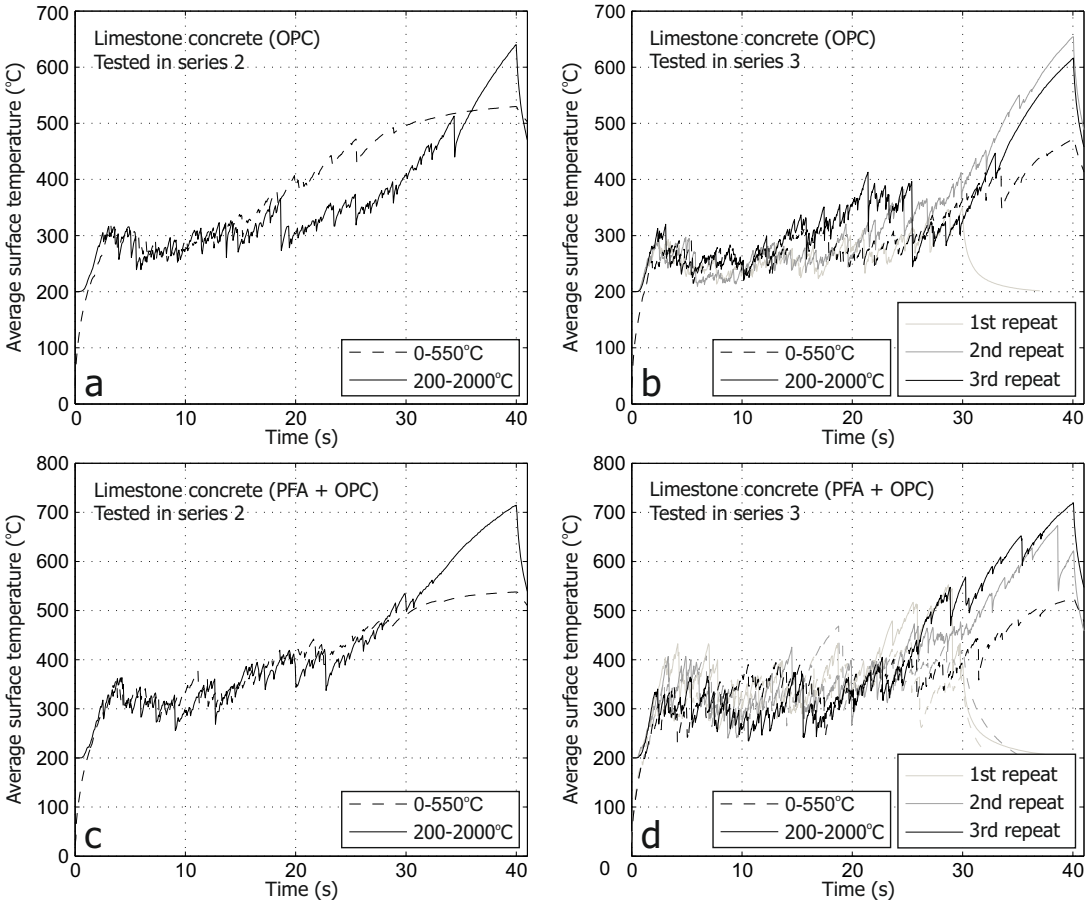

FIGURE F.5: All infra red data collected during Series 2 and the age investigation for Series 2 limestone concrete specimens.

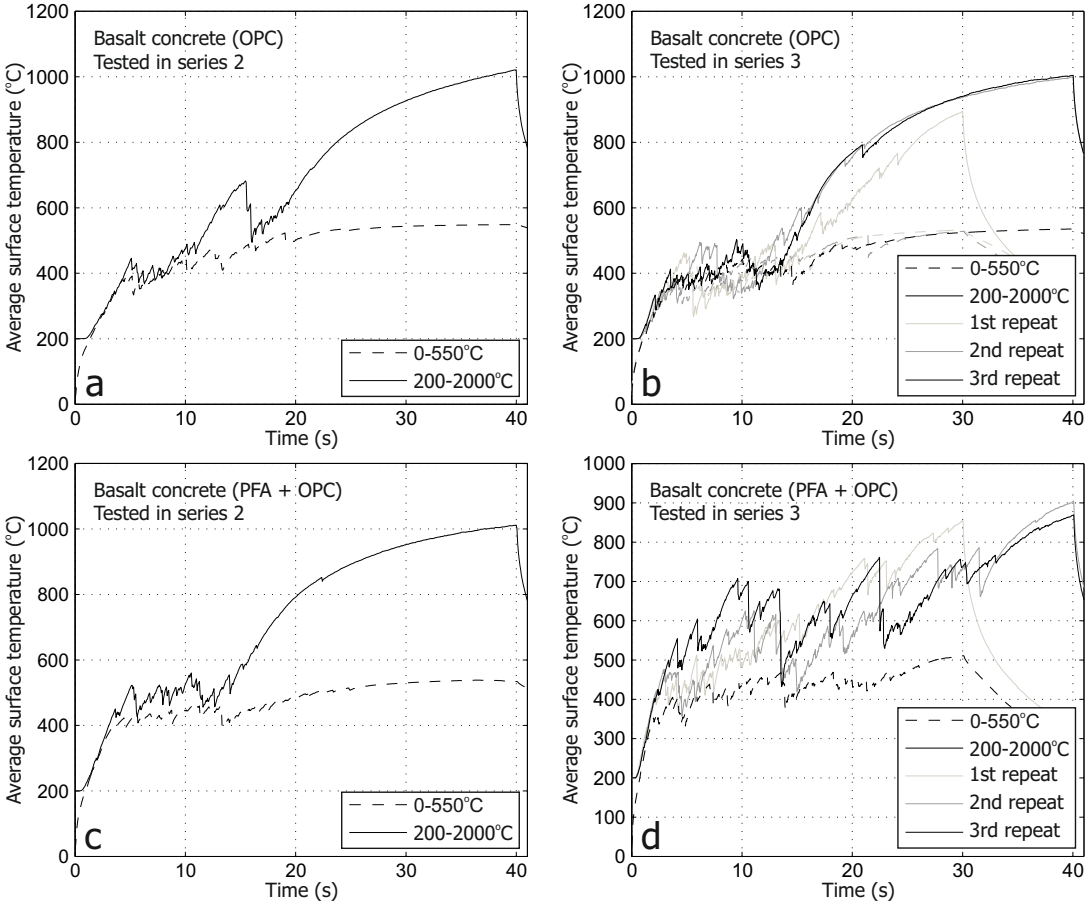

FIGURE F.6: All infra red data collected during Series 2 and the age investigation for Series 2 basalt concrete specimens.

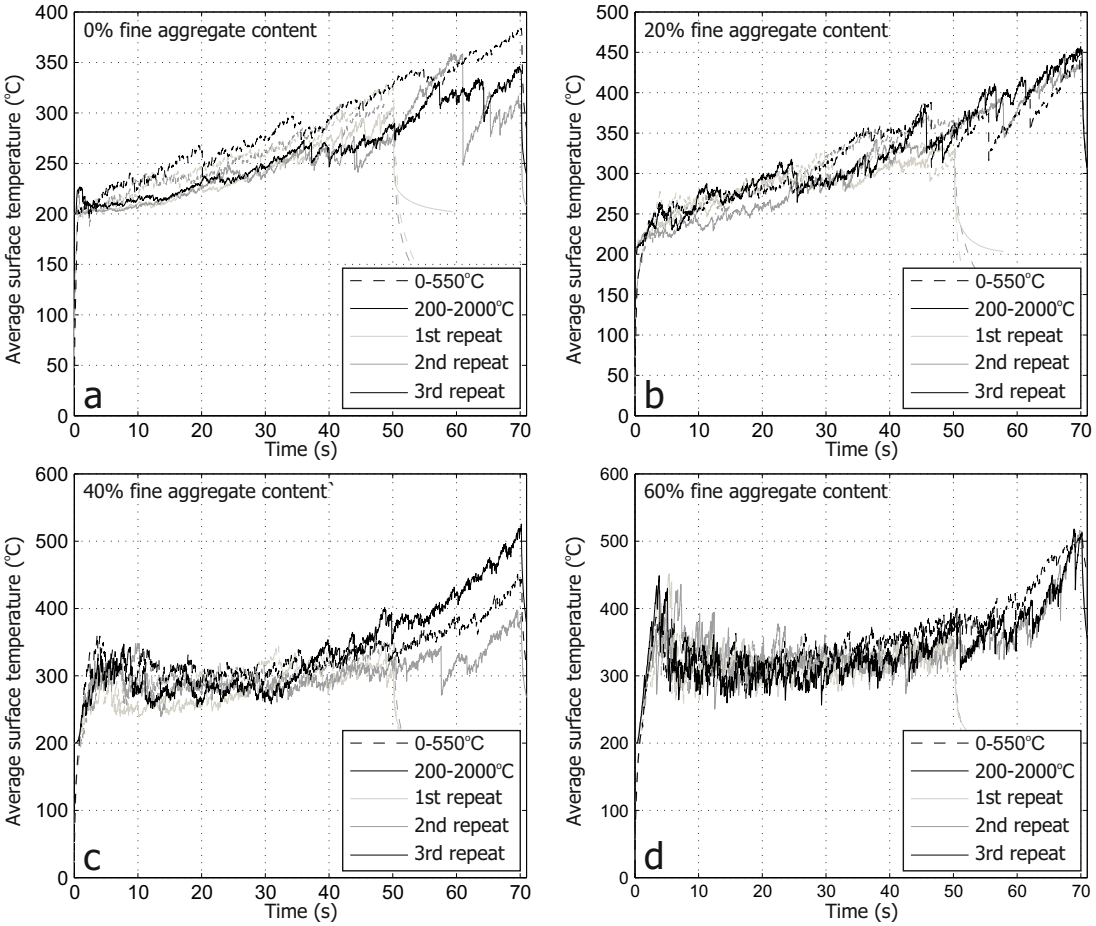

FIGURE F.7: All infra red data collected during Series 3 for mortars specimen with different aggregate contents.

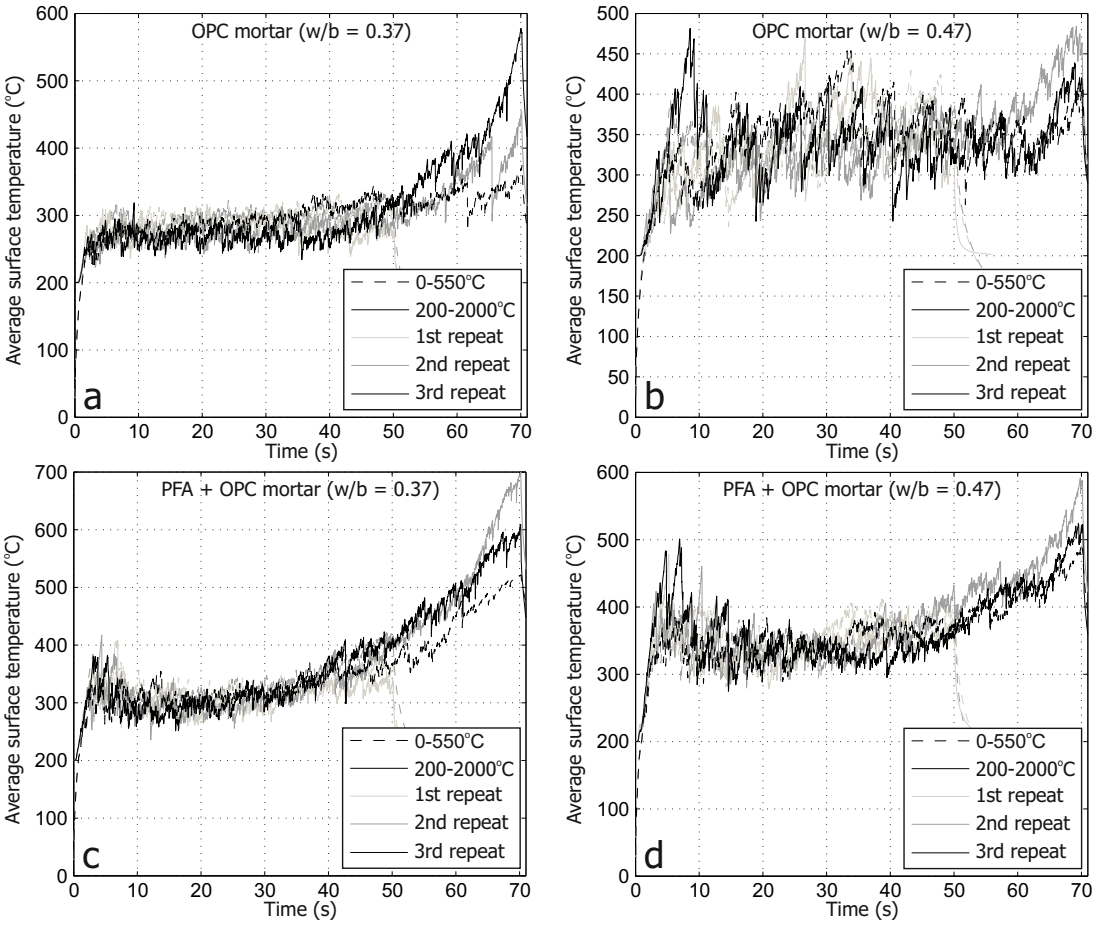

FIGURE F.8: All infra red data collected during Series 3 for mortars specimen with different water binder ratios.

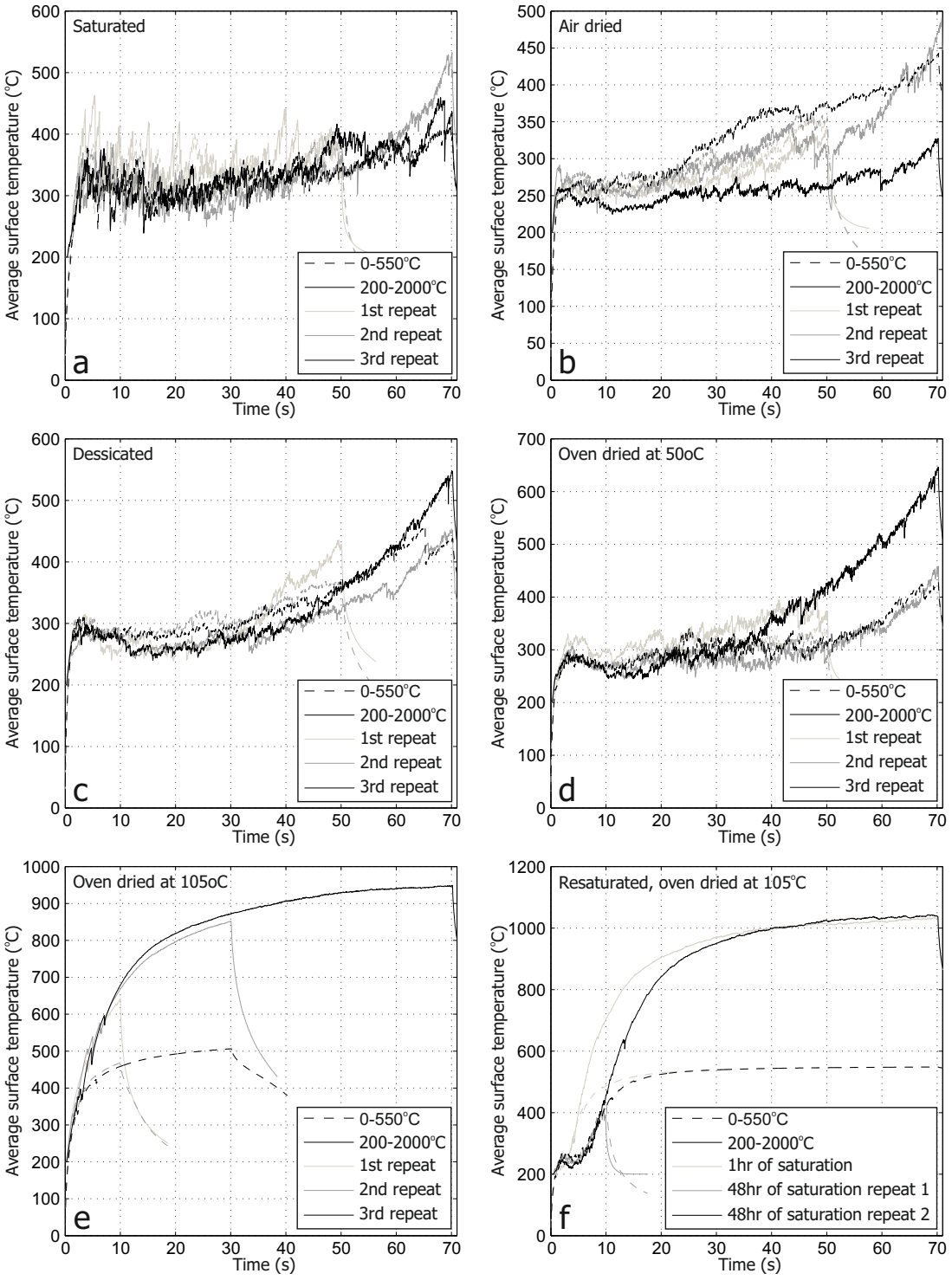

FIGURE F.9: All infra red data collected during Series 3 for mortars specimen with different free water contents.

Appendix G

Modulated and pulsed laser trials

Although laser parameters were kept constant for the main test series, some work was done on the effect of using a modulated laser beam and a pulsed laser beam, particularly in the case of the basalt concrete, in an attempt to overcome the problems of vitrification described in Chapters 4 and 5.

G.1 Modulated beam

During the second test series (Chapter 5) it was identified that vitrification of the basalt concretes generally began after 10 s laser interaction. It was hypothesised that the vitrification might be reduced, and volume removal increased, if the concrete was given chance to cool down after 10 s interaction time, and subsequently exposed to a further 10 s laser interaction once it had cooled.

To test this hypothesis three laser power configurations were used (Figure G.1). Cooling periods between laser interactions allowed the specimens to be weighed. Figure G.2 shows the comparison between the results for a continuous laser beam (first reported in Chapter 5) and the results for the modulated beam. It should be noted that the modulated beam trials were one-off experiments and not repeated.

It can be seen from Figure G.2 that all beam modulations were less successful than the continuous laser beam. This was true for both limestone and basalt concrete, suggesting that the poor performance of modulating the beam is the same for both concretes and not related to the vitrification of the basalt aggregate. This suggests it is a result of some general scabbling behaviour that reduces scabbling efficiency after the first laser interaction, potentially due to irreversible damage that takes place during the first laser exposure, reducing the tensile strength and/or increasing permeability.

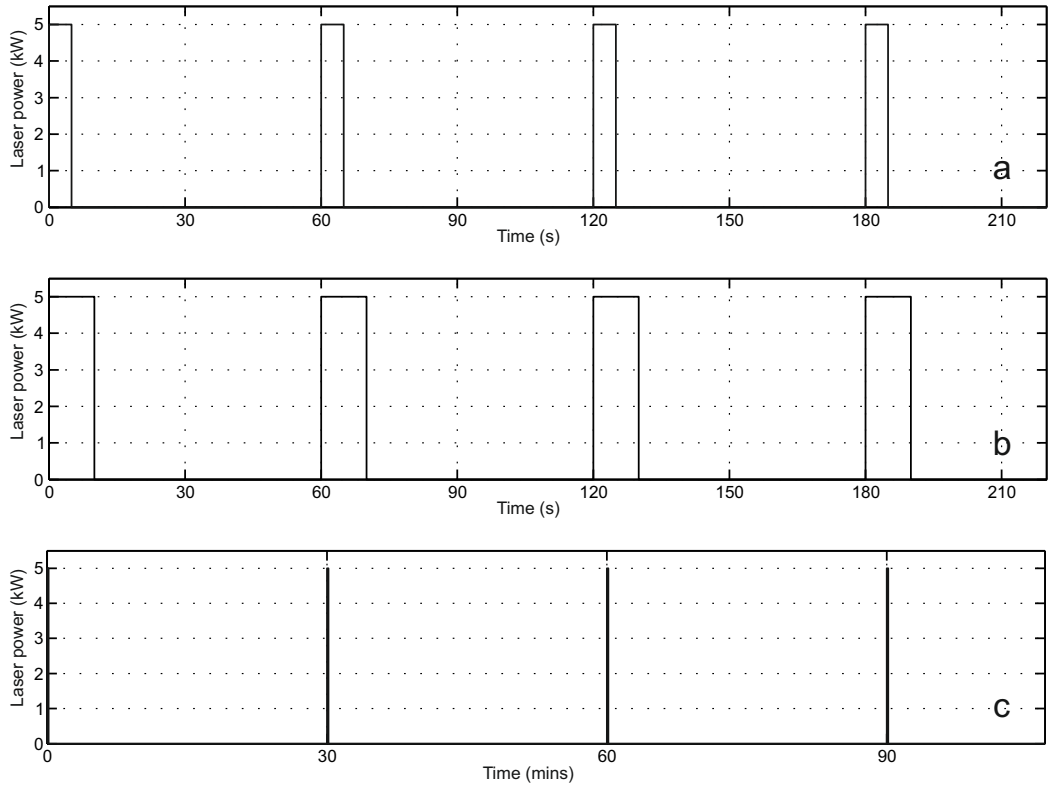

FIGURE G.1: Examples of the laser power configurations used; (a) five seconds of laser interaction per minute (5 s/min), (b) ten seconds of laser interaction per minute (10 s/min) and (c) ten seconds of laser interaction per thirty minutes (10 s/30 min), note the different scale. Cycles were continued for longer time periods as necessary. 5 s/min and 10 s/min were trialled on only the PFA + OPC basalt concrete.

Figure G.2 shows that the difference between the 10 s/30 min modulation and the continuous is larger for concrete using the PFA + OPC binder than the 100% OPC binder. The PFA + OPC binder gives a less permeable material which is therefore likely to be more sensitive to damage and experience a greater increase in permeability as a result.

Figure G.2c shows the results for the three different modulations used on the PFA + OPC basalt concrete (Bp). 5 s/min was the least successful suggesting scabbling does not fully begin after 5 s laser interaction and 10 s laser interaction is more effective. 10 s/min is more effective than 10 s/30 min, but still worse than the results for the continuous beam, showing that the more time material is given to cool, the less successful the subsequent laser exposures are.

In conclusion, all the results from this brief investigation into beam modulation suggest that allowing the concrete to cool between laser interactions is detrimental to laser scabbling of concretes. In a practical sense, the results suggest that multiple passes will be less effective and the required depth of surface removal should be targeted in the first pass.

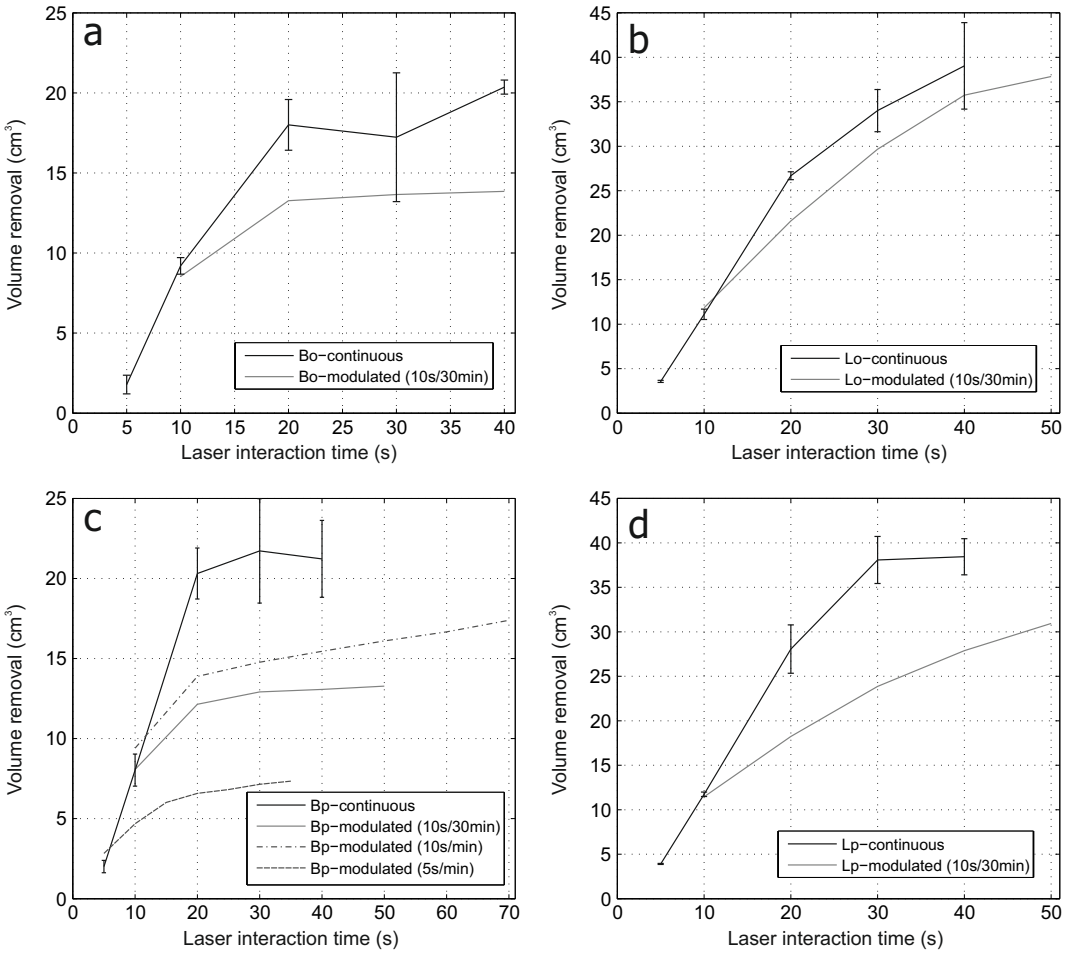

FIGURE G.2: Volume removal results plotted against cumulative laser interaction time for the modulated beam configurations and the continuous beam results reported in Chapter 5; (a) OPC basalt concrete (Bo), (b) OPC limestone concrete (Lo), (c) PFA + OPC basalt concrete (Bp), and (d) PFA + OPC limestone concrete (Lp).

G.2 Pulsed laser between continuous laser

During the third experimental programme (Chapter 6) a pulsed laser was used in between periods of continuous laser power to try and remove the vitrified layer.

The laser power configuration used can be seen in Figure G.3b, it consisted of 10 s of continuous 5 kW laser power, followed by a pulsed power of 1 s of 1 kW power every 2 s for 11s, followed by the configuration repeated. As the specimen could not be weighed between continuous beam interaction times, infra red data was collected to quantify the rate of scabbling.

It can be seen from Figure G.3a that the volume removal for the pulsed laser (which included 20 s of continuous 5 kW laser power) was similar to that of the volume removal for specimens exposed to 40 s continuous 5 kW laser power. As a result the pulsed laser configuration had a larger volume-removal/laser-energy ratio (0.27 cm^3/kJ), compared

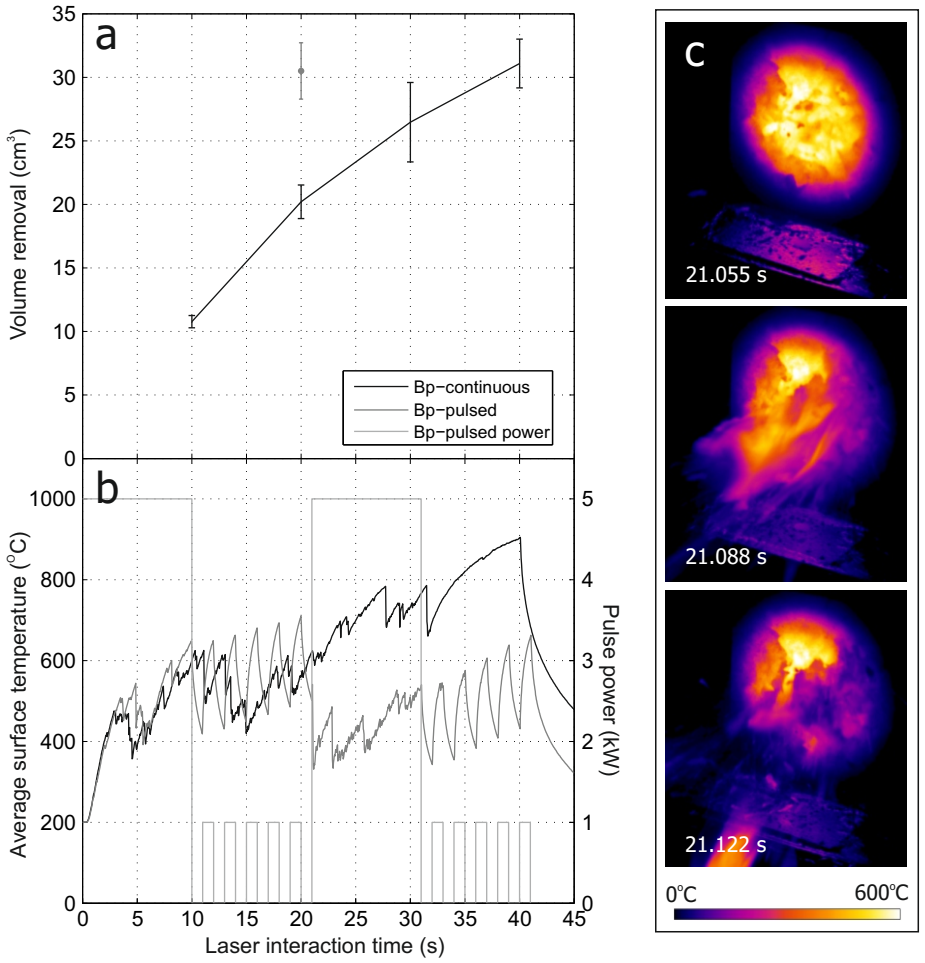

FIGURE G.3: (a) Volume removal for the continuous and pulsed laser trials on PFA + OPC basalt concrete, (b) the average surface temperature histories and pulsed laser power configuration, and (c) infra red images of the large fragment removal due to laser pulsing.

to the 20 s (0.20 cm^3/kJ) or the 40 s continuous beam (0.16 cm^3/kJ). Furthermore, it can be seen from Figure G.3b that the average surface temperature of the concrete did not exceed 700 °C and a large fragment ejection (resulting in a drop in average surface temperature of around 200 °C) can be identified immediately after the first pulse cycle, also seen in Figure G.3c. This suggests the differential thermal stresses developed in the vitrified layer and the concrete worked as a method to remove the vitrified layer, allowing the exposed surface to undergo scabbling once again.

Figure G.4 shows photographs of the specimens after the pulsed test and the 10 s, 20 s and 40 s continuous laser application. The specimen which underwent the pulsed laser application experienced less vitrification than any of the specimens which underwent continuous laser application, despite having a similar volume removal to the 40 s continuous test (Figure G.4d), and 20 s of continuous laser exposure (in total) like the 20 s continuous test (Figure G.4c).

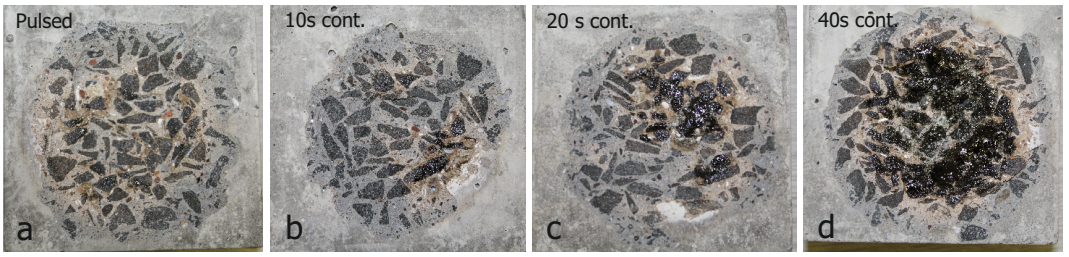

FIGURE G.4: Photographs of specimens after laser scabbling trials: (a) the pulsed configuration detailed in FigureG.3b, (b) 10 s, (c) 20 s, and (d) 40 s of continuous laser application.

In conclusion, this small investigation suggests that a pulsed laser beam can be used to remove the vitrified layer which develops when laser scabbling basalt concrete. Furthermore the laser configuration used here resulted in a much higher volume-removal/laser-energy ratio. This area has been highlighted in the further work section (Chapter 9) as a key area for future research in order increase the success of this technology in nuclear decommissioning.